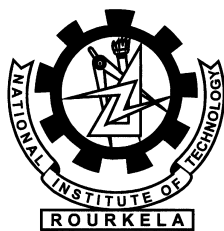# Iris Identification using Keypoint Descriptors and Geometric Hashing

Hunny Mehrotra

Department of Computer Science and Engineering
National Institute of Technology Rourkela
Rourkela-769 008, Orissa, India

Iris Identification using Keypoint Descriptors and Geometric Hashing

Thesis submitted in partial fulfillment
of the requirements for the degree of

Master of Technology

(Research)

in

Computer Science and Engineering

by

Hunny Mehrotra

(Roll: 607CS002)

under the guidance of

Prof. Banshidhar Majhi

NIT Rourkela

&

Prof. Phalguni Gupta

IIT Kanpur

Department of Computer Science and Engineering
National Institute of Technology Rourkela
Rourkela-769 008, Orissa, India
January 2010

Department of Computer Science and Engineering
National Institute of Technology Rourkela
Rourkela-769 008, Orissa, India.

January 24, 2010

Certificate

This is to certify that the work in the thesis entitled ***Iris Identification using Keypoint Descriptors and Geometric Hashing*** by ***Hunny Mehrotra*** is a record of an original research work carried out under our supervision and guidance in partial fulfillment of the requirements for the award of the degree of Master of Technology (Research) in Computer Science and Engineering. Neither this thesis nor any part of it has been submitted for any degree or academic award elsewhere.

Phalguni Gupta
Professor
CSE department of IIT Kanpur

Banshidhar Majhi
Professor
CSE department of NIT Rourkela

Acknowledgment

"The will of God will never take you where Grace of God will not protect you."
Thank you God for showing me the path. . .

I owe deep gratitude to the ones who have contributed greatly in completion of this thesis.

Foremost, I would like to express my sincere gratitude to my advisor, Prof. Banshidhar Majhi for providing me with a platform to work on challenging areas of biometrics. His profound insights and attention to details have been true inspirations to my research.

I am grateful to my co-supervisor, Prof. Phalguni Gupta who has provided me with continuous encouragement and support to carry out research. His dedication and consistent notation in my writings has motivated me to work for excellence.

I am very much indebted to Prof. Sanjay Kumar Jena, for providing insightful comments at different stages of thesis that were indeed thought provoking.

My special thanks goes to Prof. Sukadev Meher and Prof. Bibhudatta Sahoo for contributing towards enhancing the quality of the work in shaping this thesis.

I would like to thank all my friends and lab-mates for their encouragement and understanding. Their help can never be penned with words.

Most importantly, none of this would have been possible without the love and patience of my family. My family to whom this dissertation is dedicated to, has been a constant source of love, concern, support and strength all these years. I would like to express my heart-felt gratitude to them.

Hunny Mehrotra

Abstract

Iris is one of the most reliable biometric trait due to its stability and randomness. Conventional recognition systems transform the iris to polar coordinates and perform well for co-operative databases. However, the problem aggravates to manifold for recognizing non-cooperative irises. In addition, the transformation of iris to polar domain introduces aliasing effect. In this thesis, the aforementioned issues are addressed by considering *Noise Independent Annular Iris* for feature extraction. Global feature extraction approaches are rendered as unsuitable for annular iris due to change in scale as they could not achieve invariance to transformation and illumination. On the contrary, local features are invariant to image scaling, rotation and partially invariant to change in illumination and viewpoint. To extract local features, *Harris Corner Points* are detected from iris and matched using novel Dual stage approach. Harris corner improves accuracy but fails to achieve scale invariance. Further, *Scale Invariant Feature Transform* (SIFT) has been applied to annular iris and results are found to be very promising. However, SIFT is computationally expensive for recognition due to higher dimensional descriptor. Thus, a recently evolved keypoint descriptor called *Speeded Up Robust Features* (SURF) is applied to mark performance improvement in terms of time as well as accuracy.

For identification, retrieval time plays a significant role in addition to accuracy. Traditional indexing approaches cannot be applied to biometrics as data are unstructured. In this thesis, two novel approaches has been developed for indexing iris database. In the first approach, *Energy Histogram of DCT coefficients* is used to form a B-tree. This approach performs well for cooperative databases. In the second approach, indexing is done using *Geometric Hashing* of SIFT keypoints. The latter indexing approach achieves invariance to similarity transformations, illumination and occlusion and performs with an accuracy of more than 98% for cooperative as well as non-cooperative databases.

Contents

List of Figures

List of Tables

Chapter 1

Introduction

The terrorist attacks in US on 11 September 2001 has focussed more attention on personal identification. In addition to this, identification is also required in large range of civilian applications like passports, driver licenses, banking, refraining imposters from hacking into networks, stealing mails etc. There exists traditional methods for authentication like (i) token based systems: where imposters are prevented from accessing protected resources using ID cards, smart cards etc, (ii) knowledge based systems: where identity is claimed using piece of information like user id and password associated with it. Some systems use combination of token based and knowledge based approaches. However, there are various disadvantages inherent to traditional means of authentication. The problem with token based systems is that the possession could be lost, stolen, forgotten or misplaced. The drawbacks of knowledge based approaches is that it is difficult to remember passwords/PINs and easily recallable passwords can be guessed by intruders. Thus, even the combination of knowledge and token based systems could not satisfy security requirements [8]. Biometrics identification, or *biometrics* provides a trustworthy solution to the problems faced by traditional authentication approaches. It is inherently more reliable and capable compared to traditional approaches.

Biometrics is the science of establishing the identity of an individual based on physiological and behavioural characteristics. It offers reliable solution to identity management by utilising fully automated or semi-automated schemes to recognise an individual [9]. The primary advantage of biometrics over token based and knowledge based approaches is that, it cannot be misplaced, forgotten or stolen. The character-

1

Figure 1.1: Various forms of authentication. Traditional methods of authentication using token based and knowledge based approaches (left). Use of biometrics to claim identity (right)

istics are distinct and has capability to distinguish between authorised persons and imposters. It is very difficult to spoof biometric systems as the person to be authenticated needs to be physically present. Various forms of authentication are shown in Figure 1.1. A generic biometric system operates by taking an input image from the user, preprocessing the image to find region of interest, extracting features, and authenticating an individual based on the result of comparison [10]. The modules involved in the biometric system is given in Figure 1.2. An important issue to be considered while designing a biometric system is how a person is recognised. Depending upon the application context a biometric system operates in two different modes [11]. In verification mode, a person is authenticated by comparing captured biometric data with his own pre-stored template. The system conducts one to one comparison to know whether the identity claimed by an individual is genuine or not. The concept of authentication is based on *"Am I whom I claim I am?"*. The diagrammatic representation of verification system is given in Figure 1.3 (a). During identification mode, the system searches the entire database to find the identity of an individual. The system conducts one to many comparison to establish the identity of an individual. The concept of identification is based on *"Who am I?"*. The diagrammatic representation

2
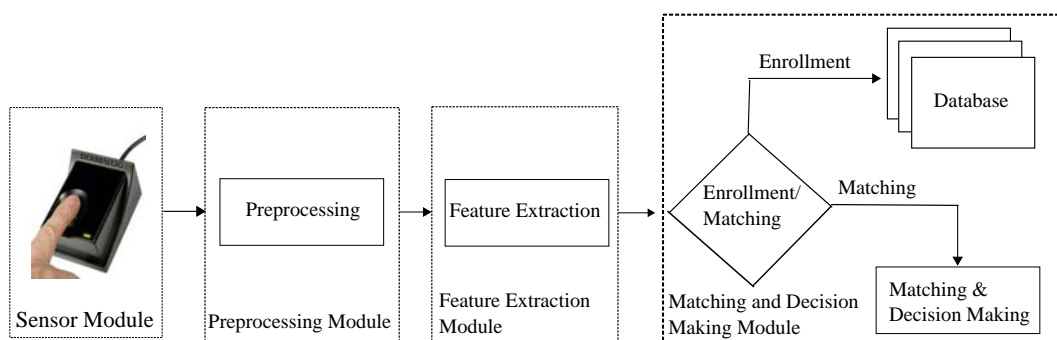
Figure 1.2: Different modules of biometrics system

of identification is given in Figure 1.3 (b).

There exists several traits like face, fingerprint, iris, ear etc. Looking at the nature of the underlying modalities, two basic categories can be identified as: Physiological (or passive) and Behavioral (or active) biometrics. Physiological biometrics are based on measurements and data derived from direct measurement of a part of the human body. Fingerprint, iris, retina, hand geometry, and face recognition are leading physiological biometrics. Behavioral characteristics on the other hand, are based on an action taken by a person. Behavioral biometrics, in turn, are based on measurements and data derived from an action, and indirectly measure characteristics of the human body. Voice recognition, keystroke dynamics, and signature are leading behavioral biometric technologies. A good biometric trait is characterised by use of features that are highly unique, stable, easy to capture and prevents circumvention.

1.1 Iris Biometrics

Reliability is particularly dependent upon the ability to acquire unique features that can be captured in an invariant fashion over change in time [12]. Although, each biometrics has several strengths and limitations and their deployment is dependent upon the application scenario. For example, fingerprint features remain unique over passage of time while face features though being unique can vary significantly with change in time and place. In addition to this, as few constraints as possible should be imposed on the user giving biometric data. Thus, fingerprint acquisition is invasive as it requires the user to make physical contact with the sensor.
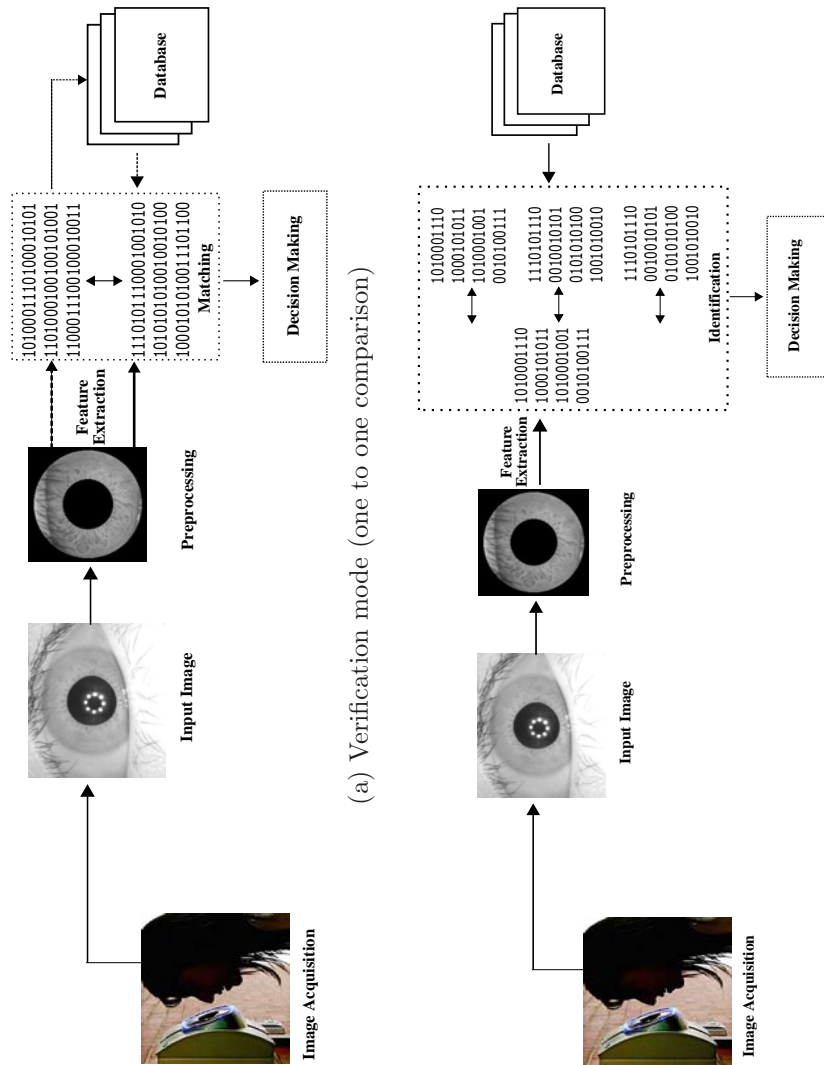
(a) Verification mode (one to one comparison)

(b) Identification mode (one to many comparisons)

Figure 1.3: Different modes of operation

Amongst various available biometric traits, iris plays a significant role to provide a promising solution to authenticate an individual using unique texture patterns [3]. Taking reliability and invasiveness into consideration, iris is proved to be the most efficient technique. From the point of view of reliability, the spatial patterns are unique to each individual. From the point of view of invasiveness, iris is protected internal organ whose random texture is stable throughout life. It can serve as a kind of living password that one need not remember but always carries along. The purpose is to provide the real-time high confidence recognition of an individual's identity by mathematical analysis of the random patterns that are visible within the iris of an eye from some distance. The randomness of iris patterns has very high dimensionality and it is one of the most reliable biometric trait available. Recognition decisions are made with confidence levels high enough to support rapid and reliable exhaustive searches through national level databases.

The most promising and significant feature in the eye image is iris (shown in Figure 1.4). The iris is in the form of circular ring that contains many interlacing minute characteristics such as freckles, coronas, stripes, furrows, crypts and so on. These minute patterns in the iris are unique to each individual and are not invasive to their users. Inside the iris, there is a central dark circle known as pupil. The iris has muscles that cause the pupil to constrict in bright light and dilate in dim light. This pupillary motion controls the amount of light entering the eye. The circumference of pupil and iris is known as pupil and iris boundary respectively. Sclera is the white portion, a tough and leather-like tissue surrounding the iris. Apart from these features, eyeball is covered by upper and lower eyelids. The upper eyelid is a stretchable membrane that can form a cover over the eye. It has a great freedom of motion, ranging from wide open to close. The lower eyelid on the other hand has a smaller degree of motion which is caused by deformation due to eyeball [13]. An eyelash is one of the hairs that grow at the edge of the eyelid and protects the eye from dust.

Image processing techniques can be employed to extract the unique iris pattern from the acquired image of an eye, and generate biometric template, which can be stored in the database. This biometric template contains a mathematical represen-
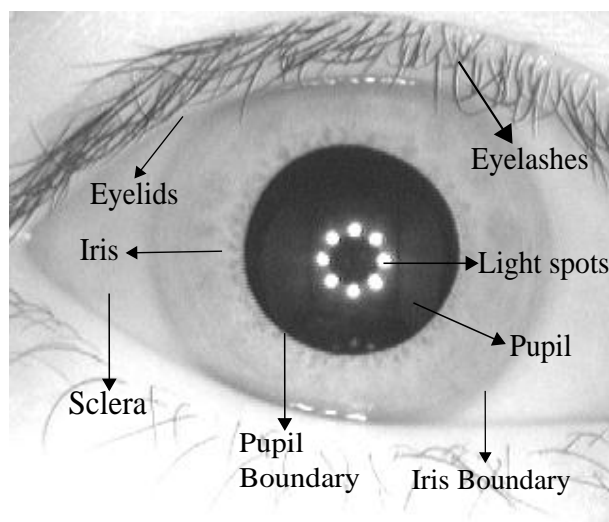
Figure 1.4: Image #: S1001R01 from CASIA database [1] that depicts the anatomy of human eye

tation of unique texture information stored in the iris, and allows comparisons to be made between individuals. When a subject wishes to be identified by an iris recognition system, their eye is first photographed, and then a template is created for their iris region. This template is then compared with the other templates stored in a database until either a matching template is found and the subject is identified, or no match is found and the subject remains unidentified.

1.2 Various Performance Measures

The correspondence between two passwords is obtained by finding a perfect match between two alphanumeric strings. However, biometrics very rarely compares exactly same templates. There is difference between two templates due to scanning conditions, change in characteristics with respect to aging, change in acquisition conditions etc. Thus, the feature sets originating from same individual does not look same. When two different biometric templates originating from same individual are different then it is known as **intra-class** variations. However, variations that occurs between templates originating from two different individuals are known as **inter-class** variations [14].

When the two biometric templates are compared to find intra-class variations then such scores are known as similarity scores/genuine scores. However, when two

biometric traits are compared to find inter-class similarity, then scores are known as imposter scores. The scores that exceed a predefined threshold value (τ), results in false acceptance. The genuine score that lies below τ results in false rejection. Figure 1.5 shows the representation of performance measures. The commonly used measures to evaluate the performance of biometrics system are:

1.2.1 False Acceptance Rate (FAR)

FAR is the frequency of fraudulent access to imposters claiming identity [15]. This statistic is used to measure biometric performance when operating in the verification mode. A false accept occurs when an individual is incorrectly matched to another individual's existing biometric template.

1.2.2 False Rejection Rate (FRR)

FRR is the frequency of rejections relative to people who should be correctly verified. This statistics is used to measure biometric performance when operating in the verification mode. A false reject occurs when an individual is not matched correctly to his/her own existing biometric template.

1.2.3 Equal Error Rate (EER)

ERR is the point where FAR is equal to FRR. In general, the lower the equal error rate value, the higher the accuracy of the biometric system. Note, however, that most operational systems are not set to operate at the equal error rate, so the measure's true usefulness is limited to comparing biometric system performance. EER is sometimes referred to as the *Crossover Error Rate.*

1.2.4 Genuine Acceptance Rate (GAR)

GAR is the fraction of genuine scores exceeding the threshold τ. It is defined as

$$GAR = 1 - FRR \tag{1.1}$$
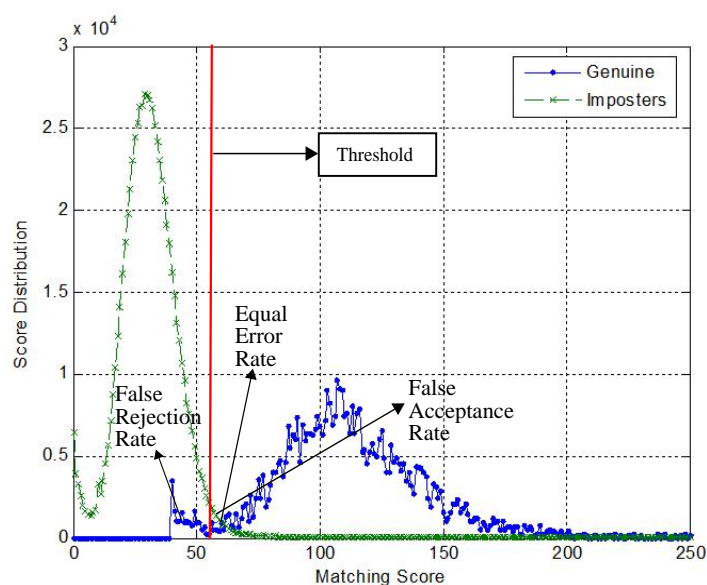
Figure 1.5: Genuine and imposter matching score distribution of biometric database showing various performance measures

1.2.5   Receiver Operating Characteristic (ROC) Curve

ROC curve is a comprehensive way to analyze the performance of a biometric system. It depicts the dependence of FAR with GAR for change in the value of threshold. The curve is plotted using linear, logarithmic or semi-logarithmic scale. In some cases, ROC can also be represented by plotting FAR against FRR at change in the threshold value.

1.2.6   Penetration Coefficient (PR)

In case of identification, the input feature set is compared to all the templates in the database. Search efficiency can be achieved by partitioning the database based on some criteria. Thus, during identification, the query template is compared to only selected templates in the appropriate partitions. The portion of total database to be scanned on an average for each search is called penetration coefficient PR, which can be defined by

$$PR = \frac{E}{N} \tag{1.2}$$

where E is the expected number of comparisons required for single input and N is

the total number of comparisons. On encountering the match, search does not stop but continues through the entire partition [14].

1.2.7   Bin Miss Rate (BM)

A bin error occurs when an attempt is placed in a bin which is not compared with the correct bin for the biometric entity used, and hence will fail to match. The error occurs due to misplacing of biometric template in the wrong bin during identification.

1.2.8   Cumulative Match Characteristic (CMC) Curve

The rank-k identification indicates the number of correct identities that occur in top k matches. Let R_k denote the number of elements of probe set in top k, then the probability of identification is given by $I = R_k/N$. CMC curve represents the probability of identification I at various ranks K [16].

1.3   Iris Databases used in the Research

To measure the performance of automated iris biometric system, extensive experiments have been carried out at various levels. This section discusses in detail about the databases used in experiments. Experimental results are obtained on various available datasets such as UBIRIS version 1 [17], BATH [18], CASIA version 3 [1] and Indian Institute of Technology Kanpur (IITK) [19] to take all possible factors into consideration like rotation, illumination, scaling and noise. These databases are classified into cooperative and non-cooperative categories based upon the restrictions imposed on the user while capturing images.

1.3.1   Cooperative Databases

These databases are acquired under ideal conditions with less imposition on the user. Such databases consider less noise factors during image acquisition. BATH and CASIA version 3 fall under this category.

BATH Database

Database available from BATH University [18] includes images from 50 subjects. For each subject, both left and right iris images are obtained, each containing 20 images of the respective eyes.

CASIA version 3

CASIA version 3 (CASIAV3) is acquired in an indoor environment. Most of the images have been captured in two sessions with an interval of atleast one month. The database comprises 249 subjects with total of 2655 images from left and right eyes. CASIAV3 is a superset of CASIAV1. The pupil regions of all iris images in CASIAV1 were automatically detected and replaced with a circular region of constant intensity to mask out the specular reflections [20].

1.3.2   Non-cooperative Databases

Non-cooperative databases are collected to bring noisy factors into consideration with less constrained image acquisition environment. UBIRIS version 1 and few images of IITK database are considered under this category.

UBIRIS version 1

UBIRIS version 1 (UBIRIS.v1) database is composed of 1877 images collected from 241 persons in two different sessions. The images for this database are acquired under noisy conditions with less restriction on the user.

Indian Institute of Technology Kanpur (IITK)

The database collected at IITK consists of over 1900 right iris images taken from 600 subjects ($\approx$ 3 images per person). The images are acquired using CCD based iris camera along with uniform light source. In addition to this, IITK database consists of few images taken in non-cooperative conditions as well. The images are acquired for change in gaze of an individual, difference in illumination, occlusion due to eyelids, etc.
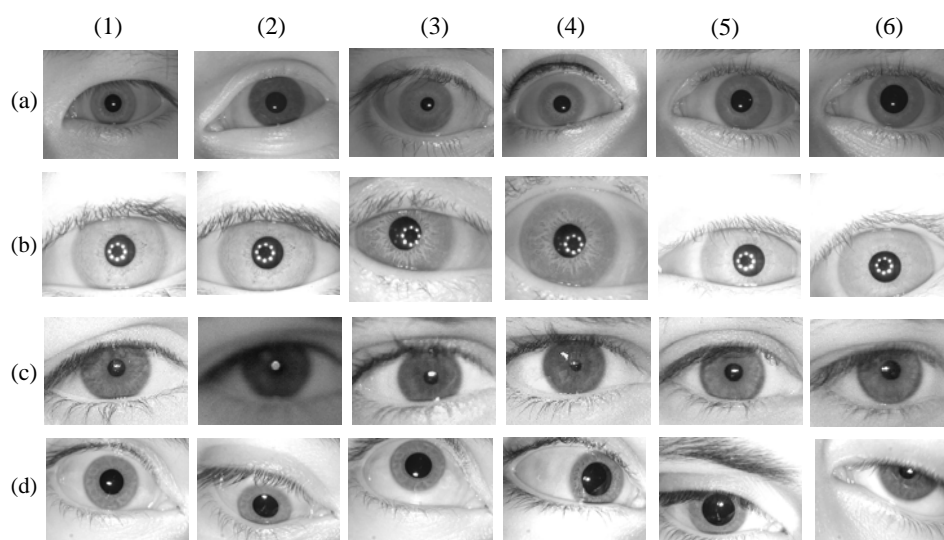
Figure 1.6: Sample iris images from various available databases: (a) BATH, (b) CASIA, (c) UBIRIS, (d) IITK.

Sample irises from various available databases are shown in Figure 1.6. BATH database is collected in controlled environmental conditions. Images a(5) and a(6) are from same subject that show the effect of illumination on iris. The size of pupil varies for both the images. Further, b(3) and b(4) depict the effect of occlusion due to eyelids. Change in orientation can be explained precisely with b(5) and b(6). The irises from UBIRIS database show the effect of blurring, noise and illumination. Images c(1) and c(2) are from same eye, collected at two different sessions with change in illumination. The iris images from IITK database are taken under controlled conditions with an exception to few samples. In order to test the robustness of proposed system, iris data for 20 subjects are collected with change in gaze and occlusion. Irises d(1), d(2) and d(3) are for same subject with less imposition on the user during image acquisition.

1.4   Problem Definition

The acquired iris image is used for detection of annular ring underlying inner pupil and outer iris boundary. This annular ring is transformed from Cartesian coordinates into doubly dimensionless polar coordinates [3]. The main objective is to achieve invariance to scale, position and orientation. Further, the images should maintain reference to same region of iris texture irrespective of camera to eye distance. Given

11

an input iris image I, the center of pupil (x_c, y_c), pupil radius r_p and iris radius r_i, normalisation is given by

$$
\begin{aligned}
N(\rho, \theta) &= I(x(\rho, \theta), y(\rho, \theta)) \\
&\text{where,} \\
x(\rho, \theta) &= (1 - \rho)x_p(\theta) + \rho x_i(\theta) \\
y(\rho, \theta) &= (1 - \rho)y_p(\theta) + \rho y_i(\theta)
\end{aligned} \tag{1.3}
$$

$x(\rho, \theta)$ and $y(\rho, \theta)$ are defined as linear combination of points lying on pupillary boundary $(x_p(\theta), y_p(\theta))$ and points lying on iris boundary $(x_i(\theta), y_i(\theta))$. The value of $\rho \in [0, 1]$ and $\theta \in [0°, 360°]$. However, traditional approaches do not take care of the problems that occurred due to polar transformation. As the size of pupil changes according to the amount of light entering the eye, variable size of pupil causes linear deformation of iris patterns and creates aliasing effect. Hugo et. al. [21] have raised the problem of aliasing that occurs during polar transformation. It has been observed that due to change in area, the recognition accuracy reduces considerably. After preprocessing, features are extracted using global transforms [22, 23, 24, 25, 26]. Global feature extraction techniques fail due to transformation of features between two image samples [7].

During identification, the number of false acceptance grows geometrically with increase in the size of the database. If FAR and FRR indicate the false accept and reject rates during verification, then rates of false accepts (FAR_N) and rejects (FRR_N) in the identification mode for database of size N are given by [27]

$$
\begin{aligned}
FAR_N &= 1 - (1 - FAR)^N \approx N \times FAR \\
FRR_N &= FRR \\
&\text{Then, total number of False Acceptance} = N \times (FAR_N) \\
&\approx N^2 \times FAR
\end{aligned} \tag{1.4}
$$

There are two approaches to reduce error rates during identification. First is by reducing FAR of matching algorithm and second is by reducing search space during identification. The FAR is limited by performance of an algorithm and cannot be reduced significantly. Thus, accuracy and speed of a biometric identification system

can be improved by reducing the number of templates against which the query has to be compared. The effect of reducing the search space during identification is given by mathematical formulation. Suppose the entire search space is reduced by a fraction L. Thus, the resultant FAR and FRR after search space reduction is given by

$$FAR_{N \times L} = 1 - (1 - FAR)^{N \times L} \approx N \times L \times FAR$$
$$FRR_{N \times L} = FRR$$

(1.5)

This minimises the number of records against which search has to be performed which in turn reduces FAR during identification. So more emphasis is required to develop an indexing scheme for retrieving the query image with less time [28].

1.5 Literature Review

The idea of automated biometrics system was proposed in 1987 by Flom and Safir [29]. The authors have suggested highly controlled conditions that includes headrest, an image to direct gaze and manual operator. To account for variation in size of iris due to expansion and contraction of pupil, the illumination has been changed to make pupil of predetermined size. In addition to this, the authors have suggested significant benchmarks that have regulated the research later. They have proposed pattern recognition tools to extract iris features and an initial method of detecting pupil using static threshold.

The first operational iris biometric system has been developed at University of Cambridge by Daugman [30]. The digital images of eye has been captured using near-infrared light source so that illumination could be controlled, that remains unaffected to users. The image acquisition system is highly robust where the algorithm maximises the spectral power by adjusting focus of the system. The next step is to find the iris in the image that uses deformable templates. A deformable template is trained with some parameters and shape of the eye to guide the detection process [31]. Daugman presumed iris and pupil boundaries to be circular thus the boundary of circle can be described with three parameters: radius r, center of the circle x_0, y_0 [22]. The operator is defined as

$$max(r, x_0, y_0)|G_\sigma(r) * \frac{\partial}{\partial r} \oint_{r,x_0,y_0} \frac{I(x,y)}{2\pi r} ds| \qquad (1.6)$$

where $G_\sigma(r)$ is a smoothing function and $I(x,y)$ is the image of the eye. The operator searches over the image domain (x,y) for the maximum in the blurred partial derivative with respect to increasing radius r of the normalised contour integral of $I(x,y)$ along a circular arc ds of radius r and centre coordinates (x_0, y_0). After iris segmentation, the next step is to describe features of iris for comparison. The first difficulty lies in iris comparison is that, all iris images are not of same size. The iris representation should be invariant to change in size, scale, orientation, etc. The distance between camera and eye affects the size of iris in an image. The iris pattern undergoes linear deformation due to change in illumination that causes pupil to dilate or contract and change in orientation of iris due to head tilt, camera position, movement of eyeball, etc. Daugman has addressed this problem by mapping iris into dimensionless polar coordinate system [22]. The normalised iris image is further used to extract phase information using 2D Gabor filters. The similarity between two iris representations generates the matching score.

An iris biometric system was developed at Sarnoff labs [23] that uses different approach compared to Daugman. For image acquisition, the authors have used diffused source of light with low level light camera. Hough transform is used for pupil and iris segmentation. For matching two iris images the system uses Laplacian of Gaussian filter at multiple scales to produce template and computes normalised correlation as a similarity measure [23]. These three models for iris recognition are taken as base and significant research is done based on the ideas laid by Flom and Safir, Daugman and Wildes. This section discusses in detail about work done in three most significant areas like preprocessing, feature extraction and identification as shown in Figure 1.2.

1.5.1 Preprocessing

Iris preprocessing involves finding the pupillary and iris boundaries that are presumed to be circular. However, few authors have also worked on detecting eyelids/eyelashes to further improve localisation performance [7]. As mentioned earlier, Daugman has

used integro-differential operator for iris localisation but the location of iris varies from image to image; so global search reduces speed. In order to improve localisation time, coarse to fine strategy is proposed by Huang et. al [32]. In the coarse stage, the technique finds outer iris boundary in the rescaled image, then using that information iris circles are found using intergro-differential operator. Further authors have proposed the method for detection of eyelids and eyelashes. Eyelids are detected by searching two curves that satisfies polynomial equation of the form $x(t) = at^2 + bt + c$, $t \in [0, 1]$. Eyelashes are also detected by checking variance for each block.

There are various approaches developed as an improvement over traditional Hough transform. In [33], the authors have used canny edge detector with Hough transform to improve localisation speed. By means of canny edges, normal line algorithm is created for finding center and inner edge. Homocentric circle algorithm is used to find outer edge. The authors in [34] have used bisection method to find inner boundary. It is quite difficult to locate the boundary between the iris and the sclera when the iris image is blurred. Hence, eyelid position is used to find the outer boundary. Further, histogram equalisation and statistical information is used to find correlate boundary. In addition to this, the authors in [35] provided an improvement over Hough transform for circle to restrict votes for center location based on direction of edges. For eyelid detection, the detected portion of iris is divided into four parts. There is an overlap of half of the pupil radius between each window. The eyelid in each of these four windows is detected and results are connected together. The algorithm proposed in [36] is used to overcome the drawback of traditional iris localisation approaches that are affected by eyelid occlusion and are time consuming. In the coarse localisation of inner boundary, the lower contour of pupil is used for estimation of parameters. In coarse localisation of outer boundary the average intensity signals on both sides of pupil are used to estimate the parameters. In fine stage, Hough transform is used to localise boundaries precisely.

Some authors have used thresholding based approaches to find coarse localisation of pupil. The authors in [37] search for pixels below a threshold as pupil and then use Hough transform and edge detection to find circles in the limited area. Further, an
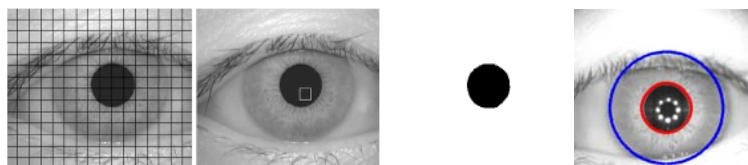
Figure 1.7: Binarizing the image using adaptive threshold (taken from [2])

automatic iris segmentation based on local areas is proposed in [2]. In this approach, iris image is divided into rectangular grid and mean is obtained for each block. The minimum value of mean is taken as threshold for binarizing the image as shown in Figure 1.7. Further, split and merge algorithm is used in [38] to detect connected regions in the image. Authors in [39] have used a concept similar to Daugman for iris segmentation. Firstly, the irregularities are removed using bilinear interpolation. Secondly, candidate locations are generated to provide initial conditions for pupil and iris boundary. Thirdly, for each seed (x, y) pupil and iris parameters are recovered. In [40], author finds the pupil using least significant bit planes.

Some work has been proposed in the direction of non-cooperative iris localisation. The authors in [41] have implemented the segmentation methodology proposed by Tuceryan [42] using the moments in small windows of the image as texture features and then applying a clustering algorithm to segment the image. Further a robust segmentation approach for non-ideal images has been developed using graph cuts [43]. Performance of some selected localisation approaches is given in Table 1.1.

1.5.2 Feature Representation

Several approaches have been developed for mathematical analysis of random texture patterns that are visible within the eye. Daugman has used Gabor filter to produce binary representation of iris [3] as shown in Figure 1.8. In [44] Gaussian filter is used for texture representation. The gradient vector field of an iris image is convolved with a Gaussian filter, yielding a local orientation at each pixel from normalised iris image. They quantize the angle into six bins. This method has been tested on CASIA database with 2255 images. Dyadic wavelet transform of a sequence of 1-D intensity signals around the inner part of the iris has been used in [24] to create a binary

16

Table 1.1: Performance of some selected localisation approaches (taken from [7])

First Author	Approach	Database	Results
Camus [39]	Multiresolution coarse to fine strategy	670 images without glasses and 30 with glasses	99.5% without glasses and 66.6% wearing glasses
Sung [34]	3176 images	Bisection method, canny edge detector and histogram equalisation	100% inner boundary and 94.5% for collarette boundary
Bonney [40]	108 CASIA v1 and 104 UNSA	Least significant bit planes	Pupil detection 99.1% and limbic detection 66.5%
Liu [35]	Modification to Hough transform	4249 images	97.08% Rank 1 recognition
Proenca [41]	Moments	1214 good quality images, 663 noisy images	98.02% good dataset and 97.88% noisy dataset
Pundlik [43]	Graph Cuts	WVU Non-ideal database	Pixel label error rate 5.9%

iris code. The system achieves 0.07% of EER. In [45] modified Log-Gabor filters are used because Log-Gabor filters are strictly bandpass filters but Gabor filters are not. Discrete Cosine Transform (DCT) is used for feature extraction in [26]. DCT is applied to rectangular patches rotated at 45 degrees from radial axis. The dimensionality of feature set is reduced by keeping three most discriminating binarized DCT coefficients. The authors in [46] have done texture analysis by computing the analytic image. The analytic image is the sum of the original image signal and Hilbert transform of the original signal. Table 1.2 shows the performance of some well known feature extraction approaches.

1.5.3 Identification

Iris based identification needs more attention because existing state-of-the-art shows that very few contributions have been made in this direction. There already exist few indexing schemes to partition the biometric database. Indexing hand geometry database using pyramid technique has been proposed in [27]. The authors have
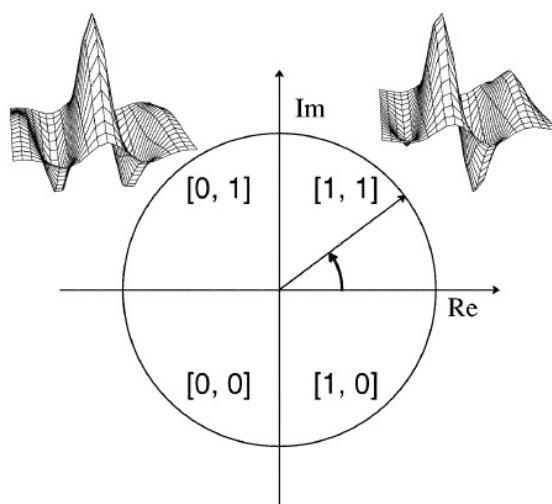
Figure 1.8: Phase demodulation process used for encoding normalised iris image (taken from [3])

Table 1.2: Performance of some well known feature representation approaches

First Author	Approach	Database	Results
Daugman [3]	2D Wavelet Demodulation	4258 different iris images	Correct Match Rate 100%
Sun [44]	Gaussian filter	CASIA	100% Correct Recognition Rate
Ma [24]	Dyadic wavelet transform	CASIA	100% Correct Recognition Rate with EER of 0.07%
Yao [45]	Log-Gabor filters		EER of 0.28%
Monro [26]	DCT	2156 CASIA images	100% Accuracy

claimed to prune the database to 8.86% of original size with 0% FRR. In [47], an efficient indexing scheme for binary feature template using B+ tree has been proposed. In [48], the authors have proposed the modified B+ tree for biometric database indexing. The higher dimensional feature vector is projected to lower dimensional feature. The reduced dimensional feature vector is used to index the database by forming B+ tree. Further, an efficient indexing technique that can be used in an identification system with large multimodal biometric database has been proposed in [49]. This technique is based on KD-tree with feature level fusion which uses the multi-dimensional feature vector. In [50], two different approaches of iris indexing have been analysed. First one

Table 1.3: Performance analysis of well known identification approaches

Author	Approach	Database	Results
Mhatre [27]	Pyramid Technique	1000 palmprint images	Penetration rate 8.86% Bin miss rate 0%
Gupta [47]	B+ Tree	360 ear images	95.8% Accuracy with penetration rate 34%
Jayaraman [48]	Modified B+ Tree	Iris database: BATH and IITK	BATH: 52.7% reduction with FRR 0% IITK: 45.6% reduction with 6.0% FRR
Jayaraman [49]	KD-Tree	5400 images of 150 subjects from IITK Multimodal database (ear, face, iris and signature)	97.4% Accuracy with penetration rate 23%
Mukherjee [50]	PCA and block based image statistics	CASIA v3.0	PCA-based: average penetration for a 80% hit rate is 17% and Block based: penetration for a 80% hit rate is only 8%

uses the iris code while second one is based on features extracted from iris texture. In [51], authors have proposed an iris indexing technique based on the iris color for noisy iris images. The performance measures shows the effectiveness of iris color for indexing very large database. The performance analysis of well known identification approaches is given in Table 1.3.

1.6 Motivation

Change in illumination causes non-affine pattern deformation due to pupillary dilation and contraction [22]. Further, transformation of iris from Cartesian to polar plane creates aliasing effect [21]. Thus, there is a stringent requirement to extract features devoid of aliasing.

Analyzing the texture of the iris has been the most popular area of research in iris biometrics [7]. The global feature extraction approaches fail to work under change in rotation, scaling, illumination and viewpoint of two iris images. The area underlying

annular iris image changes due to illumination hence global transforms are not suitable for matching two iris images of variable size. Thus, local feature descriptors are required that are invariant to change in scale, rotation, occlusion and viewpoint of two iris images.

In last few decades, good amount of work has been done for recognition but iris based identification is still in its infancy and needs careful attention. An efficient classification, clustering or indexing scheme is required to reduce the search space during identification [52, 53]. There already exist few indexing schemes to partition the biometric database. The existing indexing approaches perform well for cooperative iris databases but fail to achieve desired performance for non-cooperative images. Based on the current research directions from the literature, investigations have been made in this thesis to propose novel preprocessing, keypoint extraction and identification schemes for iris. Contributions made in the aforementioned areas are discussed below briefly in sequel.

1. During preprocessing, the problem of aliasing is removed by directly considering the annular region of iris without normalisation. Further, the annular region contains noise due to eyelids and eyelashes that should be detected and removed. In a normal gaze, the edge of the upper eyelid intersects the sclera and approximately half of the upper iris circle whereas, lower eyelid covers one-fourth of the lower iris circle. However, the left and the right regions are independent of such occlusions. Depending upon their degree of motion, upper eyelid adds more noise to the transformed strip as compared to lower eyelid. A novel sector based approach is proposed which considers these regions free from occlusions. It has been observed that, for the range of angular values θ, the regions that are not occluded due to eyelids are of range $[35°, 145°]$ and $[215°, 325°]$. For the upper and lower regions, only partial values of iris radius are taken from a sector. This generates a fixed size mask to remove eyelids from annular iris image.

2. To extract robust attributes, local features around special points known as *keypoints* are obtained and compared to find the similarity between the images. The

most valuable property of a keypoint detector is its repeatability, i.e., whether it reliably finds the same interest points under different viewing conditions [6]. To extract features around keypoints the neighbourhood of every detected point is represented by a feature vector (descriptor). In the proposed work, novel keypoint descriptors has been applied to iris to extract features robust to transformations, illumination and partial occlusions.

3. From the literature available, it can be inferred that an efficient indexing scheme is required that is invariant to possible transformations and occlusions. In this work, Geometric Hashing of keypoint descriptors is proposed for indexing large biometric database. The proposed approach uses local features and achieves invariance to various possible transformations and occlusions.

1.7 Thesis Organization

The rest of the thesis is organized as follows.

A novel preprocessing approach is given in **Chapter 2**. Many researchers have used variations of edge detection and Circular Hough Transform (CHT) for finding pupil and iris boundary [37]. But CHT requires range of radius as input and is computationally expensive. Thus, localisation approach is proposed that performs for change in rotation and viewpoint of two iris images. Further, to remove the effect of aliasing and noise due to eyelids, a novel sector based approach is proposed to form noise independent annular iris image. It has been observed that the proposed approach performs better in terms of accuracy compared to existing Masek's approaches.

Chapter 3 presents application of keypoint descriptors for iris. These descriptors have been used for object detection but their applicability to personal identification does not exist. Firstly, a Dual stage approach for keypoint detection using Harris corner detector [54] is proposed. To further improve accuracy, Scale Invariant Feature Transform (SIFT) [4] is used for extracting keypoint descriptors from annular iris. However, it has been observed that the proposed approaches are computationally expensive and hence needs more time. Thus, to further improve accuracy and reduce

computational cost an efficient keypoint descriptor called Speeded Up Robust Features (SURF)[5] has been applied to extract robust features from iris. The approaches proposed in this chapter are compared to existing global feature extraction techniques and performance analysis has been made.

The techniques presented in **Chapter 4** are used for indexing large biometric database. In this chapter two approaches are developed for search space reduction. In the first approach, energy features are extracted from the rectangular block using multiresolution subband coding of DCT coefficients. The energy histogram on extracted features are used to form keys. This key is used to traverse the B-Tree for searching the database. DCT is a global feature extraction approach and fails to work accurately for iris images taken under non-cooperative conditions. Thus, geometric hashing approach is used to index a large iris biometric database. The geometric hashing scheme allows for retrieval of model images that differ from query image by some kind of similarity transformation and occlusion.

Finally **Chapter 5** presents the concluding remarks, with scope for further research work.

Chapter 2

Noise Independent Annular Iris

The image acquisition system captures iris as a larger portion of image that also contains data from immediately surrounding eye region [23]. Thus, prior to performing feature extraction it is necessary to localise only that portion of the image that contains exclusively iris. Specifically it is important to localise the region between inner pupil and outer iris boundary. If iris is occluded by eyelids then portion below the upper eyelid and above the lower eyelid should be considered for feature extraction. Further, there exists some specular highlights on pupil region. Preprocessing is an important step that involves the process of converting the raw acquired input image into feature extraction form. The conventional steps involved in preprocessing are (i) to remove the effect of specularities lying on the pupillary area, (ii) to localise the inner and outer iris circles, (iii) to transform the iris into a rectangular block using Cartesian to polar conversion and (iv) to remove eyelids usually modelled as noise from the annular region. However, it has been observed in [21] that during polar transformation the texture features are lost due to aliasing. Hence, in the proposed research the annular region of iris is considered directly for feature extraction. Eyelids are removed from the annular ring using sector based approach to minimise occlusion. This noise independent annular iris is considered directly for feature extraction. The detailed description of steps involved in preprocessing are given as follows:
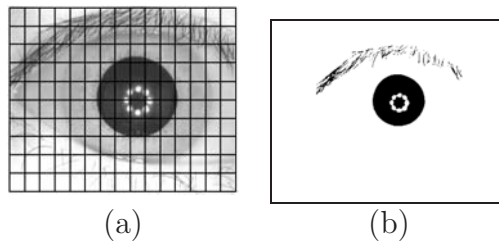
Figure 2.1: Adaptive image thresholding using grid based approach: (a) Iris image with blocks to compute threshold (b) Binary image obtained using adaptive threshold

2.1   Removal of Specular Highlights

Pupil is modelled as a dark circular disk in the eye with significantly low occlusion. However, it has been noticed that pupil contains non-singular features known as specular highlights with high gray levels. The position of specular reflection is determined by the position of light source. As pupil contains redundant information, thus the spot of light is made to fall on pupillary region. This light spot makes a hole that has to be detected and filled up to alleviate pupil segmentation process. To begin with hole filling, input iris image is binarized using adaptive threshold. The reason behind choosing an adaptive value of threshold is that static threshold cannot work for images taken under varying illumination conditions. To obtain suitable value of threshold, an input image is divided into blocks of size $w \times w$ (shown in Figure 2.1(a)). For each block, mean is obtained using the intensity values. The minimum value of mean is taken as value of threshold (T) [2]. As pupil is the darkest portion in an image, the block with minimum value of mean will lie on pupil area. The input image is compared against T to obtain the binary image as shown in Figure 2.1(b).

The image obtained in Figure 2.1(b) contains light spots known as specular highlights. These spots needs to be detected and filled because pupil localisation works more efficiently for completely filled circle. Morphological region filling approach is used to fill holes in the image [55]. To begin with hole filling operation the complement of the binary image is obtained. The convention adopted here is that the boundary pixels are labelled as 1. If non-boundary pixels are labelled as 0 then beginning with a point p inside the boundary a value of 1 is assigned. The following transformation

24

fills the region with ones

$$X_k = (X_{k-1} \oplus B) \cap A^c \tag{2.1}$$

where $X_0 = p$, $k = 1, 2, 3....$ $\oplus$ is used for dilation of X_{k-1} by B which is defined as

$$X_{k-1} \oplus B = \{z | (\hat{B})_z \cap X_{k-1} \neq \phi\} \tag{2.2}$$

B is the symmetric structuring element defined as

$$\begin{bmatrix} 0 & 1 & 0 \\ 1 & 1 & 1 \\ 0 & 1 & 0 \end{bmatrix}$$

This algorithm terminates at k^{th} iteration if $X_k = X_{k-1}$. The image generated from last iteration X_k is combined with A using bitwise OR that contains the boundary filled image. The diagrammatic representation of hole filling algorithm is given in Figure 2.2. Algorithm 1 describes the steps involved in hole filling.

2.2 Iris Localisation

Raw input image contains pupil the darkest circular region encircled by iris that consists of unique flowery pattern. The objective behind localisation is to detect the part of the image that contains iris. This is done by localising the pupil as well as iris boundary. The pupil and iris are most discriminating features of the eye with

---

Algorithm 1 Hole_Filling

Require: A: Binary Image, B: Structuring element, p: Point inside the boundary, r: Rows, c: Columns
Ensure: H: Hole filled Image
  $C \Leftarrow A^c$ {Complement of an image}
  $X_0 = zeros(r, c)$
  $X_0(p) = 1$
  $k \Leftarrow 0$
  repeat
    $k \Leftarrow k + 1$
    $X_k = (X_{k-1} \oplus B) \cap C$
  until $X_k \neq X_{k-1}$
  $H = X_k \cup A$

---

sharp variations at boundaries. The shape of iris is far more predictable compared to other biometric traits. However, iris is obscured by undesirable features like eyelids, eyelashes, eyewears etc. Thus, a robust detection approach is required that performs well under such occlusions. The important steps involved in iris localisation are —

2.2.1 Pupil Detection

Many researchers have used variations of edge detection and Circular Hough Transformation (CHT) for finding pupil and iris boundary [37]. The major drawback of Hough transform is that it requires range of radius as input from the user. Further, the transformation works in R^3 domain thus it is computationally expensive. In this work an efficient pupil detection approach is proposed that performs faster compared to Hough transformation without any estimation for radius.

In this approach, the hole filled image is re-complemented to detect center of pupil. The distance of every pixel in the binary image is obtained with nearest non-zero pixel [56]. By computing the distance between non-zero pixels, the spectrum showing the largest filled circle can be formed within the set of foreground pixels. Since the pupil is the largest filled circle in the image the overall intensity of this spectrum is maximum
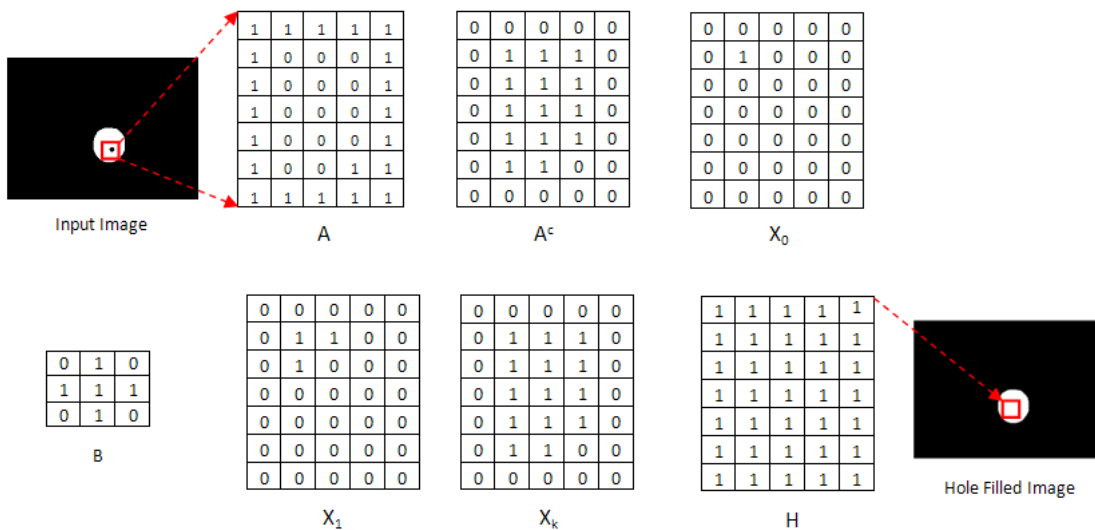
Figure 2.2: A: Block of binary image with holes, A^c: Complement of A, X_0: Image with first pixel in the boundary, X_1: Image after first iteration, X_k: Image after k^{th} iteration, H: Hole filled image, B: Structuring element
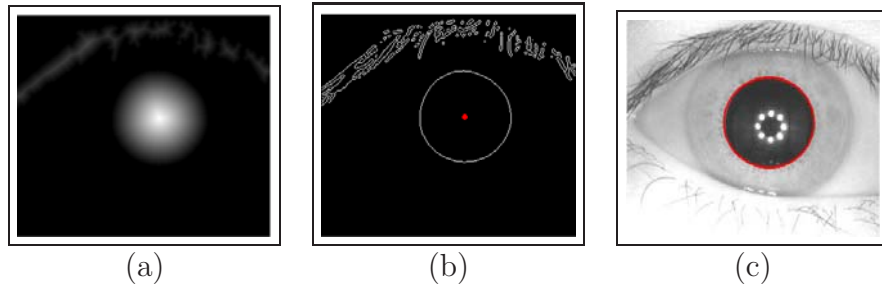
Figure 2.3: Pupil Detection: (a) Spectrum image (b) Edge detected image with pupil center (c) Pupil localised image

at the center. The spectrum image is shown in Figure 2.3 (a). Thus, the position of maximum value in the spectrum image is pupil center. To compute the pupil radius, an edge map of the hole filled binary image is obtained as shown in Figure 2.3 (b). In the edge map, the distance from the detected pupil center to the nearest non-zero pixel is the pupil radius (r_p). The pupil detected image is shown in Figure 2.3 (c). The algorithm for detecting pupil center and radius is given in Algorithm 2.

2.2.2 Iris Detection

For iris detection, the intensity image is blurred to remove external noise. But too much blurring may make it difficult to detect the outer iris boundary, separating the eyeball and sclera. Thus, a special smoothing filter such as the median filter is used on the original intensity image. This type of filtering eliminates sparse noise while preserving image boundaries [55]. After filtering, the contrast of image is enhanced to have sharp variation at image boundaries using histogram equalisation as shown in Figure 2.4 (a). This contrast enhanced image is used for finding the outer iris boundary by drawing concentric circles (Figure 2.4 (b) shows an example) of different radii from the pupil center and the intensities lying over the perimeter of the circle are summed up [24]. Among the candidate iris circles, the circle having maximum change in intensity with respect to the previous drawn circle is the iris outer boundary as shown in Figure 2.4 (c). The algorithm for detection of iris radius (r_i) is given in Algorithm 3.

27

Algorithm 2 Pupil_Detect

Require: H: Hole Filled Image

Ensure: x_c: xcenter of pupil, y_c: ycenter of pupil, r_p: Radius of pupil {Estimation of pupil center}

    $C \Leftarrow H^c$ {Complement of hole filled image}

    $[x\ y]\ =\ find(C == 1)$ {Find location of ones in an image}

    $l \Leftarrow length(x)$ {To find the number of elements in an array}

    for $i = 1$ to r **do**

      for $j = 1$ to c **do**

        for $k = 1$ to l **do**

          $D_k \Leftarrow \sqrt{(x_k - i)^2 + (y_k - j)^2}$

        end for

        $DN\ =\ sort(D)$ {Sort the values in D in increasing order}

        $S_{i,j} = DN_1$ {Take the smallest value of DN}

      end for

    end for

    $[x_c\ y_c] \Leftarrow max(S)$

    $E\ =\ edge(C)$ {Edge detection using Canny}

    $j \Leftarrow y_c$ {Estimation of pupil radius}

    $r_p \Leftarrow 0$

    while $E_{x_c,j} \neq 1$ **do**

      $r_p = r_p + 1$

      $j = j + 1$

    end while

2.3 Annular Iris

The iris patterns should be represented in the form which must achieve invariance to transformations in size, position and orientation. The size of iris depends upon the camera optical magnification factor and distance between camera and eye. The scale of iris changes due to expansion and contraction of pupil that introduces non-affine deformation of texture patterns. Further, the patterns undergo transformation due to location of iris in an image and orientation of eye. Such transformations are dependent upon head tilt and change in gaze of eye with respect to camera.

Daugman has introduced a doubly dimensionless polar coordinate system for representation of iris patterns. The coordinate system is doubly dimensionless with respect to angular variable (θ) and radial variable (ρ). The value of $\theta \in [0, 2\pi]$ whereas $\rho \in [0, 1]$. The coordinate system assigns to each point on iris a location in polar coordinate regardless of its size and pupillary dilation. The mapping of image points
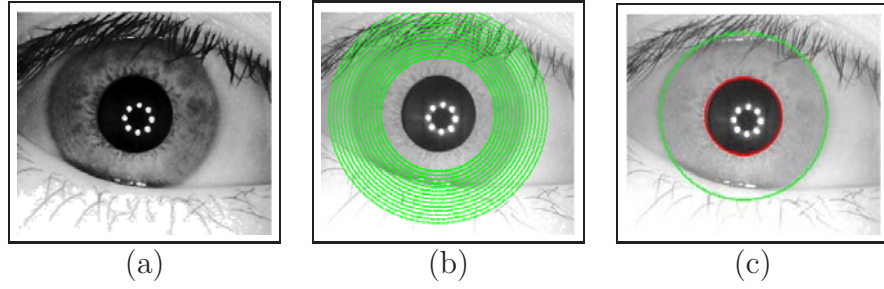
Figure 2.4: Iris Detection: (a) Contrast enhanced image (b) Concentric circles of different radii (c) Iris localised image

from Cartesian coordinate (x, y) to polar coordinate system (ρ, θ) is given by

$$I(\rho, \theta) = I(x(\rho, \theta), y(\rho, \theta)) \tag{2.3}$$

where $x(\rho, \theta)$ and $y(\rho, \theta)$ are defined as linear combination of points lying on pupillary boundary $(x_p(\theta), y_p(\theta))$ and points lying on iris boundary $(x_i(\theta), y_i(\theta))$. The linear combination is modelled as

$$
\begin{aligned}
x(\rho, \theta) &= (1 - \rho)x_p(\theta) + \rho x_i(\theta) \\
y(\rho, \theta) &= (1 - \rho)y_p(\theta) + \rho y_i(\theta)
\end{aligned}
\tag{2.4}
$$

During normalisation the segmented iris image is transformed into polar coordinate which can be regarded as sampling of original data with inherent possibility of aliasing [21]. As pupil dilates and contracts due to illumination, variable size of pupil causes linear deformation of texture features and creates aliasing effect. Figure 2.5 shows samples of same eye from CASIA database taken under varying illumination conditions. The normalized images generated using Daugman's approach are of fixed size (80×360 pixels) as given in Figure 2.5 (a.1) and (b.1) respectively.

From the images it is visually evident that though the region lying between pupil and iris boundary is not uniform in both the images, the texture features are scaled to constant size to render scale invariant image. To overcome sampling artifact, the proposed scale based approach normalises the iris image by transforming from Cartesian space to singly dimensionless polar space. Here the angular values are kept constant between $[0, 2\pi]$ whereas ρ ranges between $[0 : \rho_{inc} : 1]$ where ρ_{inc} is defined

---

Algorithm 3 Iris_Detect

Require: I: Input image, r_p: Radius of pupil, x_c: xcenter of pupil, y_c: ycenter of pupil

Ensure: r_i: Radius of iris

  $F \Leftarrow$ medianFilt(I){Median Filtering on input image}

  $H \Leftarrow$ Histeq(F) {Histogram equalisation}

  $[r\ c] \Leftarrow$ size(I) {Finding image dimensions}

  {Finding the intensity over circumference}

  for $r_i = r_p \times 1.5$ to $\frac{r}{2}$ **do**

    $sum_{r_i} \Leftarrow 0$

    for $\theta = 0$ to 360 **do**

      $x = x_c + r_i \times \cos(\theta)$

      $y = y_c + r_i \times \sin(\theta)$

      $sum_{r_i} = sum_{r_i} + H_{x,y}$

    end for

    $r_i = r_i + 2$

  end for

  {Change in intensity over circumference}

  for $i = 1$ to r_i **do**

    $D_i = |sum_i - sum_{i+1}|$

  end for

  $[d\ r_i] = \max(D)$ {Maximum change in intensity}

---

by

$$\rho_{inc} = \frac{1}{r_i - r_p} \tag{2.5}$$

Thus, the radial variable is made to vary depending upon actual distance between pupil and iris boundary as shown in Figure 2.5 (a.2) and (b.2). Hugo et. al. [21] have raised the problem of aliasing that occurs during polar transformation. The relationship between size of captured iris image and its recognition accuracy has been studied. It has been observed that due to change in area, the recognition accuracy reduces considerably. In the proposed method the problem of aliasing is removed by directly considering the annular region of iris without normalisation.

Further, the annular region contains noise due to eyelids and eyelashes that should be detected and removed. In a normal gaze, the edge of the upper eyelid intersects the sclera and approximately half of the upper iris circle whereas lower eyelid covers one-fourth of the lower iris circle. However, the left and the right regions are independent of such occlusions. Depending upon their degree of motion, upper eyelid adds more

(a) CASIA/115/L/S1115L05   (a.1)   (a.2)

(b) CASIA/115/L/S1115L10   (b.1)   (b.2)
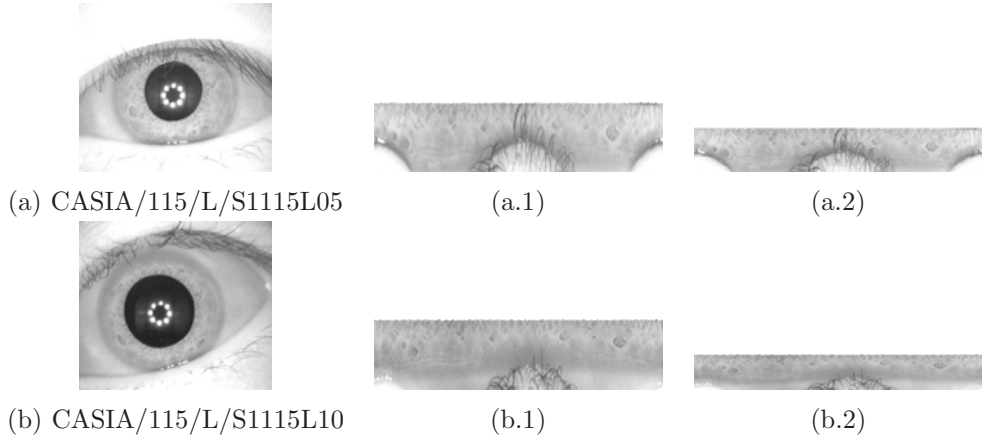
Figure 2.5: Effect of aliasing on iris normalisation using doubly dimensionless polar coordinate and singly dimensionless polar coordinate

noise to the transformed strip as compared to lower eyelid. The proposed method considers sector based approach which considers these regions free from occlusions. It has been observed that the ranges of angular values (θ) for the regions that are not occluded due to eyelids are given by $[35°, 145°]$ and $[215°, 325°]$ and for the upper and lower region, only partial values are taken from a sector. Given the center (x_c, y_c), pupil radius (r_p) and iris radius (r_i) the value of r_i changes depending upon the range of θ as defined by

$$r_i = \begin{cases} \frac{3}{4}r_i & \text{if } 0° < \theta < 35° \\ r_i & \text{if } 35° \leq \theta \leq 145° \\ \frac{1}{2}r_i & \text{if } 145° < \theta \leq 215° \\ r_i & \text{if } 215° < \theta \leq 325° \\ \frac{3}{4}r_i & \text{otherwise} \end{cases} \tag{2.6}$$

The quantisation scheme given in (2.6) is used to obtain sector based annular iris image. Figure 2.6 (b) shows the geometrical representation of sectors on annular iris circle where region underlying solid arcs are taken into consideration. The ratios $r_i/2$ and $3r_i/4$ are chosen depending upon the degree of movement and occlusion of two eyelids. The noise independent annular iris image is complimentary to aliasing that occurs due to dimensionless polar coordinate conversion. The resultant preprocessed image is shown in Figure 2.6 (c).

31
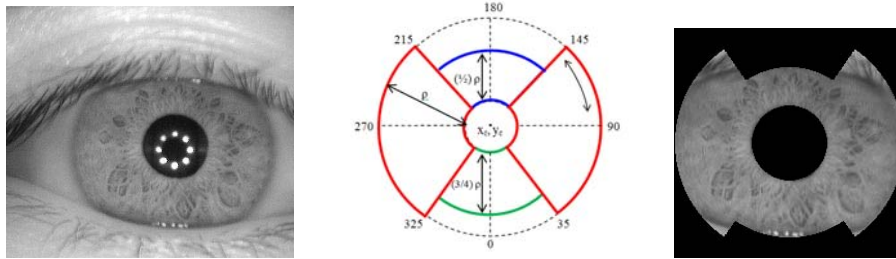
Figure 2.6: Preprocessing of iris image: (a) Input iris image, (b) Geometrical representation of sectors on iris circles, (c) Noise independent annular iris image after preprocessing

2.4   Experimental Evaluation

In this section, the localisation performance of proposed approach is compared with well known Masek's [57] approach. Masek uses circular Hough transform for detection of boundaries and linear Hough transform for masking eyelids. The proposed approach performs well compared to approaches that use adaptive mask. Masek's approach performs better for CASIA database but fails to achieve desired segmentation accuracy for non-cooperative images.

As localisation is the fundamental and significant step in iris identification, masking approach should not be erroneous as far as possible. For this purpose, eyelids are removed using predefined mask. The system has been tested on cooperative [18, 1] as well as non-cooperative [17, 19] iris databases. Table 2.1 shows the percentage of mis-localisation occurred by the proposed approach and Masek's approach [57]. It can be inferred from the table that the proposed approach performs better than the automatic eyelid detection approach proposed by Masek [57]. Figure 2.7 shows the localisation performance of Masek's approach and the proposed approach on few samples from IITK and UBIRIS database. The subject id along with image instance number is given under each displayed result. For UBIRIS database, the nomenclature is defined as ID_session_instance. The last result obtained on UBIRIS database shows that the proposed system can even localise iris for images collected at some distance from the camera. Though the outer iris circle is not localised correctly but annular region contains sufficient information to extract features.

The proposed masking approach is not unique to each image and fails to extract

Table 2.1: Mis-localisation percentage of Masek's approach and proposed approach

Database	Masek	Proposed
BATH	37.62	0.98
CASIA	05.23	0.45
UBIRIS	10.53	3.41
IITK	31.30	1.36

noise independent annular iris if degree of occlusion by upper and lower eyelids is more
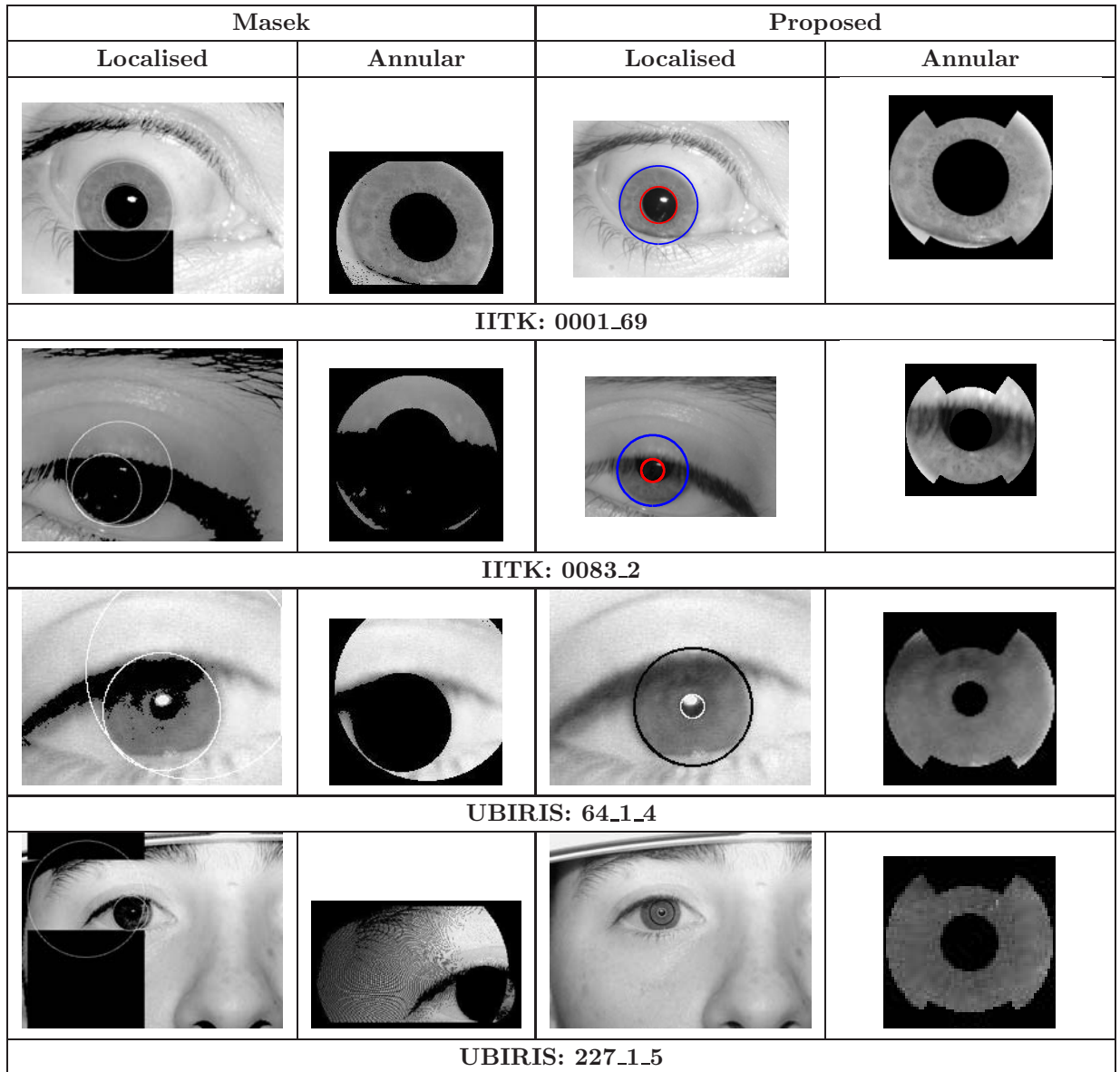
Figure 2.7: Localisation performance using Masek's approach and proposed approach on IITK and UBIRIS databases
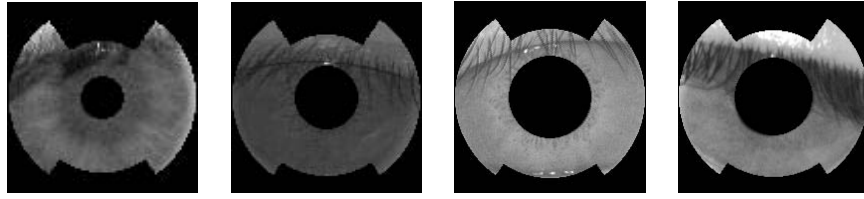
Figure 2.8: Failure to generate noise independent annular iris due to greater degree of occlusion by upper eyelid

030_S1030R07   092_S1092R08   157_S1157R09   188_S1188R09
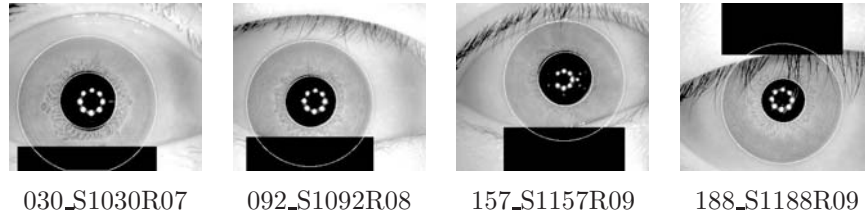
Figure 2.9: Results generated using Masek's approach on CASIA database that adaptively masks eyelids

than $\frac{1}{2}$ and $\frac{1}{4}$. Few such failure cases are shown in Figure 2.8. In such cases texture features are completely hidden due to eyelids so even the adaptive eyelid detection approaches could not help to recover hidden features. However, there still exists a need to develop an adaptive eyelid masking approach because the proposed approach masks the iris even if no occlusion occurs by upper and lower eyelids. Few such sample cases from CASIA database is shown in Figure 2.9 where an adaptive eyelid detection approach performs better compared to proposed approach.

2.5 Summary

In this chapter an endeavour has been made to develop an efficient preprocessing approach that generates Noise Independent Annular Iris. The proposed approach performs significantly better compared to conventional normalisation approach of transforming iris into doubly dimensionless polar coordinate [3]. In order to overcome noise due to eyelids, sector based approach is used. The masked annular image is directly used for feature extraction. From the experimental results it has been found that the average mis-localisation percentage of proposed approach is 1.55% which is significantly low compared to Masek's with mis-localisation of 21.17%. The proposed approach has capability to localise non-ideal iris images with severe transformations.

Chapter 3

Keypoint Descriptors for Iris

Feature extraction involves simplifying the amount of information required to describe an input image. The purpose is real time, high confidence recognition of a individual's identity by mathematical analysis of the random patterns that are visible within the iris of an eye from some distance. There already exists several global feature extraction techniques for iris [58, 57]. The main drawback of global techniques is that they fail to extract relevant features if there exists significant variations in pose, illumination and viewpoint of an individual. Local features are invariant to image scaling and rotation, and partially invariant to change in illumination and viewpoint. These local features have the capability to perform well under partial occlusions as well. In order to extract local features from iris, special points known as *keypoints* are detected where there can be a corner, an isolated point of local intensity maximum or minimum, line endings, or a point on a curve where the curvature is locally maximal. Around the neighborhood of every detected keypoint a descriptor is taken that represents the feature vector. This descriptor has to be robust to noise, detection displacements and geometric and photometric deformations [5].

In the proposed work an endeavour has been made to extract local features directly from annular iris image. As discussed earlier the reason for taking annular iris into consideration is to overcome aliasing errors due to polar transformation. To mark an improvement in terms of time and accuracy well known keypoint descriptors have been applied to iris. To begin with Harris corner points [54] were detected from the normalised iris image. Further to extract keypoint descriptor, entropy information of window around corner has been considered. But main drawback with Harris corner

35

approach is that they are very much sensitive to scale changes. Iris features are likely to undergo scale changes due to pupil expansion and contraction. Further a novel keypoint descriptor called Scale Invariant Feature Transform (SIFT) has been applied to iris [4]. SIFT has the capability to perform well for various transformations as well as occlusions due to higher dimensional descriptor. The dimension of the descriptor has a direct impact on the time it takes for recognition. Therefore less dimensions are desirable for fast interest point matching. However, lower dimensional feature vectors are in general less distinctive than their high-dimensional counterparts. Speeded Up Robust Features (SURF) [6] uses faster keypoint detection scheme with reduced dimensional descriptor. SURF has been used for machine vision applications like camera calibration and object tracking [6]. Due to inherent advantages of SURF it has been applied to iris biometrics for efficient recognition. This chapter discusses in detail about various keypoint descriptors and its applicability to iris.

3.1 Harris Corner Detector

Corner detection could find its applicability to many machine vision tasks such as tracking, localisation, matching and recognition. Such points often arise as the result of geometric discontinuities, such as the corners of real world objects, but they may also arise from small patches of texture. Three cases need to be considered for detecting corners:

1. if window is a patch (approximately constant in intensity) then all shifts results in only small change

2. if window is an edge then shift along edge results in small change but shift perpendicular to edge results in large change

3. if window is a corner point or isolated point then all shifts results in large change.

Harris corner detector provides an improvement over conventional approaches of corner detection that takes shifted patches. This approach uses determinant and trace of autocorrelation matrix for detecting corner points. The steps for finding the corner points are explained as follows:

3.1.1   Measure of Cornerness

The mathematical foundation of this can be explained as— given an intensity image I, the change E produced by shift of (x, y)

$$E(x, y) = \sum_{u,v} w(u, v)|I(x + u, y + v) - I(u, v)|^2 \qquad (3.1)$$

where w specifies the window taken into consideration. The Moravec's corner detector looks for local maxima in the minimum of the shifted image (E) above some threshold value. However, this approach suffers from various problems. The response is anisotropic because only a discrete set of shifts at every 45 degrees is considered. Further the response is noisy because the window is binary and rectangular. The operator responds too readily to edges because only the minimum of E is taken into account [54]. Harris corner detector is an improvement upon Moravec's corner detector by considering the differential of the corner score with respect to direction directly, instead of using shifted patches. This detector possess invariance to rotation, scale, illumination variation and image noise [59]. The Harris corner detector is based on the local auto-correlation function of an image which measures the local changes of the image with patches shifted by a small amount in various directions. The main objective is to find how similar the image function $I(x, y)$ at point (x, y) similar to itself when shifted by $(\Delta x, \Delta y)$. This is given by autocorrelation matrix

$$c(x, y) = \sum_{W}[I(x_i, y_i) - I(x_i + \Delta x, y_i + \Delta y)]^2 \qquad (3.2)$$

where I denotes the image and (x_i, y_i) are the points in the window W. Here W is the Gaussian window defined as $e^{\frac{-(x+y)^2}{2\sigma^2}}$ where σ defines the width of the window. Instead of using a Gaussian window a square window can also be used. But a square window results in variable distance for different directions from the center pixel of the window to the edge of the window. A square window also puts equal emphasis on all intensity variation measures regardless of their distance from the center of the window. Instead more weight should be put on values made closer to the center of the window. So, it is suggested in [54] to use circular window like Gaussian. The shifted

image is approximated by Taylor expansion truncated on the first order terms

$$I(x_i + \Delta x, y_i + \Delta y) \approx I(x_i, y_i) + [I_x(x_i, y_i) I_y(x_i, y_i)] \begin{bmatrix} \Delta x \\ \Delta y \end{bmatrix} \qquad (3.3)$$

where I_x and I_y denote partial derivatives in x and y respectively. Substituting equation (3.3) in equation (3.2) we get

$$
\begin{aligned}
c(x, y) &= [\Delta x\ \Delta y] \begin{bmatrix} \sum_W (I_x(x_i, y_i))^2 & \sum_W I_x(x_i, y_i) I_y(x_i, y_i) \\ \sum_W I_x(x_i, y_i) I_y(x_i, y_i) & \sum_W (I_y(x_i, y_i))^2 \end{bmatrix} \begin{bmatrix} \Delta x \\ \Delta y \end{bmatrix} \\
&= [\Delta x\ \Delta y] M(x, y) \begin{bmatrix} \Delta x \\ \Delta y \end{bmatrix} \qquad (3.4)
\end{aligned}
$$

where M captures the intensity structure of the local neighborhood which can be further defined as

$$M(x, y) = \begin{bmatrix} A & C \\ C & B \end{bmatrix} \qquad (3.5)$$

Thus, the autocorrelation function is approximated by

$$c(x, y) \approx [\Delta x\ \Delta y] M(x, y) \begin{bmatrix} \Delta x \\ \Delta y \end{bmatrix} = [\Delta x\ \Delta y] \begin{bmatrix} A & C \\ C & B \end{bmatrix} \begin{bmatrix} \Delta x \\ \Delta y \end{bmatrix} \qquad (3.6)$$

From autocorrelation matrix, first the measure of corner is obtained by finding the Determinant (Det) and Trace (Tr) of M as given by

$$Tr(M) = A + B \qquad (3.7)$$

$$Det(M) = AB - C^2 \qquad (3.8)$$

The formulation of corner response is given by

$$R(x, y) = Det - kTr^2 \qquad (3.9)$$

Here k is lying between 0.04 and 0.06. The intensity map, R, is compared against a threshold λ and intensity values below λ are set to zero. Positive values of R occur in corner regions, negative values in edge regions, and small values in flat regions. From the thresholded image a pixel is selected as an interest/corner point if it is local

maxima in the block. Order statistic filter is used for finding the local maxima.

3.1.2   Corner Points from Iris

Doubly dimensionless normalised iris image is used for extraction of corner points. The input image contains low contrast and non-uniform illumination. In order to highlight rich texture details, the normalised image is enhanced using block based approach as given in [24]. The normalised iris image is divided into 16×16 blocks and mean of each block is obtained. This gives the coarse estimate of background illumination. The mean image is further rescaled to the size of original image using bicubic interpolation. The background illumination image is subtracted from original image to remove illumination effect. Further the contrast of this image is enhanced using histogram equalisation. The lightening corrected image is shown in Figure 3.1(a).

The feature descriptor is formed using every detected corner points (x, y) in an image. At each detected corner point i centered at location (x_i, y_i) a window (w_i) of size $(k \times k)$ is formed. Using w_i the entropy information is obtained. Entropy is defined in terms of its probability distribution and is a good measure of randomness or uncertainty for evaluating structures and patterns. An important characteristic is to find the minimum amount of data that is sufficient to describe completely an input pattern without any loss of information. In accordance with this proposition entropy can be defined as

$$H_i = -\left(\sum_{j=0}^{N-1} p_j \log p_j \right) \tag{3.10}$$

For each detected corner point i the following information is recorded to form feature vector

1. (x, y) are the coordinates of ith corner point

2. H_i is the entropy information of window w_i

The value of i ranges from 1 to m, where m is the total number of corner points detected in an image. Steps involved Harris corner detection is shown in Figure 3.1.

(a) Strip after enhancement

(b) First derivative of image along x

(c) First derivative of image along y

(d) First derivative of image along xy
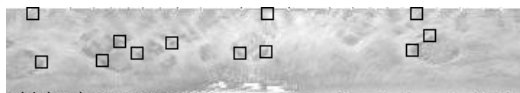
(e) Input image with detetced corner points marked by rectangles

Figure 3.1: Steps involved in Harris corner detection

3.1.3   Dual Stage Approach

For matching the corner points a traditional Euclidean distance approach has been used. The coordinates centered on corresponding corners are paired using 2D translation. But the approach fails due to lack of image statistics for finding similarity. In this thesis a novel method for matching is proposed that combines distance based approach with information theoretic local similarity measure. Here matching is done serially using dual stage approach. At first stage the matching between the two iris images is done using Euclidean distance. To compute distance for each corner from the first image, all second image corners are used. These distance values are compared against a threshold and the points satisfying the criteria are taken into consideration as candidate points for the second stage. In the next stage, the actual corner mate is found by estimating Mutual Information (MI) [60].

Let $A = \{m_1, m_2, ...m_m\}$ and $B = \{m_1, m_2...m_n\}$ be the set of interest points extracted from database and live query image respectively where each m_i is a 3-tuple comprising of $\{x_i, y_i, H_i\}$, x_i and y_i are the coordinates at particular interest point and H_i is the entropy obtained as given in (3.10). At the first level of matching the Euclidean distance between coordinates of one 3-tuple in A is obtained for all 3-tuples in B using

$$sd_l = \sqrt{(x_d - x_q)^2 + (y_d - y_q)^2} \tag{3.11}$$

where sd_l refers to the spatial distance for two points and (x_d, y_d) are the coordinates of the database tuple while (x_q, y_q) are the coordinates of the query tuple. The corner points with distances below a specified threshold τ are taken as potential corners. To find an optimal pair, Mutual Information (MI) between the entropies around potential corners is computed. MI(J) corresponding to the two entropy values H_d and H_q is defined as

$$J(d, q) = H_d + H_q - H(d, q) \tag{3.12}$$

where H_d and H_q are the entropies derived from window at one corner point in database image and another corner point in query image respectively. Moreover,
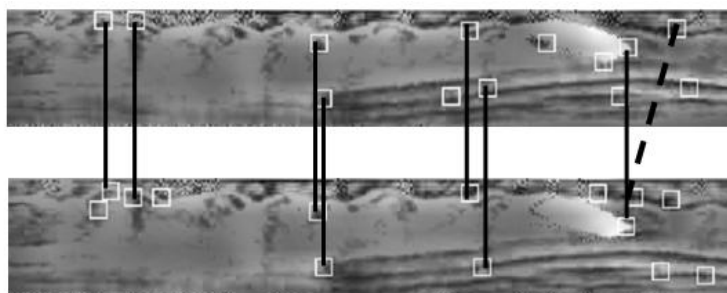
Figure 3.2: Interest point pairing. Solid lines indicate true pairs whereas dotted line indicates wrong pairing of points

$H(d, q)$ is the joint entropy defined by

$$H(d, q) = -\sum_d \sum_q p(d, q) \log p(d, q) \tag{3.13}$$

where $p(d, q)$ is joint probability distribution of values around d and q. The value of J is maximized to find an optimal pair between database and query image. A true pair/mate contains the maximal amount of information about each other. The maximum value of MI is compared against another threshold and if it passes the criteria, the two interest points are paired and removed from the list. Similarly, the steps are repeated for the remaining corner points to find an appropriate mate. Finally the total number of mates are counted and compared against threshold. Paired corner points between a gallery and probe iris image is shown in Figure 3.2. Solid lines indicate the correct pairing of corners points. Dotted line indicates that the corner points are wrongly paired.

3.1.4 Experimental Evaluation

The results are obtained on UBIRIS, BATH, CASIA and IITK iris databases. In order to study the performance of global feature extractors results were obtained using Haar wavelet [58] and Log-Gabor wavelets [57]. The accuracy of global feature extraction approaches is 79.86% and 78.50% for Haar wavelet and Log-Gabor wavelet on CASIA database. Similar results are obtained for other available databases. ROC curves for Haar wavelet and Log-Gabor wavelet on all the available databases is given in Figure 3.3. The system performs poorly using global feature extraction techniques because

the images are taken under non-ideal conditions. The features undergo transformation which in turn degrades accuracy.

The system with achieved accuracy cannot be used for high security applications. Thus, local features are detected using Harris Corner approach. For pairing these corner points three different measures have been implemented. In first session, results were obtained using Euclidean distance approach. But location of points does not represent stable features that may undergo translation. In the second session, MI based approach has been used independently to pair corner points. MI based approach alone could not produce satisfactory performance. From the results given in Table 3.1 it has been observed that these individual classifiers results in higher FAR and FRR. Subsequently, an attempt has been made to reduce the error rates using Dual stage matching approach by combining Euclidean distance and MI based approach in a hierarchical fashion. ROC curves for Euclidean distance, MI and proposed Dual stage approach is given in Figure 3.4.

Table 3.1 presents the comparative analysis of results using global and local features. For Harris corners, three approaches are used for matching corner points. From the experiments it is evident that the Euclidean distance between the points in the scale space does not promise satisfactory results. The system performs poorly for UBIRIS database and gives an accuracy of approximately 75% for BATH, CASIA and IITK database. A small change in viewpoint or orientation of individual's head may spatially translate the corner points. To overcome limitations of location based approaches, texture information around the corner point is obtained using Mutual Information. However, MI independently gives an accuracy of 78%, 73%, 87% and 90% (approx) for UBIRIS, BATH, CASIA and IITK databases respectively. These values were still not satisfactory and hence a combined approach using spatial as well texture details has been proposed.

The Dual stage system gives an accuracy of 85%, 94%, 97% and 94% for available datasets which signifies an improvement over the other two approaches. The system outperforms with an accuracy of 97% with significantly reduced FAR of 0.24% on CASIA database. From the results it can be inferred that dual stage approach

(a) UBIRIS

(b) BATH

(a) CASIA

(b) IITK
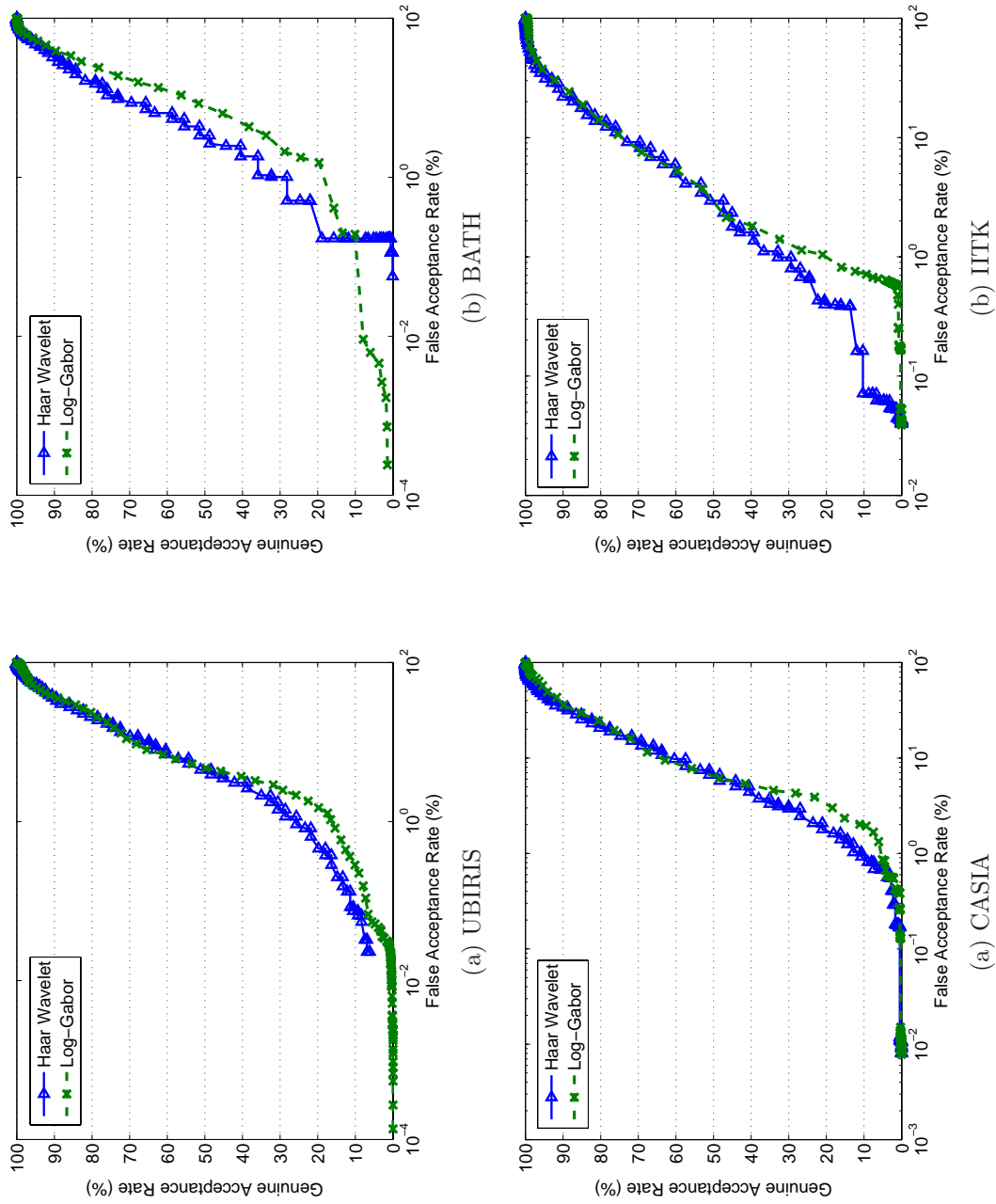
Figure 3.3: ROC curves for Haar wavelet and Log-Gabor wavelet on various available databases
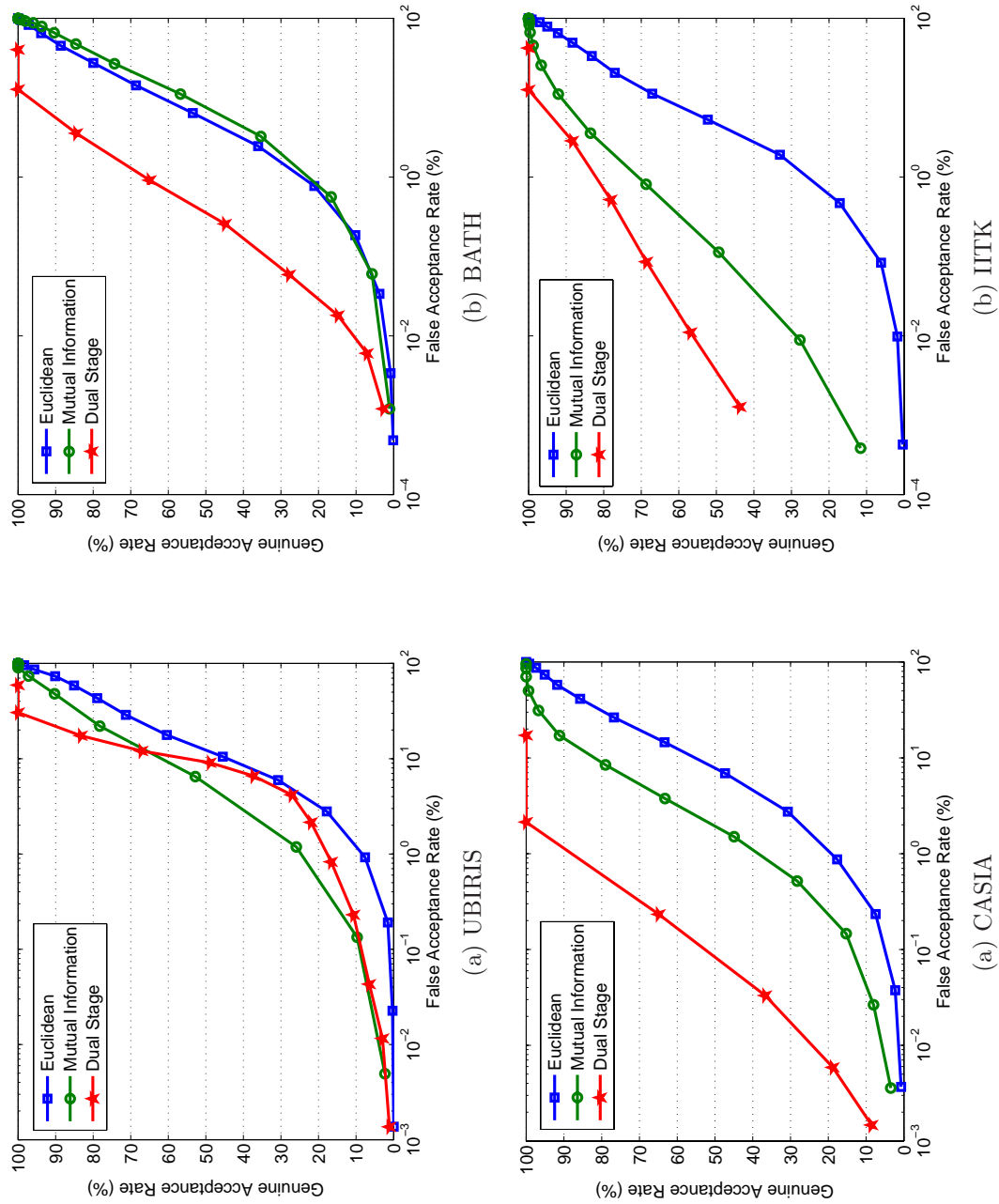
Figure 3.4: ROC curves for Euclidean distance, Mutual Information and Dual stage approach on various available databases

Table 3.1: FAR, FRR and Accuracy (ACC.) values (in %) for Log-Gabor wavelet, Haar wavelet and proposed Dual stage approach

Databases→	UBIRIS			BATH			CASIA			IITK		
Approaches↓	FAR	FRR	ACC.	FAR	FRR	ACC.	FAR	FRR	ACC.	FAR	FRR	ACC.
Log-Gabor	11.04	29.16	79.89	28.62	17.17	77.09	19.42	23.56	78.50	14.09	19.47	83.21
Haar Wavelet	20.77	19.51	79.85	16.34	18.18	82.73	25.37	14.89	79.86	15.41	16.40	84.09
Euclidean	17.74	39.60	71.32	14.31	31.40	77.14	26.40	23.25	75.17	20.57	22.97	78.22
Mutual Information	21.99	21.75	78.12	26.87	25.67	73.72	17.12	08.85	87.01	11.07	07.90	90.51
Dual Stage	07.39	23.12	84.74	06.56	06.16	93.64	00.24	05.89	96.93	08.39	04.21	93.70

Table 3.2: Average time taken (in seconds) using Harris corner approach

Approaches ↓	UBIRIS	BATH	CASIA	IITK
Euclidean	0.167	0.170	0.160	0.167
Mutual Information	0.203	0.207	0.205	0.200
Dual Stage	0.170	0.183	0.180	0.168

performs comparatively better than individual corner matching approaches. Figure 3.5 provides comparative ROC curves for global feature extraction approaches and proposed Dual stage approach. Genuine and imposter score distributions using Dual stage approach is given in Figure 3.6. Average time taken in seconds by different corner detection and matching approaches is given in Table 3.2.

(a) UBIRIS

(b) BATH

(a) CASIA

(b) IITK
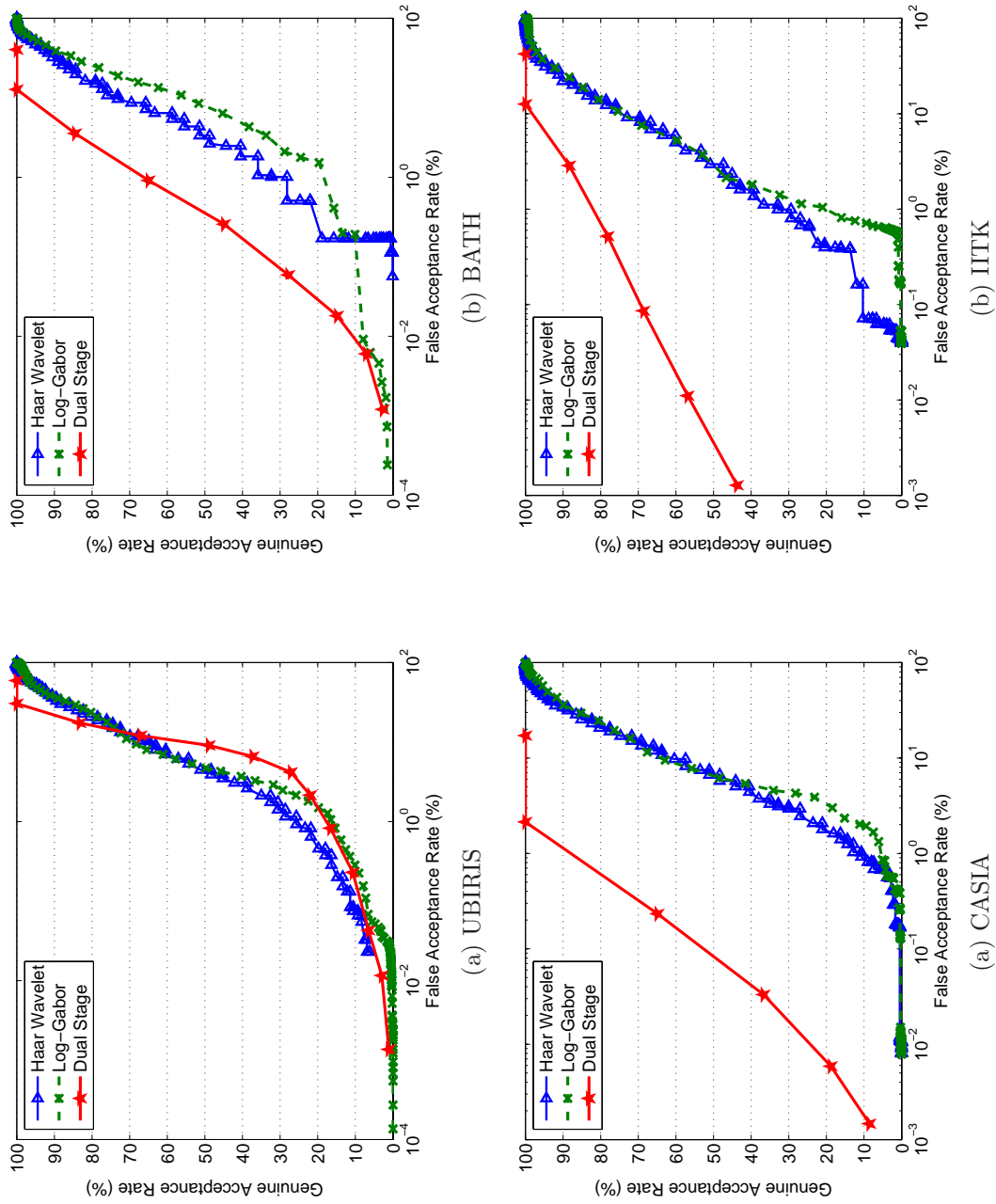
Figure 3.5: Comparative ROC curves for global feature extraction approaches and Dual stage approach

(a) UBIRIS

(b) BATH

(a) CASIA

(b) IITK
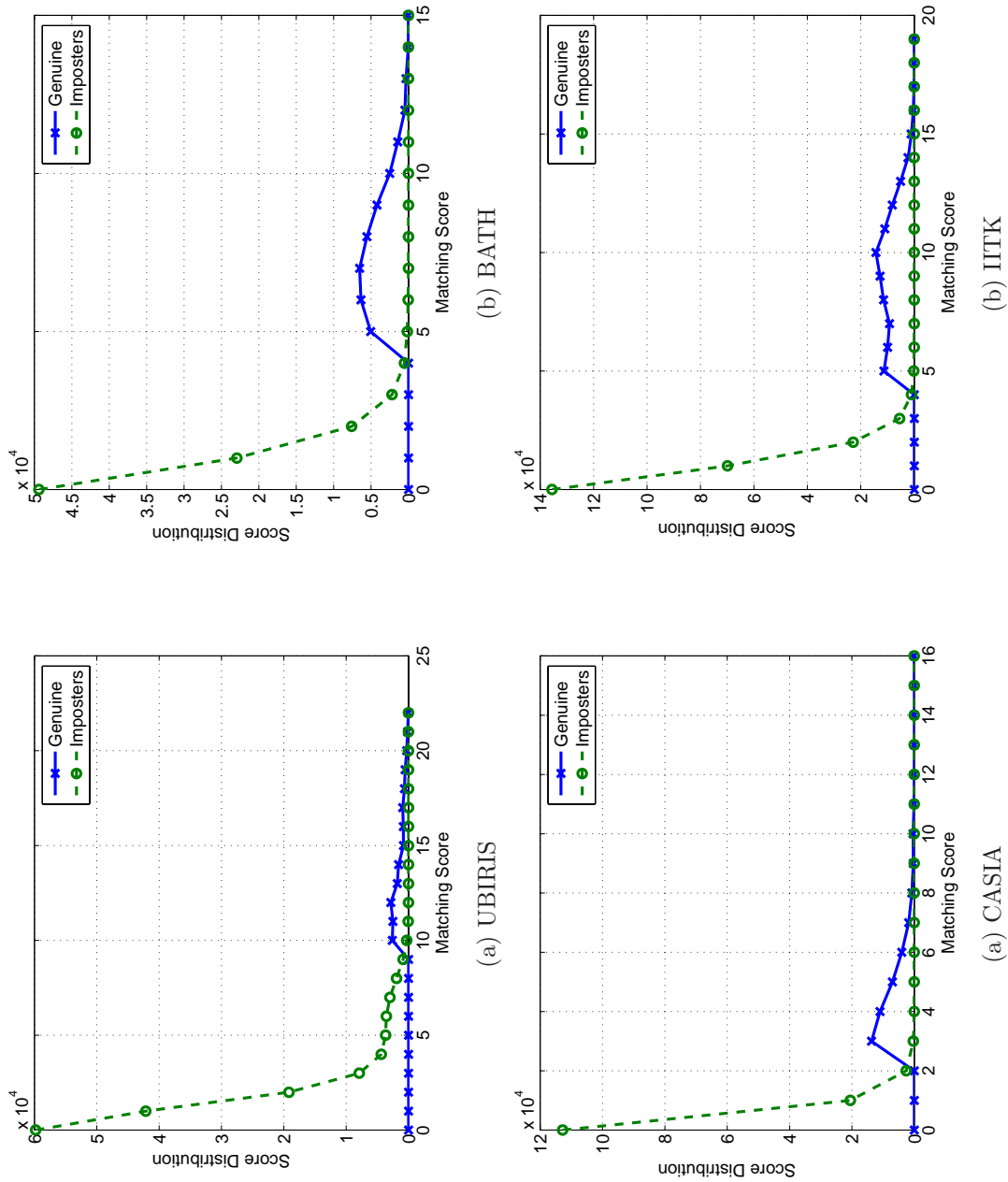
Figure 3.6: Genuine and imposter score distributions using Dual stage approach

3.2 Scale Invariant Feature Transform (SIFT)

The Harris corner detector is very sensitive to changes in image scale, so this approach could not find its applicability for matching iris images. Due to expansion and contraction of pupil as a natural phenomenon, the texture pattern of iris undergo linear deformation. Thus, enhanced keypoint descriptor is required that performs for variation in scale along with other transformations. In this thesis, a local feature descriptor coined Scale Invariant Feature Transform (SIFT) is used that provides stable set of features while being less sensitive to local image distortions. Local features from an image are computed using cascade filtering approach that minimises the feature extraction cost by applying more expensive operations at locations that pass an initial test. Keypoints are detected using difference of Gaussian (DOG) images. During feature extraction local image gradients are measured at selected scale in region around each keypoint to form descriptor vector. Detailed description of steps outlined above are gives in the following subsections.

3.2.1 Keypoint Detection

The first step is to find potential keypoints that are invariant to scale and orientation. For each detected keypoint a detailed model is fit to determine location and scale. The orientation is assigned to each location based on image gradients. The steps for keypoint detection is explained in this section.

Detection of Scale Space Extrema

The first step of keypoint detection is to identify locations that can be assigned with change in view and scale. Such locations, invariant to scale change, can be found by searching stable features across all possible scales using a continuous function of scale known as scale space [4]. The only possible scale space function is Gaussian function. Therefore scale space of image is defined as,

$$L(x, y, \sigma) = G(x, y, \sigma) * I(x, y) \tag{3.14}$$

where $I(x, y)$ is the input image with $*$ is the convolution operation in x and y.
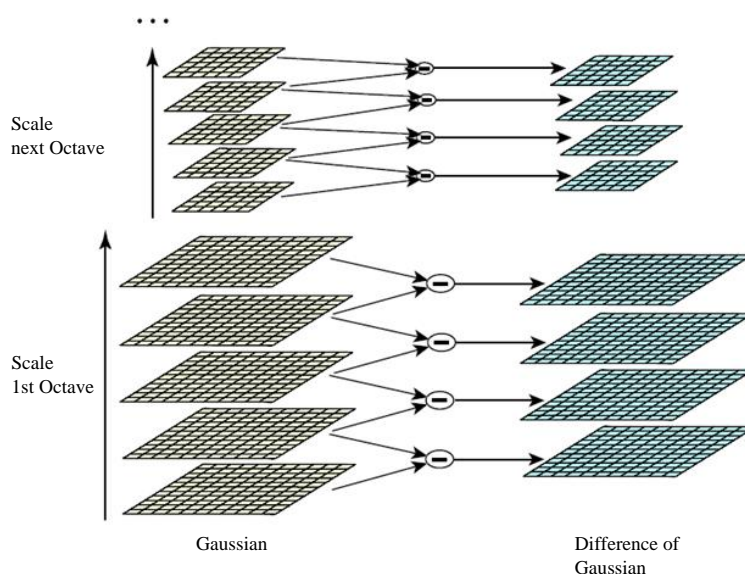
Figure 3.7: Scale space extrema for different octaves. Adjacent Gaussian images are subtracted to produce DOG images on right (taken from [4])

$G(x, y, \sigma)$ is the variable scale Gaussian defined as

$$G(x, y, \sigma) = \frac{1}{2\pi\sigma^2} e^{(-x^2+y^2)/2\sigma^2} \tag{3.15}$$

To detect stable keypoint locations in the scale space, Difference of Gaussian (DOG) function is convolved with the image. The Difference of Gaussian (DOG) for two nearby scales of an iris image I is computed as

$$\begin{aligned} D(x, y, \sigma) &= (G(x, y, k\sigma) - G(x, y, \sigma)) * I(x, y) \\ &= L(x, y, k\sigma) - L(x, y, \sigma) \end{aligned} \tag{3.16}$$

where k is a constant multiplicative factor used for changing the scale and x, y are the coordinates of a pixel in image I. The scale space for two different scales is shown in Figure 3.7. This scale invariant technique is found to be suitable for annular iris images because the size of iris changes due to expansion and contraction of pupil. Figure 3.8 shows the Gaussian blurred iris images and computation of DOG for change in octave, scale and σ. These images are generated using SIFT code [61].
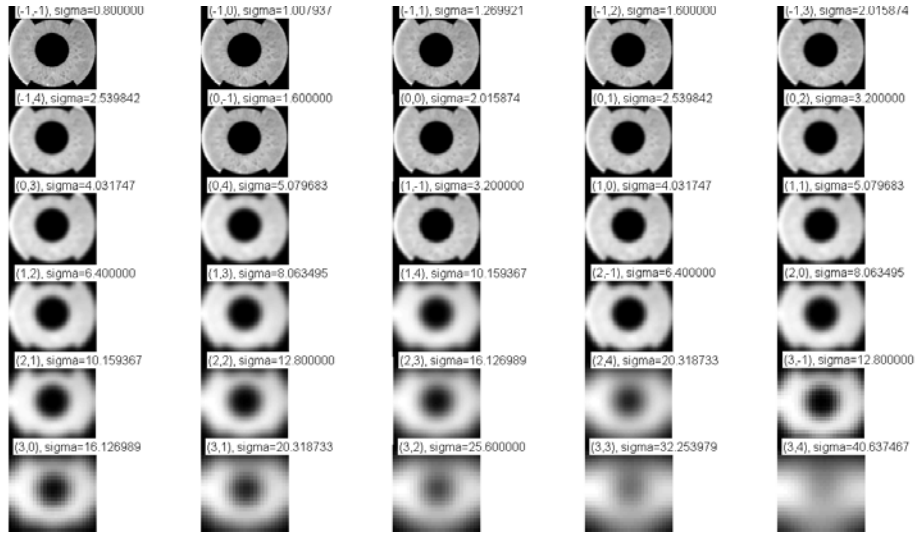
(a) Gaussian blurred annular iris images for different octave, scale and σ
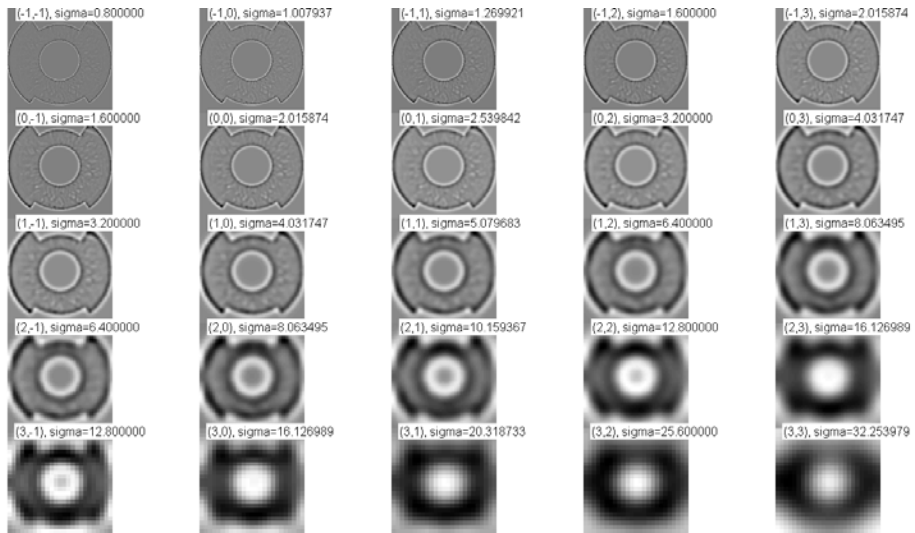
(b) Difference of Gaussian (DOG) images for change in octave, scale and σ

Figure 3.8: Detection of scale space extrema
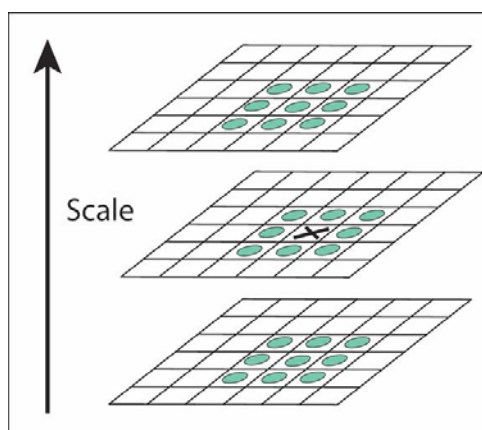
Figure 3.9: Maxima and minima of DOG images are obtained by comparing a pixel to 26 neighbors in $3 \times 3 \times 3$ regions (taken from [4])

Keypoint Localisation

DOG images are used to detect interest points with the help of local maxima and minima across different scales. Each pixel in DOG image is compared to 8 neighbours in the same scale and 9 neighbours in the neighbouring scales. The pixel is selected as a candidate keypoint if it is local maxima or minima in $3 \times 3 \times 3$ region as shown in Figure 3.9.

Once the keypoints are detected the next step is to perform the detailed fit to the nearby data for location, scale and ratio of principal curvature. The basic idea is to reject keypoints with low contrast. In [4] it is stated that keypoints with low contrast are sensitive to noise or poorly localised, hence they should not be considered. To determine the interpolated location of maximum, 3D quadratic function is fitted to local keypoint [62]. The authors have used Taylor expansion of scale space function, $D(x, y, \sigma)$ shifted so that the origin is at the sample point

$$D(\mathrm{x}) = D + \frac{\partial D^T}{\partial \mathrm{x}}\mathrm{x} + \frac{1}{2}\mathrm{x}^T\frac{\partial^2 D}{\partial \mathrm{x}^2}\mathrm{x} \qquad (3.17)$$

where D and its derivatives are evaluated at sample point and $\mathrm{x}=(x, y, \sigma)^T$ is an offset from this point. The location of extremum ($\hat{\mathrm{x}}$) is defined by taking the derivative of this function with respect to x and setting it to zero, thus giving

$$\hat{\mathrm{x}} = -\frac{\partial^2 D^{-1}}{\partial \mathrm{x}^2}\frac{\partial D}{\partial \mathrm{x}} \qquad (3.18)$$
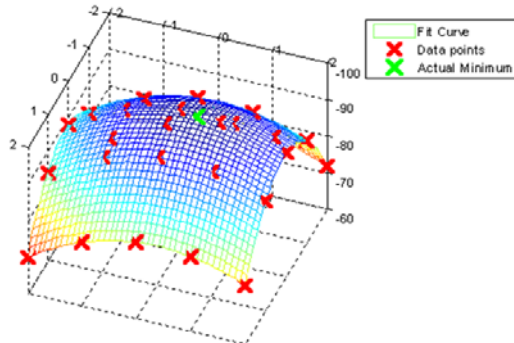
Figure 3.10: Interpolation of datapoints to estimate location of extremum

If the offset is larger than a predefined threshold then it means that $\hat{x}$ is close to different sample point. In this case sample point is changed and interpolation is performed about the point. The final offset is added to sample point to get interpolated location of extremum. Figure 3.10 shows interpolation of datapoints to get estimate of extremum. A sample iris image after detection of keypoints is shown in Figure 3.11(a).

Orientation Assignment

Orientation is assigned to each keypoint location to achieve invariance to image rotations as descriptor can be represented relative to orientation. To determine keypoint orientation, a gradient orientation histogram is computed in the neighbourhood of keypoint. The scale of keypoint is used to select Gaussian smoothed image L. For each Gaussian smoothed image $L(x, y)$, magnitude $(m(x, y))$ and orientation $(\theta(x, y))$ are computed as

$$m(x, y) = \sqrt{(L(x + 1, y) - L(x - 1, y))^2 + (L(x, y + 1) - L(x, y - 1))^2} \quad (3.19)$$

$$\theta(x, y) = \tan^{-1}\left(\frac{(L(x, y + 1) - L(x, y - 1))}{(L(x + 1, y) - L(x - 1, y))}\right) \quad (3.20)$$

Orientation histogram is then formed for gradient orientation around each keypoint. The histogram has 36 bins for 360 orientations and each sample is weighted by gradient magnitude and Gaussian weighted circular window with σ of 1.5 times of scale of keypoint before adding it to histogram. Peaks in the histogram correspond

(a)   (b)
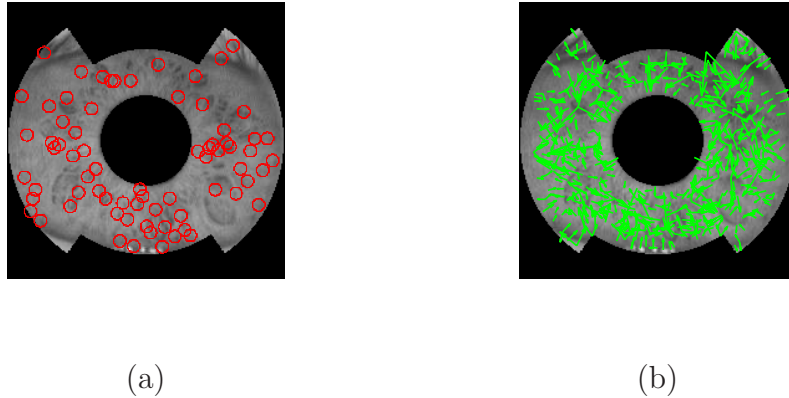
Figure 3.11: Keypoint detection on annular iris image using SIFT (a) Detected keypoints after removing noise and edge responses, (b) Scale and direction of orientation is indicated by arrows

to orientation and any other local peak within 80% of largest peak is used to create keypoint with the computed orientation. This is done to increase stability during matching [4]. The scale and direction of orientation is indicated by arrows as shown in Figure 3.11(b).

3.2.2 Keypoint Descriptor

Once orientation has been selected, the feature descriptor is computed as a set of orientation histograms on 4×4 pixel neighborhoods. The orientation histograms are relative to the keypoint orientation as shown in Figure 3.12. Histogram contains 8 bins each and each descriptor contains an array of 16 histograms around the keypoint. This generates SIFT feature descriptor of $4 \times 4 \times 8 = 128$ elements. The descriptor vector is invariant to rotation, scaling and illumination.

3.2.3 Keypoint Pairing

Let $p = \{p_1, p_2, p_3...p_n\}$ and $q = \{q_1, q_2, q_3...q_n\}$ be n dimensional feature descriptor for each point from database as well as query images respectively. The Euclidean distance between p and q is defined as

$$D(p,q) = \sqrt{\sum_{i=1}^{n}(p_i - q_i)^2} \tag{3.21}$$
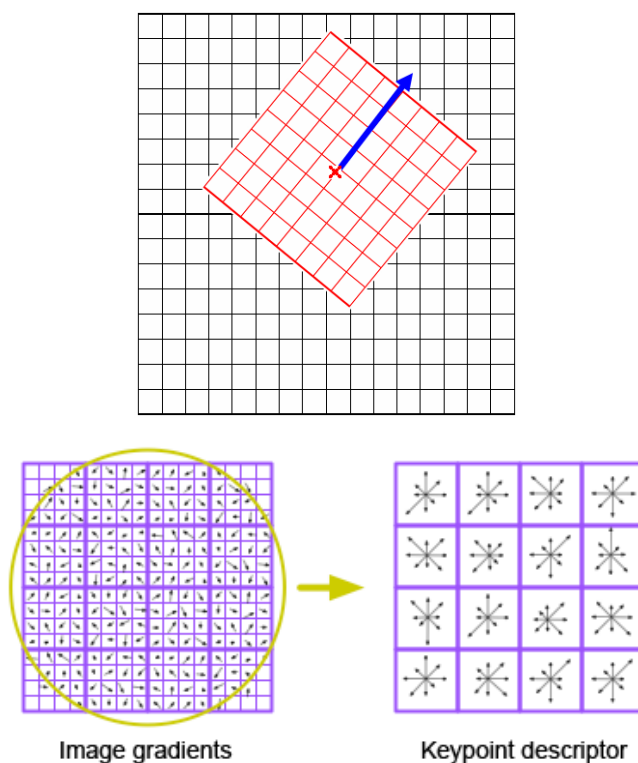
Figure 3.12: Window is taken relative to direction of dominant orientation. This window is weighted by a Gaussian and histogram is obtained for 4×4 regions

where n is 128 dimensional feature descriptor. The naive approach to nearest neighbor matching is to simply iterate through all points in the database to determine the nearest neighbor.

3.2.4 Experimental Evaluation

The accuracy of SIFT is obtained on various available databases. Results are obtained for three different forms of iris i.e., doubly dimensionless polar coordinate, singly dimensionless polar coordinate and annular iris. Table 3.3 shows the accuracy of SIFT for doubly, singly and annular iris image on various available databases. From the results it is evident that singly iris performs better compared to doubly iris for UBIRIS, BATH and CASIA database but accuracy reduces by 3% for IITK database. The reason behind is that singly iris transforms the annular region into polar form which introduces aliasing artifact. Thus, for IITK images significant texture features are lost due to such transformation.

Table 3.3: FAR, FRR and Accuracy (ACC.) values (in %) for SIFT approach

Database →	UBIRIS			BATH			CASIA			IITK		
Iris Form ↓	FAR	FRR	ACC.	FAR	FRR	ACC.	FAR	FRR	ACC.	FAR	FRR	ACC.
Doubly	13.08	32.92	77.00	08.01	10.37	90.80	07.16	19.64	86.59	7.97	5.55	93.23
Singly	22.39	09.93	83.83	05.48	06.04	94.23	11.86	01.16	93.48	16.54	02.34	90.55
Annular	06.16	00.00	96.91	05.40	05.54	94.52	02.03	04.34	96.81	0.97	04.08	97.48

(a) UBIRIS

(b) BATH

(a) CASIA

(b) IITK
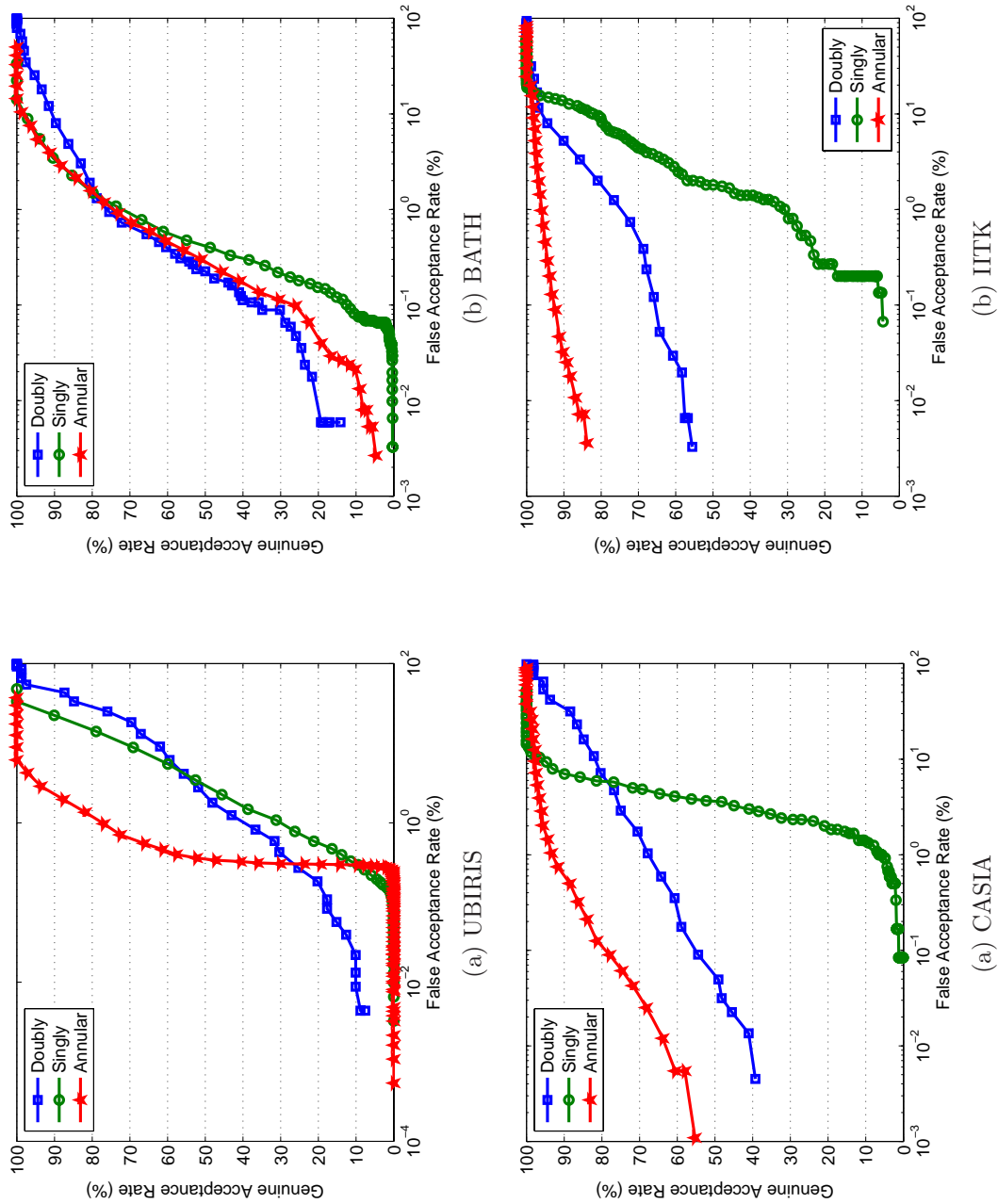
Figure 3.13: ROC curves using SIFT for doubly, singly and annular iris on various available databases

(a) UBIRIS

(b) BATH

(a) CASIA

(b) IITK
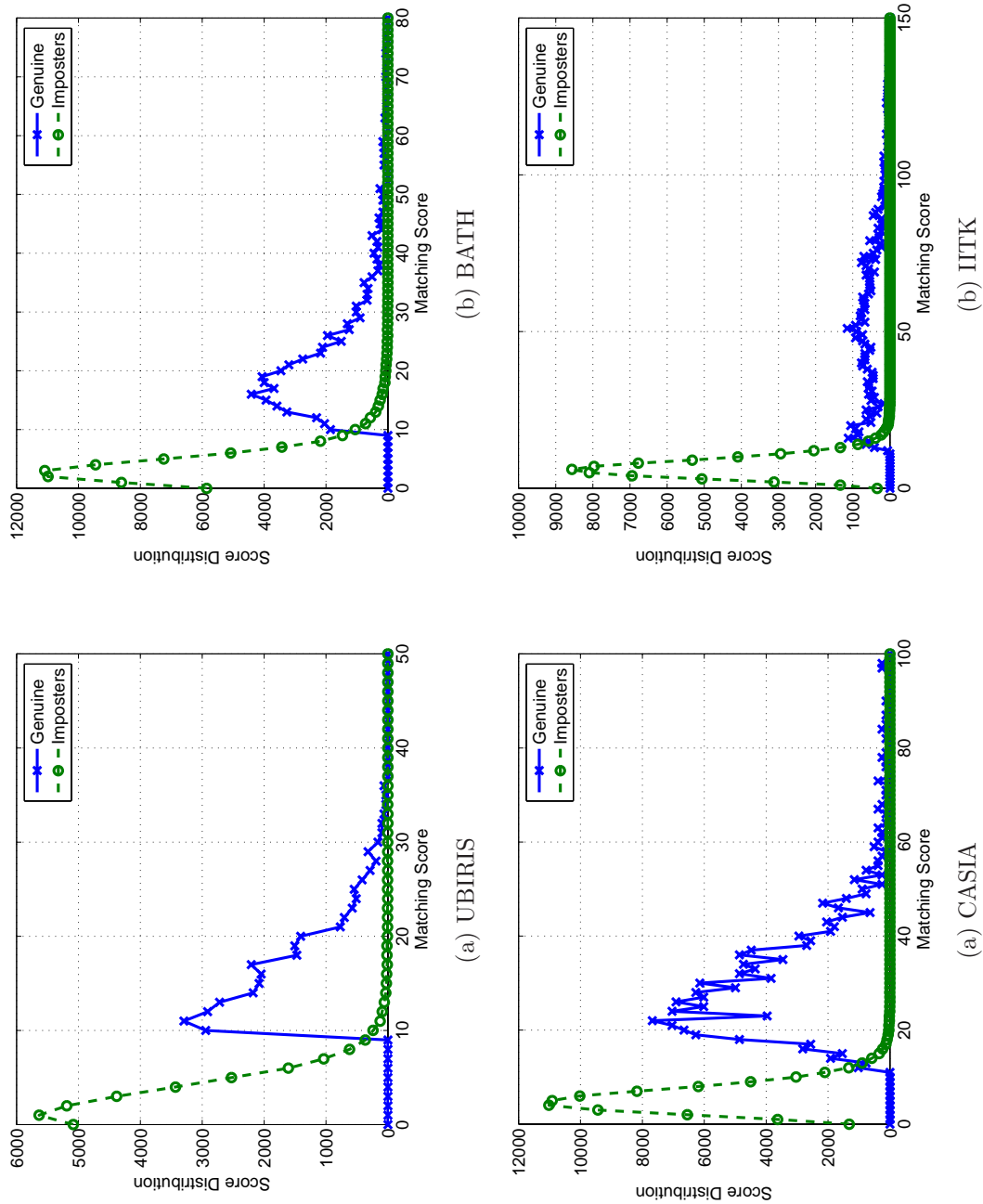
Figure 3.14: Genuine and imposter score distributions using SIFT

Table 3.4: Average time taken (in seconds) using SIFT

Iris Forms ↓	UBIRIS	BATH	CASIA	IITK
Doubly	1.463	0.977	0.911	1.504
Singly	0.368	0.543	0.899	0.927
Annular	0.233	0.480	1.340	1.297

Finally, results are obtained directly on annular iris image which marks an improvement in performance. The accuracy for UBIRIS increases considerably to 96.91% from 77% for doubly iris. Similarly there is improvement in accuracy for all other databases. ROC curves for UBIRIS, BATH, CASIA and IITK is shown in Figure 3.13. From the results it is evident that local features extracted directly from annular iris image performs better compared to conventional approaches. Genuine and imposter score distributions for SIFT is shown in Figure 3.14. Time required to claim recognition also reduces for SIFT as shown in Table 3.4. This validates the applicability of keypoint descriptors for annular iris recognition.

3.3   Speeded Up Robust Features (SURF)

Speeded Up Robust Features (SURF) detector and descriptor are not only faster, but far more repeatable and distinctive [6] compared to state-of-the-art approaches [4, 63, 64]. The essential requirement is to apply feature descriptor that, in comparison to existing keypoint approaches, are fast to compute while not sacrificing performance. This can be achieved by simplifying the detection scheme while keeping it accurate, and reducing the descriptor's size while keeping it sufficiently distinctive [5]. SURF is more robust compared to existing keypoint detectors because Hessian-based detectors are more stable and repeatable than their Harris-based counterparts. Further, due to descriptor's low dimensionality, any matching algorithm is bound to perform faster.

SURF has two significant advantages over SIFT. Firstly, SURF uses sign of Laplacian to have sharp distinction between background and foreground features. Secondly, SURF uses only 64 dimensions compared to SIFT using 128 dimensional vector. This reduces feature computation time and allows quick matching with increased robustness simultaneously [65]. SURF has been applied to iris recognition for the first time in literature. The operator extracts keypoints using Hessian matrix and describes a distribution of Haar Wavelet responses from a window around the interest point as descriptors. There are two steps involved to determine local descriptor vector and they are (1) Detection of keypoints (2) Keypoint descriptor. The above mentioned steps are explained as follows:

3.3.1   Detection of Keypoints

For interest point detection SURF uses Hessian Matrix approximation. For faster computation of interest points integral images are used as proposed in [66]. Integral images uses the concepts of boxlets as proposed by Simard et al. [67].

Integral Images

Integral images reduces the computation time drastically by allowing the faster computation of box type convolution filters. The entry of an integral image $I_{\sum}(\mathrm{x})$ at a location $\mathrm{x} = (x, y)^T$ represents the sum of all pixels in the input image I within a
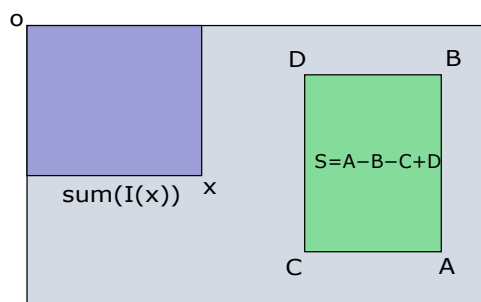
Figure 3.15: Integral images are used to calculate the sum of intensities inside a rectangular region of any size.

rectangular region formed by the origin and x

$$I_\Sigma(\text{x}) = \sum_{i=0}^{i \le x} \sum_{j=0}^{j \le y} I(x, y) \tag{3.22}$$

After computing the integral images it takes three additions to calculate sum of intensities over the integral area as shown in Figure 3.15. The calculation time is independent of the filter size.

Hessian Matrix based Interest Points

Hessian matrix based detection is used because of its increased performance. For detection of keypoints determinant of Hessian matrix is used for selecting location and scale. Given a point $P = (x, y)$ in an image I, the Hessian matrix $H(P, \sigma)$ in P at scale σ is defined as follows

$$H(P, \sigma) = \begin{bmatrix} L_{xx}(P, \sigma) & L_{xy}(P, \sigma) \\ L_{xy}(P, \sigma) & L_{yy}(P, \sigma) \end{bmatrix} \tag{3.23}$$

where $L_{xx}(P, \sigma)$ is the convolution of the Gaussian second order derivative $(\frac{\sigma^2}{\sigma x^2} g(\sigma))$ with the image I at the point P and similarly $L_{xy}(P, \sigma)$ and $L_{yy}(P, \sigma)$ are obtained. Gaussian is discretised and cropped as shown in Figure 3.16. These approximate Gaussian second order derivatives can be evaluated at a very low computational cost using integral images. The calculation time therefore is independent of the filter size. The 9×9 box filters as shown in Figure 3.16 are approximations of a Gaussian at σ = 1.2. These are denoted by D_{xx}, D_{xy} and D_{yy} [68]. By choosing the weights for the box filters adequately, the approximations for the Hessian's determinant are computed

using

$$Det(H_{approx}) = D_{xx}D_{yy} - (0.9D_{xx})^2 \tag{3.24}$$

Scale Space Representation

Due to the use of box filters and integral image it is not required to iteratively apply the same filter to the output of previously filtered image. This can be made computationally efficient by applying box filter of any size on the original image as shown in Figure 3.17. Therefore scale space is analysed by upscaling the filter size rather than reducing the image size. The output of the 9×9 filter, introduced in previous section, is considered as the initial scale layer. Subsequent layers are obtained by filtering image with larger masks to localise keypoints invariant to scale. The advantage of such scale space creation is that it is computationally efficient as image is not downsampled so there is no effect of aliasing.

The scale space is divided into *octaves*. Each octave is represented by series of filter responses obtained by convolving input image with filter of increasing size. Each octave is subdivided into a constant number of scale levels. The length (l_0) of positive or negative lobe of partial second order derivative in direction of derivation (x or y) is set to third of filter size length. For the 9×9 filter, this length l_0 is 3. For two successive levels, the size is increased by a minimum of 2 pixels (1 pixel on every side) in order to keep the size uneven and thus ensure the presence of the central pixel. This results in a total increase of the mask size by 6 pixels as shown in Figure 3.18.

Scale space construction starts with the initial 9×9 filter for which scale s=1.2 (approximating Gaussian derivatives with $\sigma = 1.2$). Then, filters with sizes 15×15, 21×21, and 27×27 are applied, by which even more than a scale change of two has
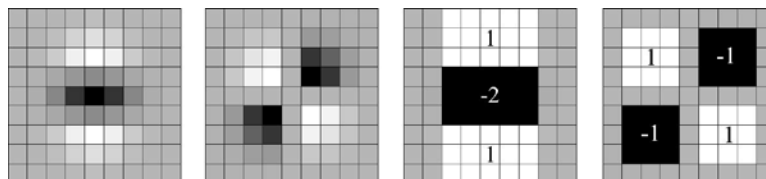
Figure 3.16: Left to right: discrete Gaussian second order derivative in y and xy direction. Approximation for the second order Gaussian partial derivative in $y-(D_{yy})$ and xy-direction (D_{xy}) (taken from [5]).

been achieved. The filter size increase is doubled for every new octave (from 6-12 to 24-48). The filter size is increased for corresponding octaves until image size is larger than the filter size.

Interest Point Localisation

Keypoints are localised in scale and image space by applying a non maximum suppression in a 3×3×3 neighbourhood. The local maxima found on the determinant of Hessian matrix are interpolated to image space as proposed in [62]. Figure 3.19 shows the detected interest points on the annular iris image.

3.3.2   Keypoint Descriptor

For description of every interest point, Haar wavelet responses are obtained in x and y direction. The descriptor is obtained using integral images with only 64 dimensions for speed. The first step consists of finding orientation using circular window around the interest point. Then, a square region aligned to the selected orientation is considered to extract the SURF descriptor.

Orientation Assignment

To achieve invariance to image rotation the orientation is identified for each keypoint. For this purpose, Haar wavelet responses are calculated in x and y direction within a circular neighbourhood of radius $6s$ around the interest point, with s the scale at which the interest point was detected. The size of wavelets are scale dependent and set to side length of $4s$. Once the wavelet responses are calculated and weighted with a Gaussian ($\sigma = 2s$), the dominant orientation is obtained by calculating sum
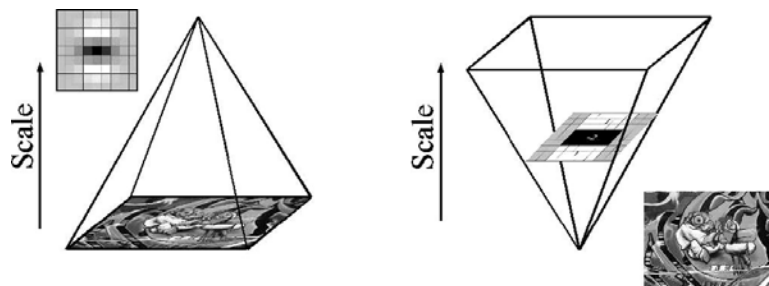
Figure 3.17: Use of integral images for upscaling filter masks (taken from [6])
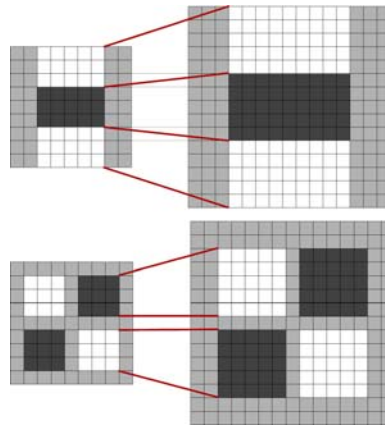
Figure 3.18: Filters D_{yy} (top) and D_{xy} (bottom) for two successive filter sizes (9×9 and 15×15) [5].

of all responses within a sliding orientation window of size $\frac{\pi}{3}$ (see Figure 3.20). The horizontal and vertical responses within the window are summed. The longest such vector over all windows defines the orientation.

Keypoint Descriptor

The descriptor vector is obtained around every detected keypoint by taking a square window of size $20s$ centered around the interest point and aligned relative to the direction of orientation. The region is split into smaller 4×4 sub-regions to preserve spatial information as shown in Figure 3.21. For each sub-region, Haar Wavelet responses are obtained in horizontal (d_x) and vertical direction (d_y). To increase the robustness towards geometric deformations and localisation errors, the responses d_x and d_y are first weighted with a Gaussian ($\sigma = 3.3s$) centered at the interest point.
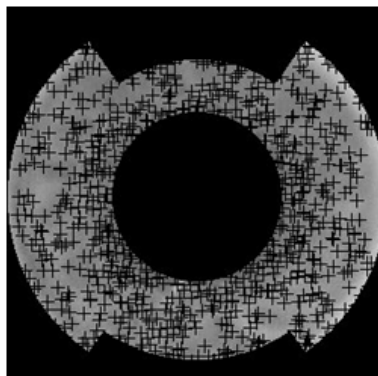
Figure 3.19: Detected interest points on annular iris image
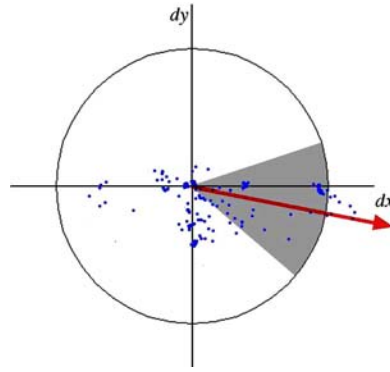
Figure 3.20: Orientation assignment by taking a sliding window of size $\frac{\pi}{3}$ indicated by shaded region [5]

Finally the descriptor vector is summed up for each sub-region to form elements of feature vector. To bring in information about the polarity of the intensity changes, the sum of the absolute values of the responses are obtained ($|d_x|$ and $|d_y|$). Thus, each sub-region is a 4D feature vector comprising of

$$v = \left\{ \sum d_x, \sum d_y, \sum |d_x|, \sum |d_y| \right\} \tag{3.25}$$

Concatenating this for all 4×4 sub-regions results in a descriptor vector of length 64. Figure 3.22 shows the property of a descriptor for three different image-intensity patterns within a sub-region. For a homogeneous sub-region (left of Figure 3.22) all values are relatively low. For the presence of frequencies in x direction, the value of $\sum |d_x|$ is high but all others are low (middle). If intensity is gradually decreasing in
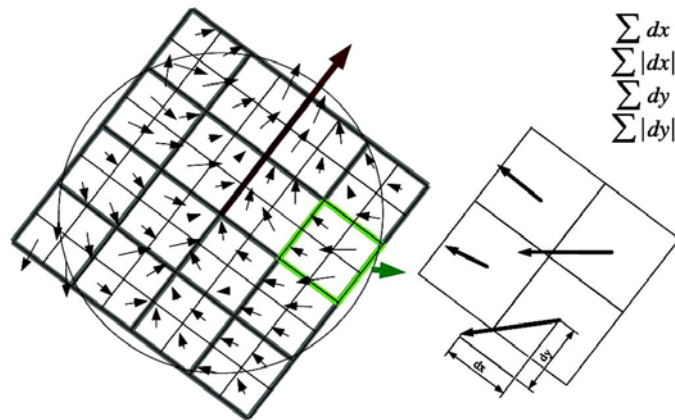
Figure 3.21: An oriented window with 4×4 sub-regions is taken in direction of orientation. For each sub-region wavelet responses are obtained [5].
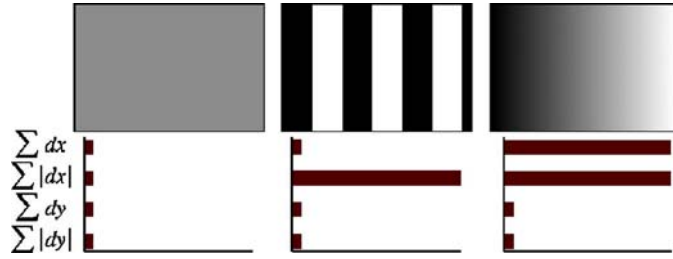
Figure 3.22: Descriptor entries of a sub-region represent the nature of the underlying intensity pattern [5].

x direction, both the values of $\sum d_x$ and $\sum |d_x|$ are high.

3.3.3 Keypoint Pairing

After detection of keypoints in database image (A) and query image (B), matching is done using interest point pairing approach. The best candidate match for each keypoint in A is found by identifying the closest pair from the set of keypoints in B. The nearest neighbor is defined as the keypoint with minimum Euclidean distance for the invariant descriptor vector. Let $L = \{l_1, l_2, l_3.....l_m\}$ and $E = \{e_1, e_2, e_3.....e_n\}$ be vector arrays of keypoints of A and B respectively obtained through SURF.

The descriptor array l_i of keypoint i in L and descriptor array e_j of keypoint j in E are paired if the Euclidean distance $||l_i - e_j||$ between them is less than a specified threshold α. Threshold based pairing results in several number of matching points. To avoid multiple matches, the keypoints with minimum descriptor distance if less than threshold are paired. This results in a single matching pair, and is called as nearest neighbourhood matching method. In SURF, the matching method applied is similar to the nearest neighbor matching, except that the thresholding is applied to the descriptor distance ratio between keypoints. The method used in SURF is called as nearest neighbor ratio method. Thus, the keypoints are matched if

$$\frac{||l_i - e_j||}{||l_i - e_k||} < \alpha \tag{3.26}$$

where, e_j is the first nearest neighbor and e_k is the second nearest neighbor of l_i. The paired points (l_i, e_j) are removed from L and E respectively. The matching process is continued until there are no more key-points. Based on the number of pairs

between query image A and enrolled image B, a decision is taken about candidate's identity. Figure 3.23 shows keypoint pairing between two annular iris images. Results are shown for samples taken from IITK database. The number of keypoints paired for each comparison along with image instance number is shown below the figure. This is an illustrative example to prove the capability of keypoint descriptors to achieve scale invariance.

3.3.4   Experimental Evaluation

This section discusses the performance of SURF for UBIRIS, BATH, CASIA and IITK databases using various forms of iris. Table 3.5 shows the performance comparison for all the databases. From the experimental evaluation, it has been found that SURF performs well for doubly iris with an accuracy of 92.93% on IITK database but still there is a scope for further improvement. To measure the robustness of the system, ROC curve is obtained for doubly dimensionless iris as shown in Figure 3.24. In the next stage of simulation the results are obtained for singly iris as shown in Figure 3.25. Accuracy improves for sinlgy iris for BATH, CASIA and IITK databases. The system gives an accuracy of 95.77% for IITK database. But there is reduction in value of accuracy for UBIRIS database. UBIRIS fails to perform due low resolution and reduced quality of input image.

At the final stage, features are extracted using SURF directly from annular iris. From the results it is evident that SURF performs with an accuracy of 98% on IITK database. The accuracy values has improved significantly for all other databases. ROC curve for annular iris recognition using SURF is shown in Figure 3.26. Distribution of genuine and imposter scores for all databases is given in Figure 3.27. Table 3.6 gives time required in milliseconds to perform recognition. The time to claim identification has reduced considerably for SURF compared to existing keypoint descriptors.

(b) 0001_12 with 0067_4
No of Pairs: 54

(b) 0001_12 with 0001_5 (0.5 scaled)
No of Pairs: 91

(a) 0001_12 with 0001_5
No of Pairs: 179
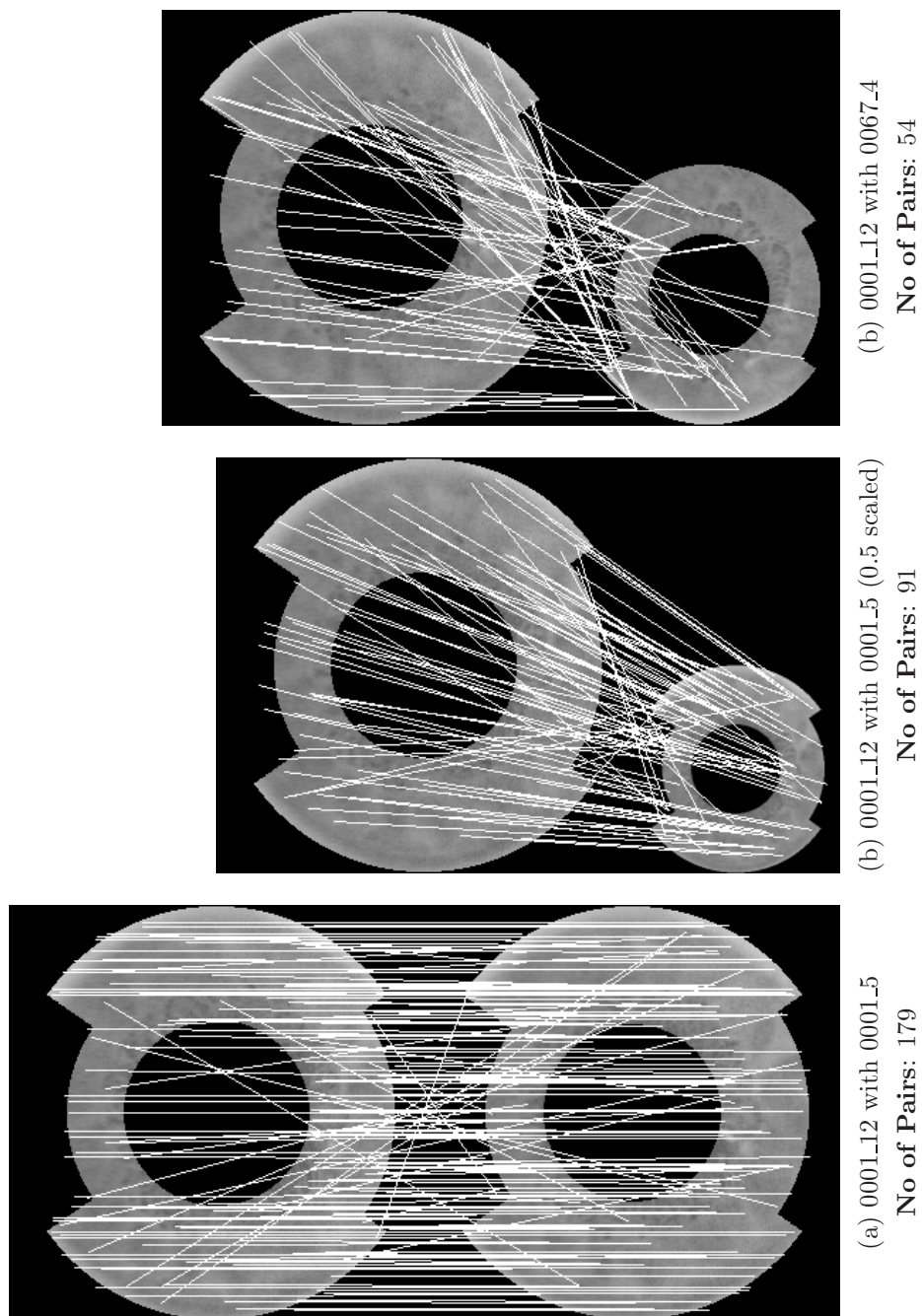
Figure 3.23: Keypoint pairing between two annular iris images from IITK database using SURF

69
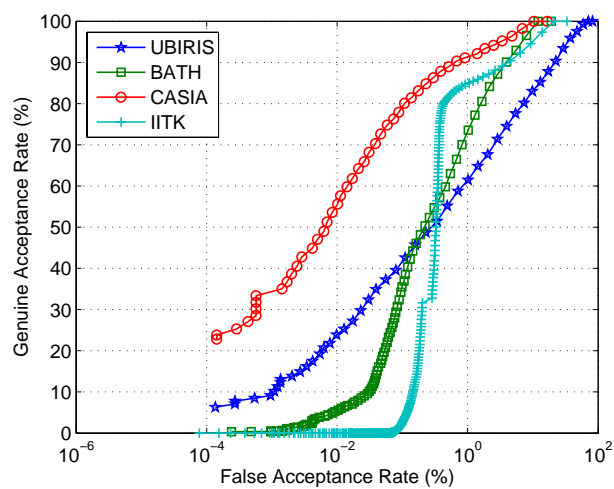
Figure 3.24: ROC curve for doubly dimensionless iris strip
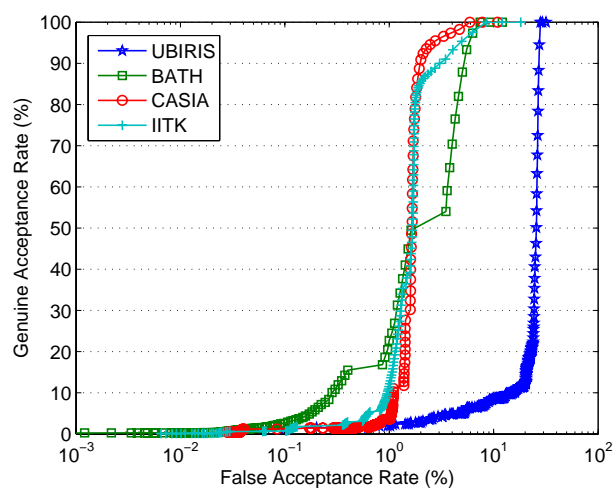
Figure 3.25: ROC curve for singly dimensionless iris strip

Table 3.5: FAR, FRR and Accuracy (ACC.) in % using SURF on various available databases

Databases →	UBIRIS			BATH			CASIA			IITK		
Iris Forms ↓	FAR	FRR	ACC.	FAR	FRR	ACC.	FAR	FRR	ACC.	FAR	FRR	ACC.
Doubly	09.85	16.98	86.57	07.98	03.46	94.27	03.39	04.78	95.91	06.41	07.71	92.93
Singly	28.02	00.00	85.98	04.20	03.20	96.30	03.30	02.60	97.05	03.22	05.23	95.77
Annular	9.15	14.25	88.29	1.44	2.06	98.24	2.16	4.78	96.52	1.28	1.92	98.39

Table 3.6: Average time taken (in milliseconds) using SURF

Iris Form ↓	UBIRIS	BATH	CASIA	IITK
Doubly	282.67	156.94	267.97	304.22
Singly	43.18	53.17	154.23	201.45
Annular	50.06	100.13	387.48	305.98
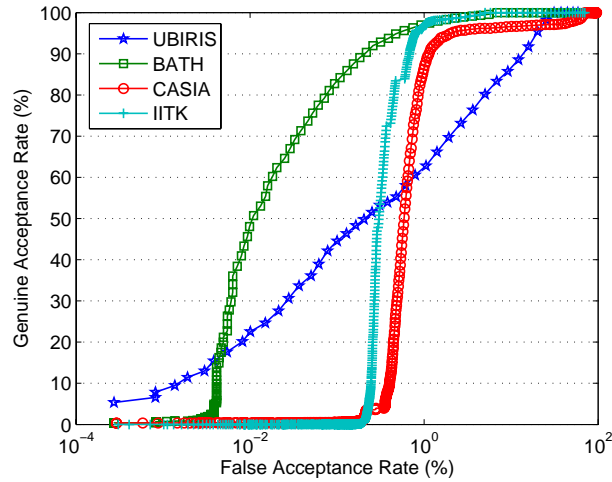
Figure 3.26: ROC curve for annular iris image

3.4   Summary

In this chapter, three well known keypoint descriptors are studied and applied to iris. In order to prove the merits of keypoint descriptors, Harris corner detector is compared to existing global feature extraction approaches like Haar and Log-Gabor wavelets. From the results it has been found that Harris corner detector performs with an average accuracy of 92.25% which is much better than global approaches. However, Harris corner detector could not achieve invariance to scale changes. In order to achieve scale invariance, SIFT is applied to annular iris that is robust to all possible transformations as well as partial occlusions. The system using SIFT performs with an average accuracy of 96.37%. The performance has improved compared to Harris corner approach but the time required to recognise an individual is more due to higher dimensionality of feature descriptor. Thus, one of the recently developed keypoint descriptor coined SURF is applied to annular iris. SURF performs better compared to existing keypoint descriptors in terms of reliability, accuracy and speed. SURF
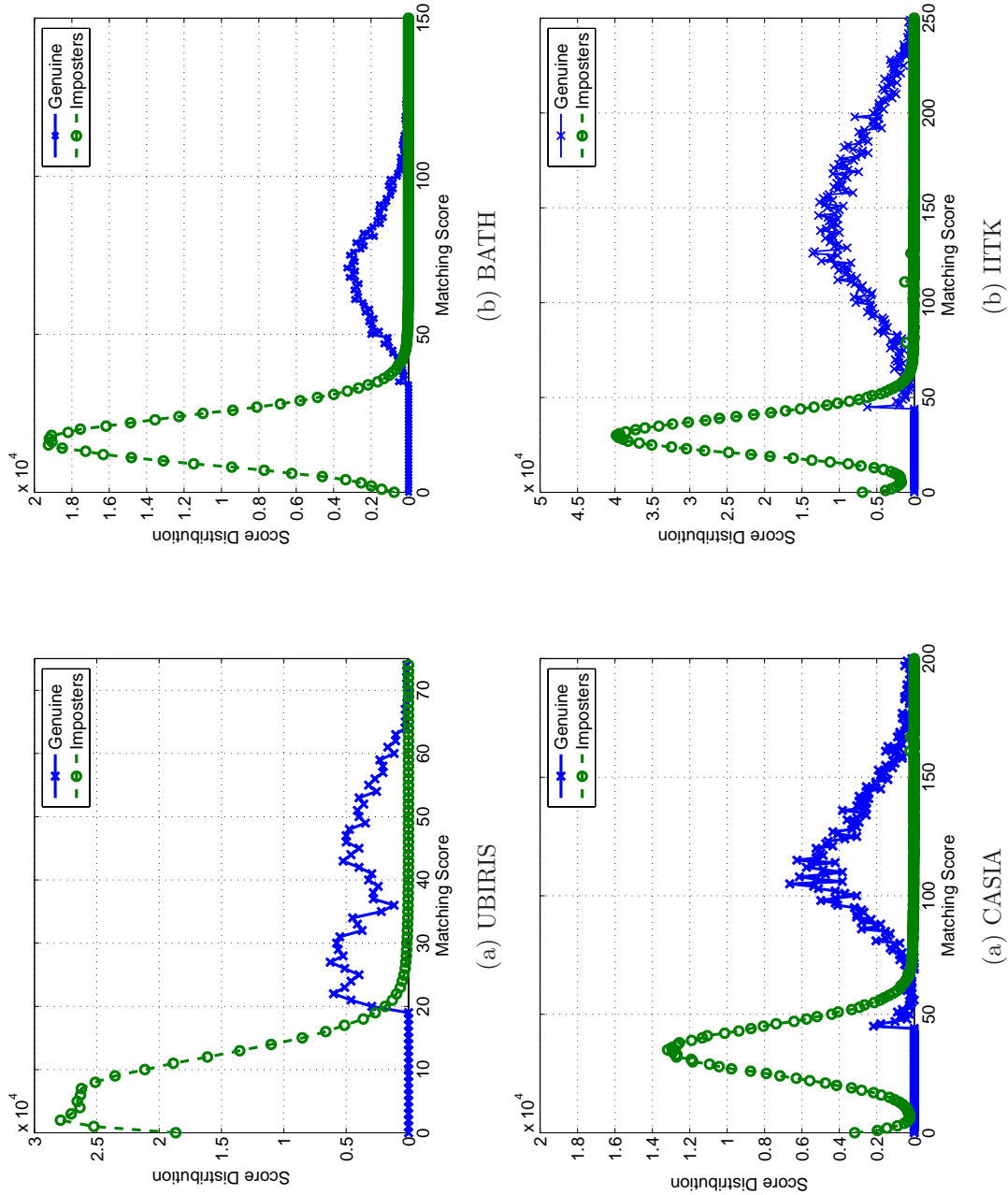
Figure 3.27: Genuine and imposter score distributions using SURF

is giving an average accuracy of 97.7% on cooperative as well as non-cooperative databases. Further, the time required to claim identification using SURF is reduced considerably to 200 ms (approx). Based on the experimental study it has been inferred that SURF can be used as one of the most reliable matching approach where iris images are obtained under non-ideal conditions.

Chapter 4

Iris Identification

During identification mode, the system recognises an individual by searching the templates of all the users in the database for a match. Therefore, the system conducts a one-to-many comparison to establish an individual's identity. For a system to operate in identification mode there are two challenges that need to be addressed. Firstly, any identification system suffers from an overhead of large number of comparisons in the database. As the size of database increases the time required to declare an individual's identity increases significantly [8]. Secondly, it has been observed mathematically that the number of false positives (FAR) also increases geometrically with increase in the database size [11, 27].

Thus, there are two ways to improve the performance of a biometric system: (i) by reducing the number of false positives and (ii) by reducing the search space [27]. The FAR of a system is dependent upon the recognition algorithm and cannot be reduced indefinitely. Thus, accuracy can be improved by reducing search space (N). The search space can be reduced by using classification, clustering and indexing approaches on the database. Applying some traditional database binning approaches do not yield satisfactory results. The reason behind is that biometrics does not possess any natural or alphabetical order. As a result, any traditional indexing scheme cannot be applied to reduce the search time. Thus, the query feature vector is compared sequentially with the all templates in the database. The retrieval efficiency in sequential search depends upon the database size. This leaves behind a challenge to develop a non-traditional indexing scheme that reduces the search space in the large biometric database. The general idea of indexing is to store closely related feature vectors
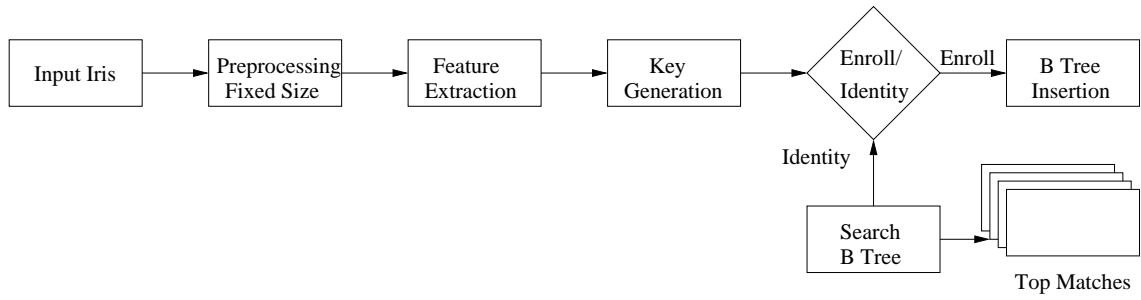
Figure 4.1: Block diagram of DCT based indexing scheme

together in the database at the time of enrolment. During identification, the part of the database that has close correspondence with query feature vector is searched to find a probable match. In the proposed work a novel iris database indexing scheme is developed using energy histogram of DCT coefficients. This scheme uses doubly dimensionless normalized iris image for indexing. This approach works well for cooperative databases but fails to perform indexing for non-cooperative irises. The reason behind is that DCT is a global feature extraction approach and fails to handle variations due to illumination and transformations. Thus, there is a need to develop an indexing scheme using local features like keypoints. A robust indexing scheme known as Geometric Hashing [69] is applied on detected keypoints to render an efficient iris identification system. The two identification approaches are discussed in sequel:

4.1   Indexing using Energy Histogram of DCT

In this thesis, an efficient indexing scheme based on energy histogram of iris database has been studied. The acquired iris image is preprocessed and transformed into fixed size normalized image. Energy features are extracted from the rectangular block using multiresolution subband coding of DCT coefficients. The energy histogram on extracted features are used to form keys. This key is used to define the B Tree and store the iris templates at the leaf node that shares similar texture information. The block diagram of system modules is given in Figure 4.1.

4.1.1 Feature Extraction using DCT

Features are extracted from fixed size normalized strip using Discrete Cosine Transformation (DCT) [70]. DCT has strong energy compaction property and its coefficients represent some dominant grey level variations of the image. Thus, it is the most promising approach for texture classification. The input iris strip is divided into non-overlapping 8×8 pixel blocks which are transformed to generate DCT coefficients. The reason behind using block based DCT approach is that it extracts block based details of an image. It has been observed that multiresolution decomposition provides useful discrimination between texture. Each block of the computed DCT coefficients has to be reordered to form subbands like 3 level wavelet decomposition. The block of size 8×8 is reordered to transform coefficients into multiresolution form. For a coefficient $D(u, v)$ of the block, ordering is done and stored in S_i where i is defined by

$$i = \begin{cases} 0 & \text{for } m = 0 \\ (m - 1) \times 3 + (a/m) \times 2 + (b/m) & \text{otherwise} \end{cases} \tag{4.1}$$

Let $m = max(a, b)$ for $2^{a-1} \leq u \leq 2^a$ and $2^{b-1} \leq v \leq 2^b$, a and b are the integer values and i ranges from 1 to 10. After reordering, the coefficients $D(1, 1), D(1, 2), D(2, 1)$ and $D(2, 2)$ are stored in subband S_1, S_2, S_3 and S_4 respectively. The multiresolution subband ordering for 8×8 block is shown in Figure 4.2. After reordering all the DCT blocks, the coefficients from each block belonging to a particular subband are grouped together. Energy value E_i of each subband S_i is obtained by summing up the square of coefficients as

$$E_i = \sum S_i(x, y)^2 \tag{4.2}$$

Note that the sum of square increases the contribution of significant coefficients and suppresses insignificant coefficients. The feature vector consists of different energy values obtained from 10 subbands.

4.1.2 Indexing Iris using B Tree

It is expected that the query response time should depend upon the templates similar to the query template and not the total number of templates in the database.

Figure 4.2: Multiresolution reordering of 8×8 DCT coefficients
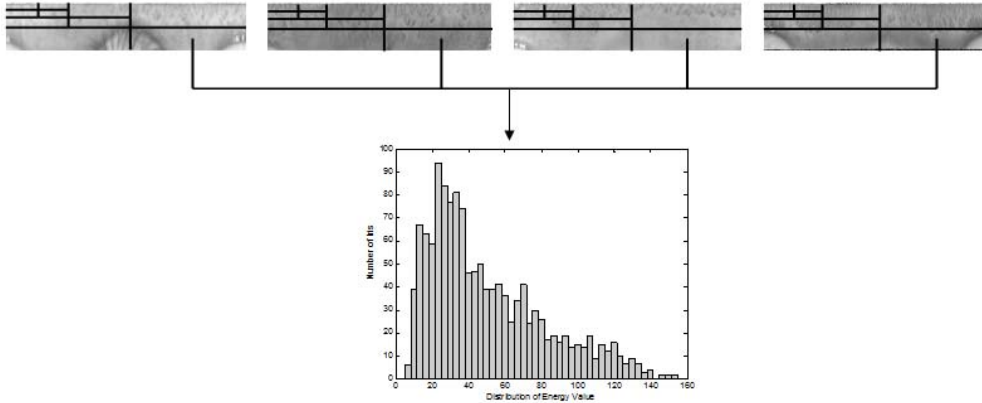
Figure 4.3: Energy histogram of S_{10} region

Thus, the database should be logically partitioned such that images having similar texture patterns are indexed together. To search the large visual databases, content based image indexing and retrieval mechanism based on energy histogram of wavelet coefficients has been proposed in [71]. The scheme provides fast image retrievals. Similar approach has been proposed by considering the energy histogram of reordered DCT coefficients [72]. In the proposed approach, biometrics database is indexed using energy histogram of reordered coefficients as given by [72]. The steps involved in indexing are given as follows:

Key Generation

The feature vector obtained from each image contains 10 different energy values one from each subband. The energy histogram (H_i) is build for each subband (S_i) using all the images in the database. This presents the distribution of energy for each subband. Figure 4.3 shows the histogram for region S_{10} using all images in the database.

The histogram generated from each subband (H_i) is divided into bins to form logical groups. The texture details of iris strip that have similar energy values (E_i) are placed together in the same bin to have more accurate matches. The size of the bin can be fixed or variable. Here the size of the bin is fixed for experiments. The bins are enumerated in numerical order starting from 1 as shown in Figure 4.5. The images falling under each bin are represented on each bar of the histogram. Each image falls under a particular bin of the histogram H_i. This bin number is used to form a global key for indexing. Image key consists of bin number corresponding to each subband. The bin numbers for each subband are combined together using Morton order traversal which places low-frequency coefficients before high-frequency coefficients. The schematic diagram for Morton order traversal is shown in Figure 4.6. For example the image I using Morton order forms the key as (3-5-7-8-2-1-4-5-6-7). Similarly all the images in the database obtains keys.

Database Creation and Searching

The key is used for inserting an image in the database during enrollment. To store an iris template B tree data structure is used. The degree of the tree is total number of bins that has been constructed for each subband. The height of tree is the number of subbands i that has been taken into consideration. The root node of the tree represents subband S_0 with bins as children that are formed using energy histogram. The leftmost branch represents the first bin and then the next branch represents the second bin and so on. Each node in the second level of the tree corresponds to the immediate following subband. To insert a template in the database, B tree is traversed using the image key generated in Section 4.1.2. After reaching at the leaf node the template is inserted in the database. Each leaf node in the tree is denoted as a class that contains iris templates. The tree structure used for indexing is given in Figure 4.4. Thus, more the number of classes lesser will be the retrieval time. The algorithm for inserting an image in the database is given in Algorithm 4.

The best match for query strip is obtained by searching the database using the key. Each block of the image is divided into subbands using multiresolution reordering of coefficients. The coefficients of each subband is used to compute the energy values.
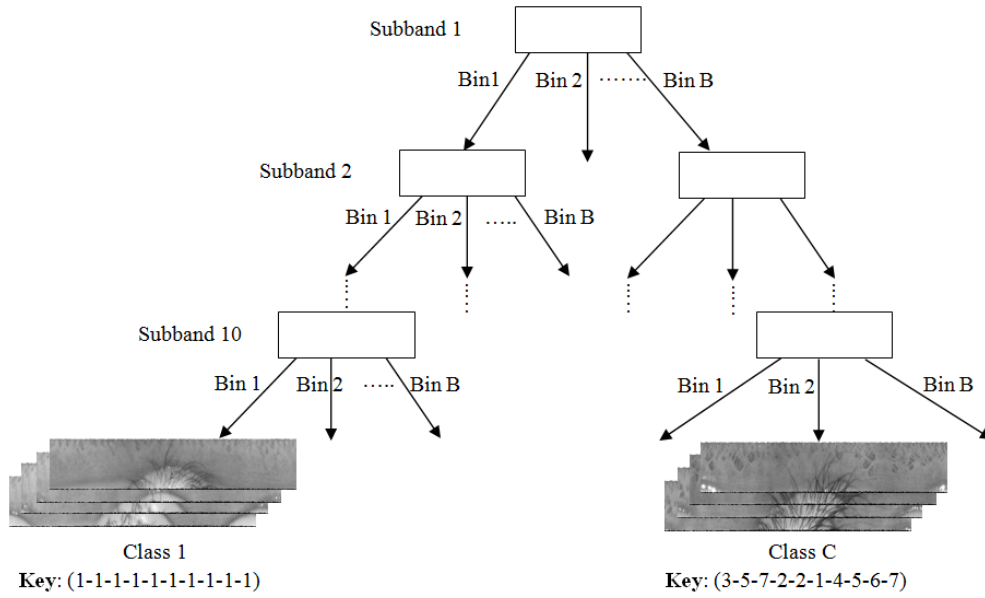
Figure 4.4: B-tree data structure for storing iris templates

Algorithm 4 btree_indexing(n: total number of iris strips)

---

1. For each image I in the database
2. Find DCT for each 8×8 block
3. Reorder the coefficients using subband coding
4. Find total energy value of each subband (S_i)
5. Construct energy histogram (H_i) for each subband using n images
6. Divide each histogram into bins and enumerate them
7. Obtain a key for I using bin numbers of each (H_i)
8. Traverse the tree using key
9. Store the image at the leaf node

The key for query image is calculated by finding bin number of each subband using bin allocation scheme given in Section 4.1.2. This key is used for traversing the tree to arrive at the leaf node and retrieve the images stored in a particular class. The query image is compared with the retrieved images to find a suitable match. However, if the complete key is used for traversing the tree then the probability of finding exact match becomes less. Thus, partial key is used that is constructed from the first B subbands where B is less than total number of subbands i. The images that fall in the same bin for the first B subbands are retrieved and compared with the query template. The step-wise process for finding a query is given in Algorithm 5.
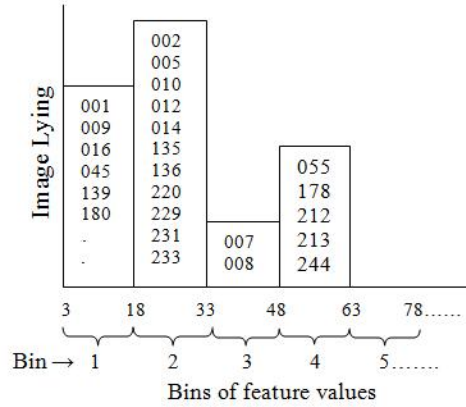
Figure 4.5: Logical grouping of energy histogram
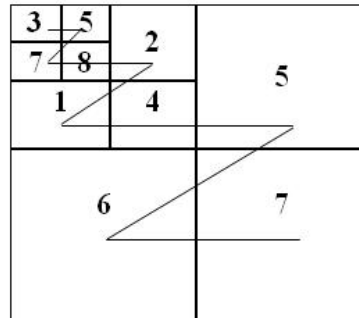
Figure 4.6: Global key formation using Morton order traversal

4.1.3 Experimental Evaluation

The proposed indexing algorithm has been tested on UBIRIS, BATH, CASIA and IITK iris databases. A comparative study on performance rates is done by changing the number of subbands. The number of subbands determines the length of the key. To find an exact match the tree is traversed using all the subbands. However, to obtain similar matches the tree traversal will stop before reaching the leaf and images having the same partial key is retrieved to find a match. The large set of images will be obtained using partial match which in turn increases the penetration rate. For database construction, an input image is divided into 10 subbands using 8×8 block. Further energy histogram of each subband is divided into 5 bins. Thus, every node in B tree is of degree 5. For the sake of convenience fixed number of bins are taken into consideration.

The bin miss rate and penetration rate is obtained by varying the number of

---

Algorithm 5 btree_searching(q: query strip)
1. Find blockwise DCT coefficient of q
2. Reorder the coefficients using subband coding
3. Find energy value of each subband (S_i)
4. Construct query image key using histogram bins
5. Traverse the tree using complete/partial key
6. Retrieve all K images stored in a class
7. Perform comparisons of q with K
8. Find the probable match

---

subbands. With the change in the number of subbands the number of classes formed at leaf node also changes. Table 4.1 shows the number of classes, penetration rate and bin miss rate by varying the number of subbands for UBIRIS, CASIA, BATH and IITK databases. From the table it has been observed that with increase in the number of subbands the number of classes (#) also increases. This is because with less number of subbands the length of global key reduces. The tree is not traversed completely till the leaf node and the images that have same partial key are used to find the match. Hence probability of finding an image is higher in partial traversal compared to complete traversal. The bin miss rate reduces for partial traversal. However, partial traversal gives higher penetration rate due to increase in the number of templates stored in each class. If number of subbands is 2, CASIA database shows bin miss rate of 0.22 with penetration rate of 25.90%. However, if number of subbands is 10, the penetration rate reduces significantly to 0.50% with increased bin miss. Similar results are obtained for UBIRIS, BATH and IITK databases (Table 4.1). Thus, there exists a trade off between the two evaluation rates. The number of subbands used for traversal should be chosen carefully so that both bin miss rate and penetration rate are optimal. Figure 4.7 shows change in bin miss rate for change in number of classes. The graph is plotted for all the four databases. Similarly penetration rate is plotted for different number classes as shown in Figure 4.8. Figure 4.9 represents the relationship between the penetration rate and bin miss rate.
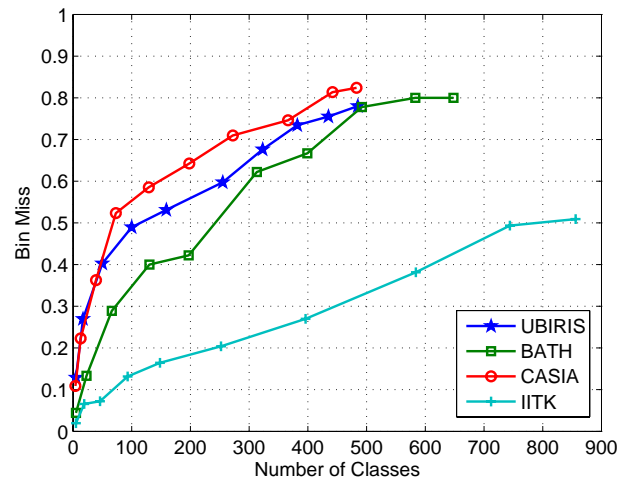
Figure 4.7: Bin Miss rate for change in number of classes
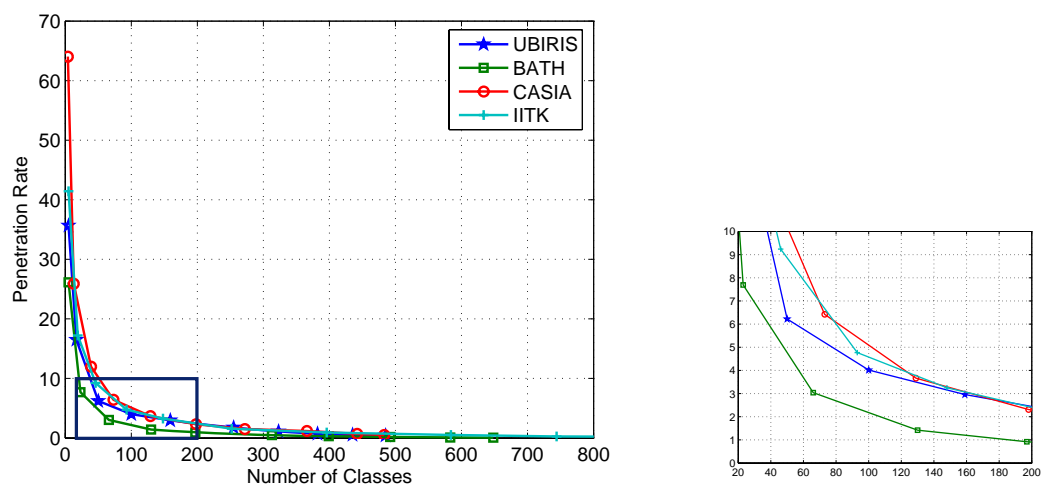
Figure 4.8: Penetration rate for change in number of classes with enlarged view of the selected portion on the right

Table 4.1: Performance rates for change in the number of classes for UBIRIS, CASIA, BATH and IITK datasets. **BM:** Bin Miss Rate, **PR:** Penetration Rate in (%), **C:** Class

| Databases → | UBIRIS | | | BATH | | | CASIA | | | IITK | | |
Subband ↓	C	BM	PR	C	BM	PR	C	BM	PR	C	BM	PR
1	5	0.1286	35.65	5	0.0444	26.14	4	0.1088	64.04	5	0.0197	41.44
2	17	0.2697	16.48	23	0.1333	07.69	13	0.2228	25.90	19	0.0658	17.21
3	50	0.4025	06.22	66	0.2889	03.04	39	0.3627	11.99	46	0.0724	09.24
4	100	0.4896	04.02	130	0.4000	01.42	73	0.5233	06.42	93	0.1316	04.77
5	159	0.5311	02.96	197	0.4222	00.92	129	0.5855	3.67	148	0.1645	03.25
6	255	0.5975	01.75	313	0.6222	00.49	198	0.6425	02.31	252	0.2039	01.56
7	323	0.6763	01.11	399	0.6667	00.30	272	0.7098	01.51	396	0.2697	00.92
8	382	0.7344	00.71	492	0.7778	00.16	366	0.7461	01.16	584	0.3816	00.50
9	435	0.7552	00.54	583	0.8000	00.09	442	0.8135	00.68	744	0.4934	00.27
10	485	0.7801	00.43	648	0.8000	00.06	483	0.8238	00.50	856	0.5089	00.20
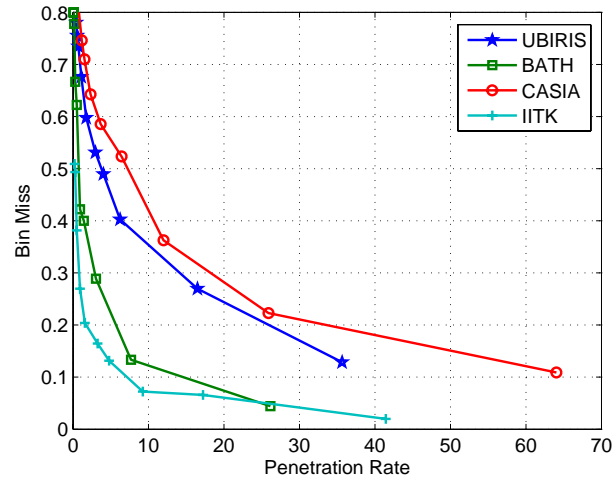
Figure 4.9: Graph showing relationship between Penetration rate versus Bin Miss rate

4.2 Indexing based on Geometric Hashing

Indexing iris database using DCT coefficients works well for cooperative images but fail to perform identification for non-cooperative data. Thus, an efficient indexing scheme is required that is invariant to possible transformations and occlusions. Geometric hashing is an indexing technique for model based object recognition that uses location of keypoints which are invariant to similarity transformation as an index to the hash table [73, 69]. During image retrieval, keypoint locations are computed for the query image and are used to index into the hash table to find the possible matches [74]. The primary advantage of geometric hashing is that it speeds up the search and recognises the object efficiently. Due to aforementioned advantages, geometric hashing technique could find its applicability to biometrics. In [75], automated fingerprint recognition system is proposed that uses geometric hashing to overcome nonlinear distortions and noise obtained during image capture process. In addition to this, geometric hashing along with flash algorithm addresses the requirement of non-criminal fingerprint identification [76].

In the proposed work, geometric hashing approach is used to index large iris biometric database. The block diagram of proposed approach is given in Figure 4.10. The keypoints are detected directly from noise independent annular iris image using SIFT. Geometric invariants are obtained for detected keypoints and stored in
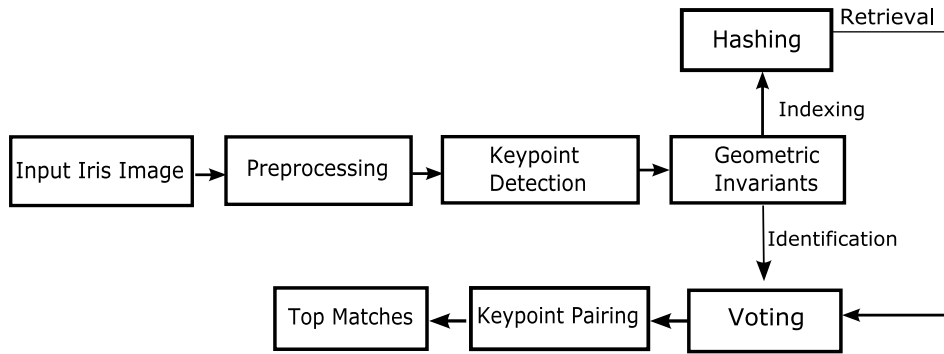
Figure 4.10: Block diagram for geometric hashing based indexing approach

the quantized hash table during indexing. During identification, the hash table is accessed using the invariants and votes are casted. Entries that receive more than certain number of votes are considered as candidate irises. The steps involved in indexing are explained in the following sub-sections.

4.2.1 Indexing

The geometric hashing scheme allows for retrieval of model images that differ from query image by some kind of similarity transformation [77]. It is used for model based object recognition that forms indices from a subset of model points. One of the advantages of geometric hashing is that it is inherently parallel. It has been observed in [78] that with minimal communication and maintenance costs, the concept of geometric hashing is parallel and can be shared among number of cooperating processors. Further, the technique remains invariant to similarity transformations and its representation performs well under partial occlusion.

Index Generation

The detected keypoints on annular iris image are used for indexing the database. The basic idea is to extract local features from an image that remain invariant to similarity transformations. The property of invariance can be explained with the help of a model. The points detected from a sample iris image are plotted on a 2D plane and represent a model (M_i) of ith image in the database. Figure 4.11(a) shows an example. Let us take a pair of keypoints (k_1 and k_2) as an ordered basis to reference model M_i (represented in Figure 4.11(a)). The keypoints are chosen for different

combinations of basis pair with an assumption that k_2 should lie in positive x axis. Thus, for n keypoints the possible basis pairs are atmost $\binom{n}{k}$. The keypoints are scaled such that the magnitude of $\overrightarrow{k_1 k_2}$ is equal to 1. The midpoint between k_1 and k_2 is placed at the origin such that k_1 and k_2 have positive x axis. The remaining points of M_i are placed at different locations. For each choice of basis, the remaining points P of model M_i are computed using

$$P = uP_x^i + vP_y^i + P_0^i \tag{4.3}$$

where $P = [x \; y]$ is the keypoint to be indexed, (u, v) is the location of P after similarity transformation. P_x^i and P_y^i are defined by

$$P_x^i = \frac{k_2 - k_1}{2} \tag{4.4}$$
$$P_y^i = \mathrm{Rot}_{90}(P_x^i) \tag{4.5}$$

where Rot_{90} refers to rotation of coordinate locations by 90 degrees. The midpoint P_0^i between k_1 and k_2 is defined by

$$P_0^i = \frac{k_1 + k_2}{2} \tag{4.6}$$

The keypoints after transformation of model M_i for basis pair k_1 and k_2 are shown in Figure 4.11(b). However, since iris is occluded by upper and lower eyelids thus there is a possibility that the basis (k_1, k_2) may not occur in every instance of model M_i. Thus, different combinations of possible basis pair are used to obtain the geometric invariants as shown in Figure 4.11(c).

Hash Table Organisation

For the formation of hash table, the possible ordered basis pairs for all model images are selected to obtain transformation invariant coordinates (u, v) of the remaining points (x, y). The values of u and v computed from (4.3) remain invariant under similarity transformation and their quantisation allows to have an index (u_q, v_q) into the hash table. In the proposed method discrete intervals are assigned within the range so that each coordinate is quantized to the nearest interval. Each interval is set

(a)   (b)

(c)
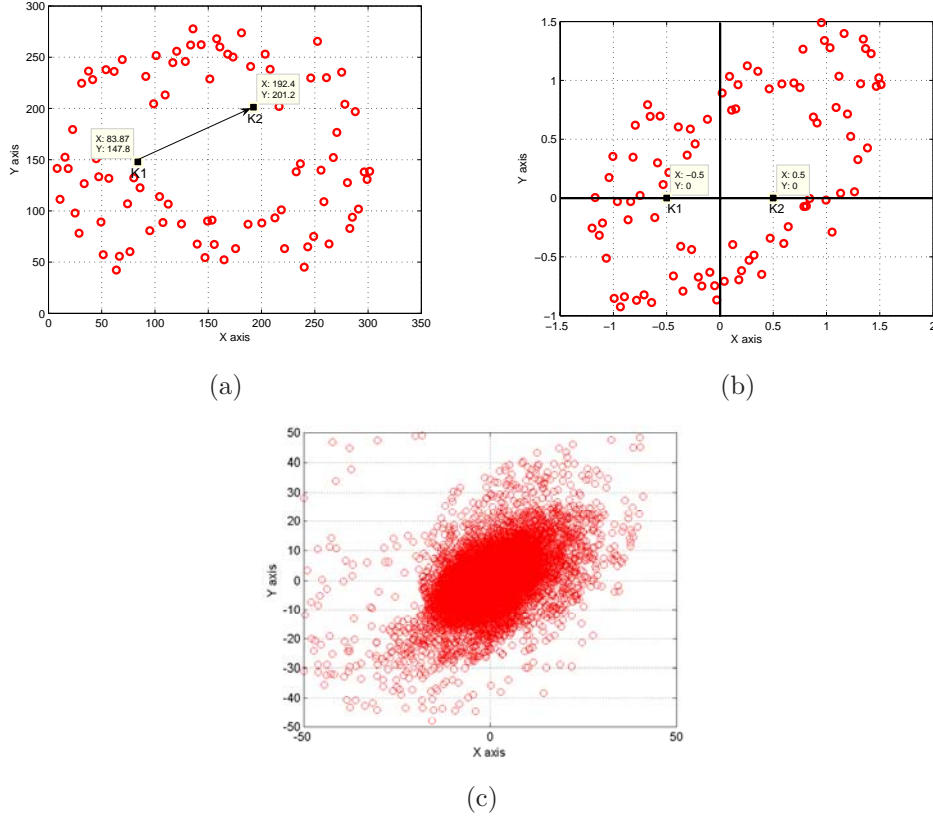
Figure 4.11: Similarity transformation: (a) 2D representation of detected keypoints from annular iris image, (b) Keypoints after similarity transformation for basis pair k_1k_2 and (c) Keypoints after similarity transformation of possible basis pairs

to 0.05 within the range from -25 to 25 in both x and y directions [79]. So there are 1000×1000 entries in the hash table. The hash table at (u_q, v_q) contains entry of the form (M_i, k_1, k_2) for model M_i with basis pair $\overrightarrow{k_1k_2}$. The distribution of data over the hash table is shown in Figure 4.12 for BATH, CASIA, UBIRIS and IITK databases. The hash bin occupancy for quantized hash table is non-uniform and consists of peak that accumulates large number of entries. A uniform distribution of entries over hash table is required to reduce the data retrieval and execution time. Thus, Rigoutsos and Hummel [78] have proposed an efficient technique for uniform distribution of entries in the hash table. If the distribution of data over quantized hash table follows a Gaussian distribution and keypoints detected from iris undergo similarity transformations then probability density $(f(u, v))$ can be defined by

$$f(u, v) = \frac{3}{\pi} \frac{1}{(u^2 + v^2 + 3)^2} \tag{4.7}$$

88

where u and v are invariant coordinates after geometric transformation. After computing the probability density a transformation is performed to map the distribution of entries uniformly in a hash table using rehashing. The rehashing function is applied to transformed coordinates so that equally spaced bins have uniform occupancy. Rehashing function for similarity transformation is given as [78]

$$h(u', v') = (1 - \frac{3}{u^2 + v^2 + 3}, atan2(v, u)) \tag{4.8}$$

where u and v are transformed coordinates and $atan2$ is four quadrant inverse tangent. The uniform distribution of hash bin occupancy after rehashing is given in Figure 4.13. The entries are accumulated uniformly over hash table with several low peaks. The height of peak reduces from 84 to 14 for BATH database with other entries in the hash table being near to uniform distribution. Similarly, there is reduction in peak size for CASIA (613 to 23), UBIRIS (17 to 11) and IITK (384 to 16) databases. This has reduced the accumulation of data at a particular region in the hash table. At $h(u', v')$ an entry is stored in the hash table with (model,basis) pair. The keypoint descriptor obtained using SIFT is stored in the feature database corresponding to a particular iris image. The algorithm for indexing iris biometric database is given in Algorithm 6.

4.2.2   Iris Retrieval

During identification, iris images that have close proximity with the query image are retrieved from the database. The query image is preprocessed to detect annular portion of iris. The keypoints are localised on the annular query iris image and arbitrarily two keypoints are chosen as ordered basis pair and transformed such that its midpoint coincides with the center of origin with direction in the positive x axis. The magnitude of basis vector has unit length. The coordinates of remaining keypoints are defined using (4.3) for chosen basis pair. Each transformed entry is quantized and mapped to the hash table. For each entry found in the corresponding hash table bin, a vote is casted.

The basic assumption is that in case the query image contains basis that corre-

(a) BATH

(b) CASIA

(c) UBIRIS

(d) IITK
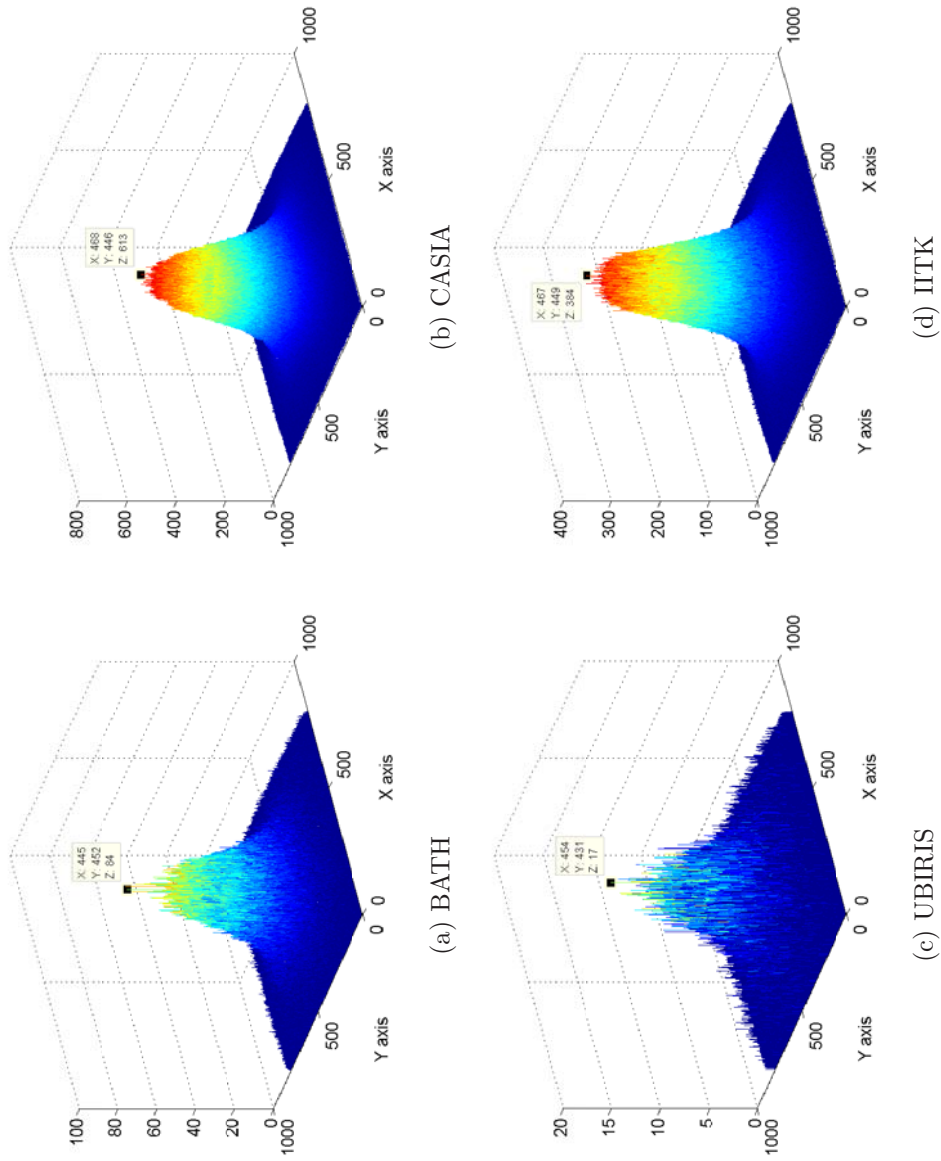
Figure 4.12: Hash bin occupancy prior to rehashing

(a) BATH

(b) CASIA

(c) UBIRIS

(d) IITK
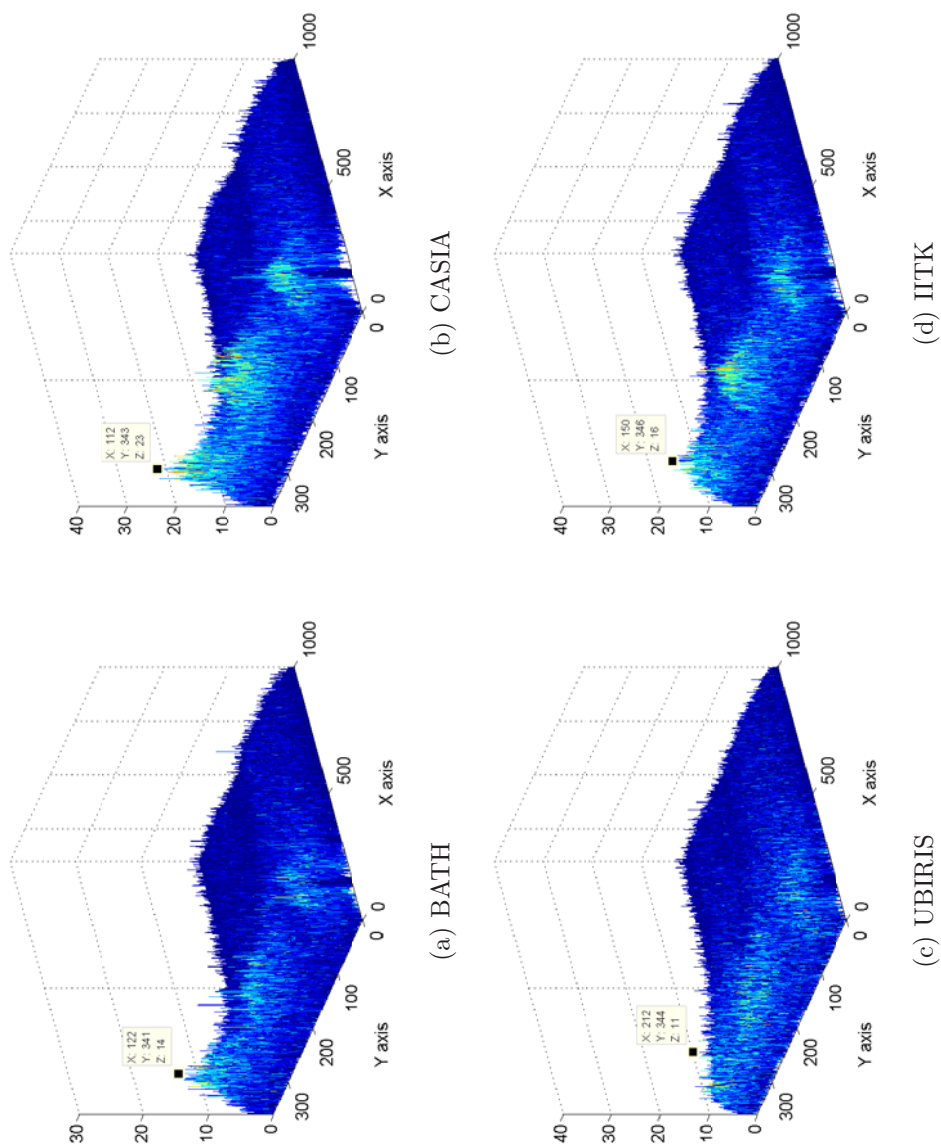
Figure 4.13: Hash bin occupancy after rehashing

sponds to that of model image from database, then it is expected to receive votes from all other unoccluded points. The total number of votes for various basis pairs corresponding to each model image is determined. If the number of votes received for each model images are greater than a threshold (λ) then these images are considered to be potential matches for query image. The algorithm for iris retrieval is given in Algorithm 7. Further the keypoint descriptor for query and candidate model images are compared to find top best matches.

Algorithm 6 Indexing Database

Require: P: Detected Keypoints, n: Number of keypoints, M: Model iris image
Ensure: h: Hash Table
  {Hash Table creation}
  for $i = 1$ to n **do**
    for $j = 1$ to n **do**
      if $i \neq j$ & $P_j(x) - P_i(x) > 0$ **then**
        $P_x = \frac{P_j - P_i}{2}$
        $P_y = \text{Rot}_{90}(P_x)$
        $P_0 = \frac{P_i + P_j}{2}$
        $P = uP_x + vP_y + P_0$
        {Rehashing coordinates}
        $u' = 1 - \frac{3}{u^2 + v^2 + 3}$
        $v' = atan2(v, u)$
        $h(u', v') = (i, j, M)$
      end if
    end for
  end for

4.2.3 Experimental Evaluation

To measure the performance of the proposed iris indexing algorithm, extensive experiments are carried out at two distinct levels. At first level of experiments the accuracy of SIFT classifier is obtained prior to indexing. The performance of SIFT is also compared with one of the known implementation provided by Masek [57]. At the second level of experiment the database is indexed using geometric hashing and probabilities of identification at various ranks are obtained. Detailed discussion of various levels of experiments is given in the following sub-sections

---

Algorithm 7 Retrieval

Require: h: Hash Table, Q: Query keypoints, m: Number of query keypoints, λ: Threshold

Ensure: K: Top K Matches

  {Mapping and Voting}

  for $i = 1$ to m **do**

    for $j = 1$ to m **do**

      if $i \neq j$ & $Q_j(x) - Q_i(x) > 0$ **then**

        Obtain (u, v) using (4.3)

        Obtain (u', v') using (4.8)

        {Cast a vote in the hash table}

        $h(u', v') = h(u', v') + 1$

      end if

    end for

  end for

  {Histogram and Thresholding}

  $H = \text{hist}(h)$

  $K = H \geq \lambda$

Exhaustive Search

During exhaustive search, each point in the probe set is matched with all points in the gallery set (union of gallery sets) without binning. For sequential search the proposed approach uses SIFT for feature extraction without hashing. The results of SIFT without hashing are compared with Masek's approach [57] which uses 1D Log-Gabor wavelets for feature encoding and Hamming distance for matching. The CMC curves for Masek's and SIFT are given in Figure 4.14(a) and 4.14(b) respectively. Identification probabilities at various ranks are given in Table 4.2. Using SIFT the identification probability for UBIRIS, BATH, CASIA and IITK databases is 0.36, 0.32, 0.66 and 0.91 for the top most match respectively. The probability increases to 0.71, 0.96, 0.94 and 0.96 for all databases at rank 100. There is significant improvement in the results for higher ranks. However, the rate of improvement for UBIRIS is low compared to other databases. The reason behind this is, UBIRIS database contains low quality images with several noise factors. Thus, few good quality images taken under ideal illumination conditions fall under rank 1 identification. This analysis shows that number of false acceptances is quite high for higher ranks. This is the reason that the true identity falls at 100th rank. The number of false accep-

tance increases with the increase in the number of comparisons during identification [27]. Similar results are obtained for Masek's approach as given in Table 4.2. Masek's approach gives identification probabilities of 0.33, 0.24, 0.55 and 0.19 for top most match. The identification probability is very low for IITK database due to presence of non-ideal images that leads to errors due to mis-localisation. Masek's approach could not attain desired performance in terms of time as well as accuracy.

ROC curve for two approaches are given in Figure 4.15. Table 4.3 shows the percentage accuracy at EER for SIFT and Masek. From the results it is evident that the accuracy of SIFT is fairly high compared to Masek's approach. This is mainly due to localisation performance. In addition to this, SIFT is invariant to similarity transformations and occlusion. However, the two approaches perform equally well for CASIA as the percentage mis-localisation is less for Masek's approach. Table 4.4 shows average time taken (in seconds) by different approaches. Masek's approach takes more time compared to SIFT due to masking and feature extraction. For IITK database, both the approaches take more time because images are collected at varying sizes to check scale invariance. The average penetration coefficient for exhaustive search is 1 as whole database is scanned to find a match with bin miss rate of 0.

Index based search

To improve the performance in terms of time as well as accuracy, the databases are indexed using geometric hashing of SIFT keypoints. Probability of identification at various ranks is shown in Table 4.5. The rank 1 identification increases to 0.82, 0.45, 0.82 and 0.95 for UBIRIS, BATH, CASIA and IITK databases respectively. Identification probability for databases is 1.00, 0.98, 0.99 and 1.00 at rank 100. The performance improves considerably after indexing. BATH database gives reduced identification probability due to low texture resolution that leads to reduction in the number of keypoints. UBIRIS database performs better after indexing where the probability of identification improves from 0.36 to 0.82 at rank 1. IITK database gives identification probability of 1 at rank 3. The reason behind is that images from IITK database consists of rich quality texture features with higher resolution. The probability of identification becomes 1.00 for all the databases at 250 ranks. This is a
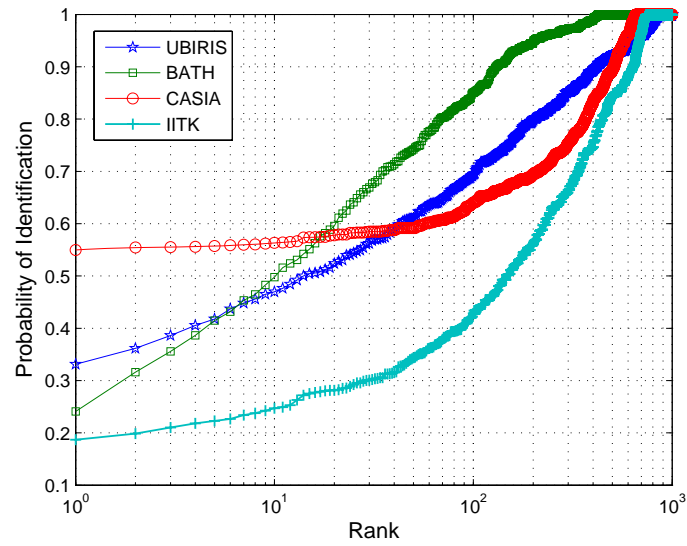
(a) Masek's approach
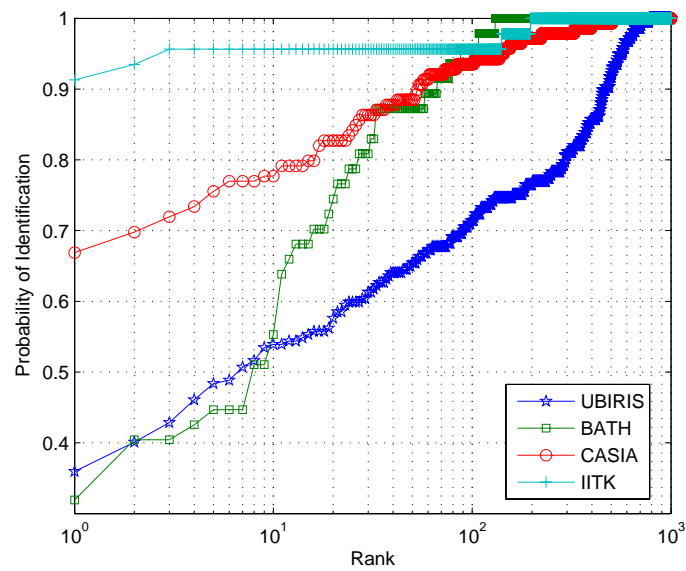
(b) SIFT without hashing

Figure 4.14: CMC curve for exhaustive search

Table 4.2: Identification probabilities at various ranks for exhaustive search

Ranks	UBIRIS		BATH		CASIA		IITK	
	M	S	M	S	M	S	M	S
1	0.33108	0.35945	0.24091	0.31915	0.54973	0.66187	0.18676	0.91304
2	0.36149	0.40092	0.31591	0.40426	0.55429	0.69784	0.19856	0.93478
3	0.38626	0.42857	0.35568	0.40426	0.55505	0.71942	0.21035	0.95652
5	0.41892	0.48387	0.41477	0.44681	0.55733	0.75540	0.2228	0.95652
10	0.46959	0.53917	0.49773	0.55319	0.5634	0.77698	0.24705	0.95652
50	0.61374	0.65438	0.74205	0.87234	0.5915	0.88489	0.34338	0.95652
100	0.69932	0.71429	0.85	0.95745	0.64085	0.93525	0.42857	0.95652
200	0.80405	0.76498	0.94659	1.00	0.694	0.97122	0.56029	1.00
250	0.82995	0.77880	0.96364	1.00	0.72513	0.97842	0.63172	1.00
500	0.91892	0.91705	0.99886	1.00	0.8937	1.00	0.84273	1.00
1000	0.99887	1.00	1.00	1.00	1.00	1.00	0.99934	1.00

M: Masek's approach and **S:** SIFT without hashing
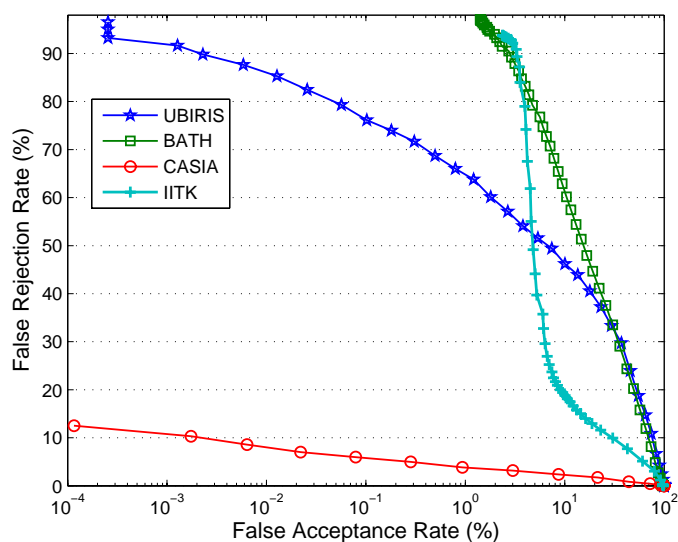
(a) Masek's approach
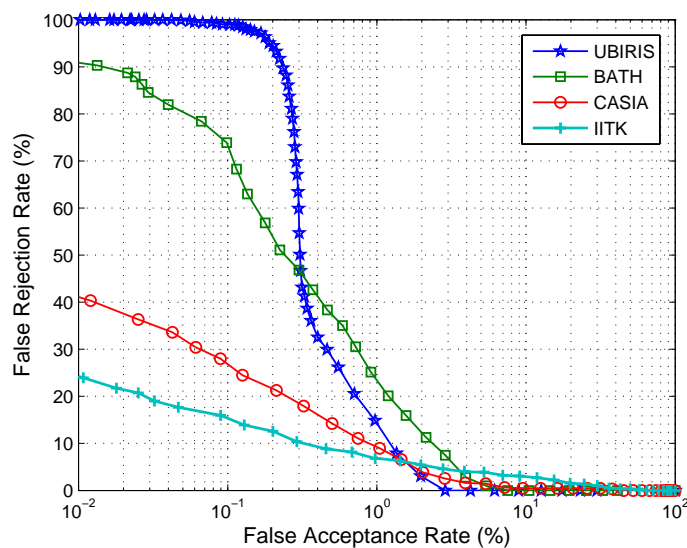
(b) SIFT without hashing

Figure 4.15: ROC curve for exhaustive search

Table 4.3: Accuracy at EER (in %) using exhaustive search (Prior to indexing) for SIFT and Masek's approach

Database	Masek's Approach	SIFT Without Hashing
UBIRIS	71.87	97.48
BATH	68.33	94.82
CASIA	97.61	97.06
IITK	85.62	96.03

Table 4.4: Average time (in seconds) by individual searching approaches

Approach ↓ Database →	UBIRIS	BATH	CASIA	IITK
Masek's Approach	11.3290	11.4319	28.9373	263.7545
SIFT Without Hashing	05.6888	03.5450	19.4371	39.5302
SIFT with Geometric Hashing	03.5882	01.1375	09.2196	10.7490

significant reduction in comparison to exhaustive search using SIFT without hashing and Masek's approach where probability of identification becomes 1.00 at 1500 ranks.

The efficiency of identification system is further measured in terms of penetration coefficient and bin miss rate. The penetration coefficient is obtained for change in threshold (λ). Here the value of λ is chosen by keeping a bound on the number of votes. Figure 4.16 shows relationship between penetration coefficient and threshold while Figure 4.17 provides the relationship between bin miss rate and threshold. From the graphs it can be seen that penetration coefficient decreases with increase in the value of threshold while bin miss rate shares direct relationship with threshold. Thus, there exists a trade off between two evaluation rates. The value of threshold should be chosen depending upon the deployment of the identification system. If the demand of application is highly secure than bin miss rate should be made as low as possible. In case of low secure applications where time is a major constraint, the penetration rate is reduced at acceptable bin miss rate. However, neither penetration rate nor bin miss rate can be reduced to an insignificant small value. Figure 4.18 shows the relationship between two performance rates. The threshold value is chosen where two curves intersects i.e., PR=BM. The values given in Table 4.5 are obtained for threshold with bin miss 0. However, if bin miss is reduced to 0 the penetration rate becomes close to 1. The CMC curve is obtained after indexing as shown in Figure 4.19 for chosen threshold λ where BM=PR.

Average time required to claim identification also reduces due to binning as shown in Table 4.4. The ROC curve for index based search is given in Figure 4.20. The accuracy at EER after indexing, given in Table 4.6, shows that the proposed indexing approach performs better than the exhaustive search. The proposed approach gives an accuracy of 98.29% for BATH database in comparison to 94.82% obtained using

Table 4.5: Identification probabilities at various ranks using indexing scheme for threshold where BM=0

Ranks	UBIRIS	BATH	CASIA	IITK
1	0.82028	0.44681	0.82014	0.95652
2	0.86636	0.51064	0.84892	0.97826
3	0.88018	0.51064	0.86331	1.00
5	0.91705	0.61702	0.87050	1.00
10	0.94009	0.80851	0.87770	1.00
50	0.99078	0.91489	0.97122	1.00
100	1.00	0.97872	0.98561	1.00
200	1.00	0.97872	1.00	1.00
250	1.00	1.00	1.00	1.00

Table 4.6: Accuracy at EER (%) for proposed indexing approach

Database	UBIRIS	BATH	CASIA	IITK
Accuracy	97.57	98.29	98.55	99.61

exhaustive search. There is not substantial improvement for CASIA and UBIRIS but for IITK database it outperforms with an accuracy of 99.61%. Experimentally it has been observed that the accuracy of SIFT operator on IITK database is 96% for exhaustive search. The value of accuracy increases to 99.61% after indexing. The reason behind variation in the value of accuracy for the same database using same classifier is that during exhaustive search the error rates are quiet high due to increased number of comparisons while during indexing the size of database reduces which in turn reduces the number of comparisons and false acceptances.

The experiments done on non-cooperative database include images with various transformations, occlusions and variation in illumination. The system has been tested for such cases with change in illumination (cases for UBIRIS), occlusion (CASIA) and similarity transformations (IITK and CASIA). Few sample instances are shown in Figure 4.21 that represents the rank of identification for the true match. An instance which represents an element from the probe set is shown on the left with corresponding match from the gallery set along with the rank on the right side.
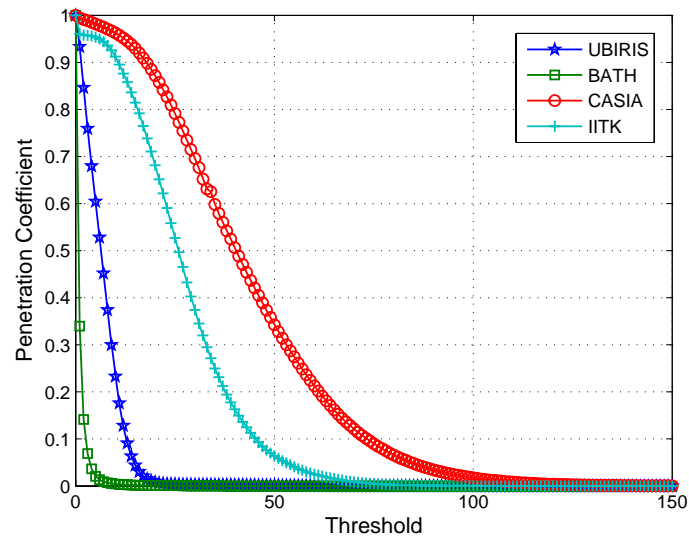
Figure 4.16: Relationship between Penetration coefficient and threshold
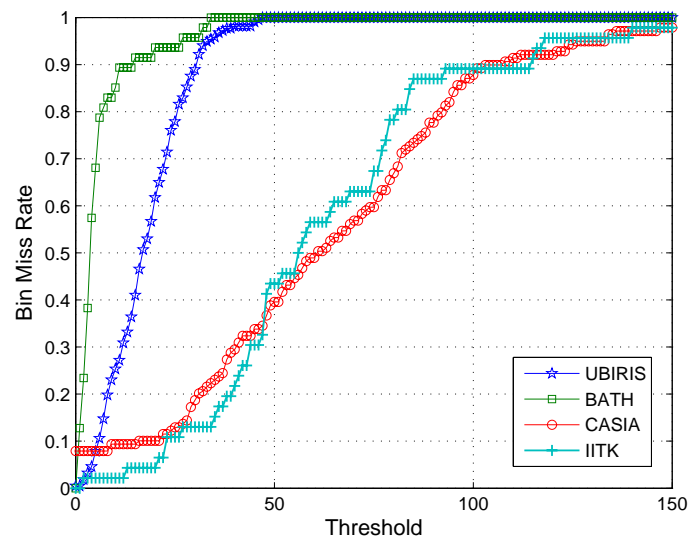
Figure 4.17: Relationship between Bin Miss rate and threshold
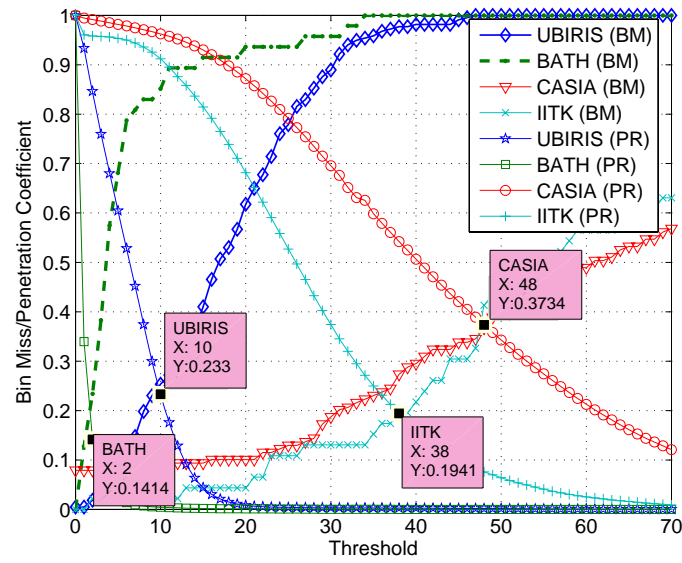
Figure 4.18: Relationship between Penetration coefficient and Bin Miss rate
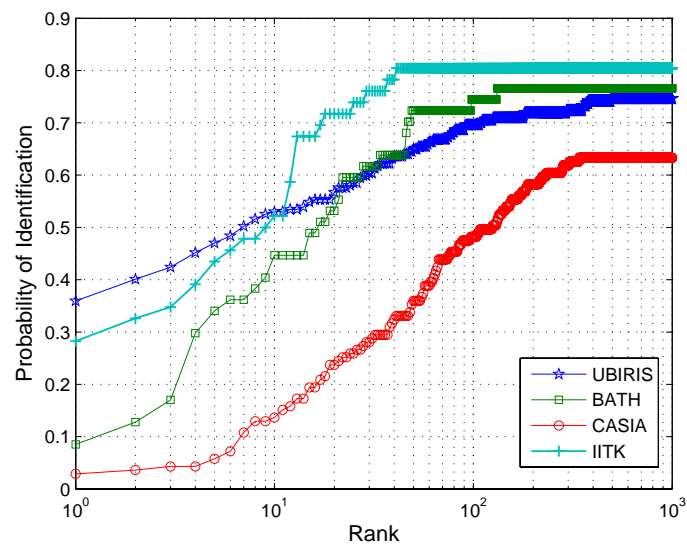
Figure 4.19: CMC Curve for geometric hashed based indexing scheme for threshold where PR=BM
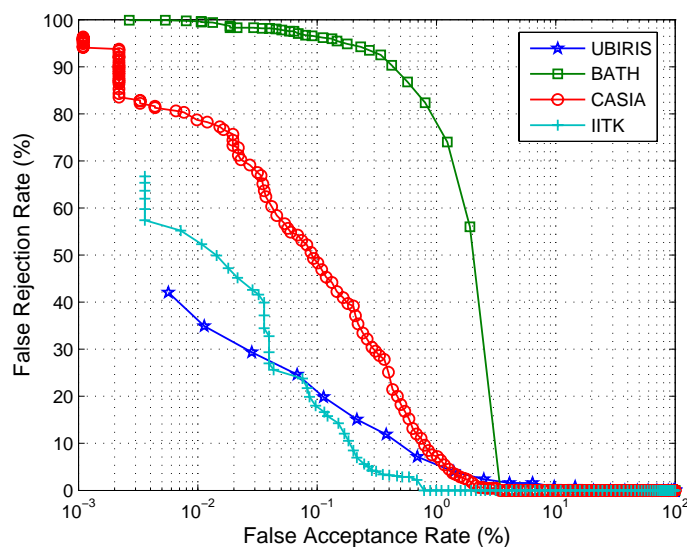
Figure 4.20: ROC curve of geometric hashed based indexing approach
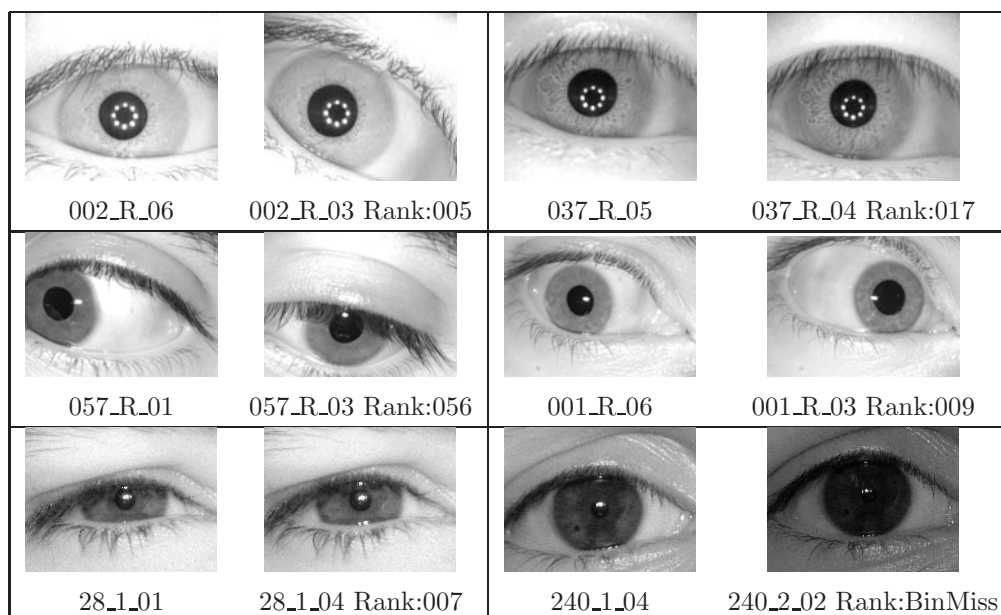
Figure 4.21: Correct matches using geometric hashing technique. For each test case, image on the left is an element from probe set whereas image on right is an element from gallery set along with rank of identification. Row 1, 2 and 3 represents instances from CASIA, IITK and UBIRIS databases respectively.

4.3 Summary

In this chapter two novel approaches are proposed for indexing iris biometric database. The first approach uses energy histogram of DCT coefficients from doubly dimensionless polar iris image. The system prunes database to approximately 20% of the original size with low bin miss rate. However, this approach uses polar transformed image that introduces aliasing errors. Further, DCT is a global feature extraction approach that fails for work for non-cooperative images. The second approach uses geometric hashing for indexing. It is found to be robust to similarity transformations, occlusion as well as non-uniform illumination. Features are extracted directly from annular iris image to overcome the effect of aliasing. Performance for exhaustive search and indexing based search are critically analyzed. Exhaustive search using SIFT classifier gives an identification probability of 0.91 at top most match for IITK database. The probability of identification for Masek's approach is considerably low due to mis-localisations and inability of feature extractor to handle variations between genuine and imposter templates. Further, the number of false acceptances grows geometrically with increase in the size of the database and this leads to the reduction in the performance. Searching an indexed IITK database using geometric hashing gives identification probability of 1.00 at rank 3. The time required for iris retrieval also reduces significantly by 29 seconds (approx). The accuracy at EER is obtained within each bin and system is performing with an average accuracy of 98.5%. After indexing the total amount of database to be searched with acceptable bin miss rate is obtained. The penetration rate and bin miss rate can be varied depending upon the choice of threshold. In the proposed work, threshold is chosen where BM=PR which gives an average penetration rate and bin miss rate of 0.24. The system can handle several variations in the probe set as tested empirically. Results show that the proposed iris identification system can be deployed for applications where both speed and accuracy cannot be compromised.

Chapter 5

Conclusions and Future Work

This thesis proposes novel preprocessing, feature extraction and identification approaches for cooperative as well as non-cooperative iris databases. The first contribution is made to develop an efficient preprocessing approach that segments non-ideal iris imagery. The proposed approach removes specular highlights and localises pupil boundary using spectrum image. In order to overcome the problem of aliasing due to polar transformation, the annular region underlying pupil and iris boundary is considered directly for feature extraction. From the annular image, the occlusion due to eyelids is removed using sector based approach to generate *Noise Independent Annular Iris* image. The experiments are done using proposed preprocessing approach and known Masek's approach on various available databases. From the results it is found that the average mis-localisation percentage is 1.55% which is significantly low compared to Masek's approach.

The second contribution is made to develop local feature extraction approach for iris. The main drawback of global approaches is that the they fail to work for large variations in individual's pose, illumination and occlusion. The accuracy is obtained for well known global feature extraction approaches such as Haar wavelet and Log-Gabor wavelet. The system is performing with an average accuracy of 79.67%. Further, global approaches are not suitable for noise independent annular iris as the size of iris varies due to illumination. In order to overcome these issues, an attempt has been made to devise local keypoint descriptors for iris. Local features are less sensitive to variations since the features are extracted from the subset regions around interest points. At first level *Harris Corner Detector* is applied to iris and corner

points are paired using Euclidean distance. However, distance based measure gives an average accuracy of 75.46% which is relatively low. The position of corner point features may change due change in head position or viewpoint of an individual. Thus, entropy information is obtained for a block around every detected corner point. For corner point pairing, a novel *Dual Stage* approach is developed that combines spatial distance and mutual information of entropy hierarchically. This approach performs with an average accuracy of 94% which still leaves behind a scope to further explore techniques to improve performance. At second level, one of the well known keypoint descriptor known as *Scale Invariant Feature Transform* (SIFT) has been applied to iris for feature extraction and matching. The approach has been tested for various forms of iris and performs with an enhanced accuracy of 96.43% for annular iris. But the main drawback of SIFT is that it is computationally costly due to higher dimensionality of feature descriptor. At last level, recently developed keypoint descriptor called *Speeded Up Robust Features* (SURF) is applied to annular iris. SURF has already been proposed for camera calibration and object recognition but its applicability is new to iris. SURF based recognition system performs with an average accuracy of 97.72% using noise independent annular iris. This marks an improvement in performance for BATH, CASIA and IITK databases but accuracy reduces for UBIRIS database. SURF approximates or even outperforms previously proposed keypoint descriptors with respect to repeatability, distinctiveness, robustness and time.

The last and most valuable contribution is made to develop an identification approach for iris that performs better than the state-of-the-art system. We have investigated two different techniques for iris database indexing. First approach indexes the database using energy histogram of DCT coefficients. DCT based approach performs with bin miss rate of 0.22 and penetration rate of 20%. However, the proposed DCT based approach suffers from few limitations like considering the doubly dimensionless iris image for indexing introduces aliasing artifacts and DCT is incapable to handle large variations in the input data. The second approach addresses the aforementioned issues by indexing the database using *Geometric Hashing* of SIFT keypoints. This approach performs significantly well with an average accuracy of 98.5% at the threshold

where BM=PR which gives an average penetration rate and bin miss rate of 0.24.

To conclude with this thesis, the proposed approaches have been critically analysed and few limitations have been observed. These limitations can be studied and refined that promotes further research in the proposed area. The sector based preprocessing approach uses fixed size mask for removing eyelids. This fails for images with no occlusion or occlusion greater than the mask size. Thus, an adaptive mask is required that can automatically detect eyelids by fitting curves on the lower and upper eyelid edge segments. Performance of SURF can be further improved for UBIRIS and computational cost can be reduced by applying box filters of varying sizes on the original image in parallel. The accuracy of geometric hashing can be further improved by extracting features using SURF. SURF extracts more number of keypoints which in turn increases the number of basis pairs $\binom{n}{2}$ for indexing. Thus, keypoints extracted from SURF can be filtered by applying some dimensionality reduction approaches while still preserving recognition time and accuracy. Finally, the concept of geometric hashing can be inherently made parallel by using fully connected machines.

Bibliography

[1] CASIA Database. http://www.cbsr.ia.ac.cn/english/IrisDatabase.asp.

[2] G. Xu, Z.F. Zhang, and Y.D. Ma. Automatic iris segmentation based on local areas. In *International Conference on Pattern Recognition*, volume 4, pages 505–508. IEEE Computer Society, 2006.

[3] J. Daugman. The importance of being random: statistical principles of iris recognition. *Pattern Recognition*, 36(2):279 – 291, 2003.

[4] D. G. Lowe. Distinctive image features from scale-invariant keypoints. *International Journal of Computer Vision*, 60(2):91–110, 2004.

[5] H. Bay, A. Ess, T. Tuytelaars, and L. Van Gool. Speeded-up robust features (surf). *Computer Vision and Image Understanding*, 110(3):346 – 359, 2008.

[6] H. Bay, T. Tuytelaars, and L. V. Gool. Surf: Speeded up robust features. In *9th European Conference on Computer Vision*, Graz Austria, 2006.

[7] K.W. Bowyer, K. Hollingsworth, and P. J. Flynn. Image understanding for iris biometrics: A survey. *Computer Vision and Image Understanding*, 110(2):281–307, 2008.

[8] R. Bolle and S. Pankanti. *Biometrics Personal Identification in Networked Society*. Kluwer Academic Publishers, Norwell, MA, USA, 1998.

[9] A. K. Jain, A. Ross, and S. Prabhakar. An introduction to biometric recognition. *IEEE Transactions on Circuits and Systems for Video Technology*, 14:4–20, 2004.

[10] A. K. Jain, P. Flynn, and A. A. Ross. *Handbook of Biometrics*. Springer-Verlag New York, Inc., Secaucus, NJ, USA, 2007.

[11] A. K. Jain and D. Maltoni. *Handbook of Fingerprint Recognition*. Springer-Verlag New York, Inc., Secaucus, NJ, USA, 2003.

[12] J. L. Wayman, A. K. Jain, D. Maltoni, and D. Maio. *Biometric Systems: Technology, Design and Performance Evaluation*. Springer-Verlag New York, Inc., Secaucus, NJ, USA, 2004.

[13] S. Sirohey, A. Rosenfeld, and Z. Duric. Eye tracking. Technical Report CAR-TR-922, Center for Automation Research, University of Maryland, College Park, 1999.

[14] J. L. Wayman. Error rate equations for the general biometric system. *IEEE Robotics & Automation Magazine*, 6(1):35–48, 1999.

[15] M. Golfarelli, D. Maio, and D. Maltoni. On the error-reject trade-off in biometric verification systems. *IEEE Transactions on Pattern Analysis and Machine Intelligence*, 19(7):786–796, 1997.

[16] A. Y. Johnson, J. Sun, and A. F. Bobick. Predicting Large Population Data Cumulative Match Characteristic Performance from Small Population Data. In *AVBPA*, pages 821–829, 2003.

[17] H. Proenca and L. A. Alexandre. UBIRIS: A noisy iris image database. In *13th International Conference on Image Analysis and Processing - ICIAP 2005*, volume LNCS 3617, pages 970–977. Springer, 2005.

[18] BATH University Database. http://www.bath.ac.uk/elec-eng/research/sipg/irisweb.

[19] Database of Indian Institute of Technology Kanpur. http://www.cse.iitk.ac.in/users/biometrics.

[20] L. Ma, T. Tan, Y. Wang, D. Zhang, and C. Boyce. Critique: Efficient iris recognition by characterizing key local variations. *IEEE Transactions on Image Processing*, 13(6), 2008.

[21] H. Proenca and L.A. Alexandre. Iris recognition: An analysis of the aliasing problem in the iris normalization stage. In *International Conference on Computational Intelligence and Security*, volume 2, pages 1771–1774, 2006.

[22] J. Daugman. How iris recognition works. In *International Conference on Image Processing 2002*, volume 1, pages 33–36, 2002.

[23] R.P. Wildes. Iris recognition: an emerging biometric technology. *Proceedings of the IEEE*, 85(9):1348–1363, 1997.

[24] L. Ma, T. Tan, Y. Wang, and D. Zhang. Efficient iris recognition by characterizing key local variations. *IEEE Transactions on Image Processing*, 13(6):739–750, 2004.

[25] W. W. Boles and B. Boashash. A Human Identification Technique using Images of the Iris and Wavelet Transform. *IEEE Transactions on Signal Processing*, 46(4):1185–1188, 1998.

[26] D. M. Monro, S. Rakshit, and D. Zhang. DCT-based Iris Recognition. *IEEE Transactions on Pattern Analysis and Machine Intelligence*, 29(4):586–595, 2007.

[27] A. Mhatre, S. Chikkerur, and V. Govindaraju. Indexing biometric databases using pyramid technique. In *International Conference on Audio and Video Based Biometric Person Authentication (AVBPA)*, pages 841–849, 2005.

[28] M. Kokare, B. N. Chatterji, and P. K. Biswas. Cosine-modulated wavelet based texture features for content-based image retrieval. *Pattern Recognition Letters*, 25(4):391 – 398, 2004.

[29] L. Flom and A. Safir. Iris recognition system. U.S. Patent 4,641,349, 1987.

[30] J. Daugman. Biometric personal identification system based on iris analysis. U.S. Patent No. 5,291,560, 1994.

[31] A.L. Yuille, D.S. Cohen, and P.W. Hallinan. Feature extraction from faces using deformable templates. In *IEEE Computer Society Conference on Computer Vision and Pattern Recognition*, pages 104–109, 1989.

[32] Y. Huang, S. Luo, and E. Chen. An efficient iris recognition system. In *International Conference on Machine Learning and Cybernetics*, volume 1, pages 450–454, 2002.

[33] Y. Liu, S. Yuan, X. Zhu, and Q. Cui. A practical iris acquisition system and a fast edges locating algorithm in iris recognition. In *20th IEEE Conference on Instrumentation and Measurement Technology*, volume 1, pages 166–168, 2003.

[34] H. Sung, J. Lim, J. Park, and Y. Lee. Iris recognition using collarette boundary localization. In *17th International Conference on Pattern Recognition*, volume 4, pages 857–860, 2004.

[35] X. Liu, K.W. Bowyer, and P.J. Flynn. Experiments with an improved iris segmentation algorithm. In *Fourth IEEE Workshop on Automatic Identification Advanced Technologies*, pages 118–123, 2005.

[36] X. Feng, C. Fang, X. Ding, and Y. Wu. Iris localization with dual coarse-to-fine strategy. In *18th International Conference on Pattern Recognition*, volume 4, pages 553–556, 2006.

[37] Q. Tian, Q. Pan, Y. Cheng, and Q. Gao. Fast algorithm and application of hough transform in iris segmentation. In *International Conference on Machine Learning and Cybernetics*, volume 7, pages 3977–3980, 2004.

[38] A. Zaim, M. Quweider, J. Scargle, J. Iglesias, and R. Tang. A robust and accurate segmentation of iris images using optimal partitioning. In *18th International Conference on Pattern Recognition*, volume 4, pages 578–581, 2006.

[39] T.A. Camus and R. Wildes. Reliable and fast eye finding in close-up images. In *16th International Conference on Pattern Recognition*, volume 1, pages 389–394, 2002.

[40] B. Bonney, R. Ives, D. Etter, and D. Yingzi. Iris pattern extraction using bit planes and standard deviations. In *Conference Record of the Thirty-Eighth Asilomar Conference on Signals, Systems and Computers*, volume 1, 2004.

[41] H. Proenca and L.A. Alexandre. Iris segmentation methodology for non-cooperative recognition. *IEE Proceedings on Vision, Image and Signal Processing*, 153(2):199–205, 2006.

[42] M. Tucceryan. Moment-based texture segmentation. *Pattern Recognition Letters*, 15(7):659–668, 1994.

[43] S.J. Pundlik, D.L. Woodard, and S.T. Birchfield. Non-ideal iris segmentation using graph cuts. In *IEEE Computer Society Conference on Computer Vision and Pattern Recognition Workshops*, pages 1–6, 2008.

[44] Z.A. Sun, T.N. Tan, and Y.H. Wang. Robust encoding of local ordinal measures: A general framework of iris recognition. In *ECCV Workshop on Biometric Authentication*, pages 270–282, 2004.

[45] P. Yao, J. Li, X. Ye, Z. Zhuang, and B. Li. Iris recognition algorithm using modified log-gabor filters. In *Proceedings of the 18th International Conference on Pattern Recognition*, pages 461–464, 2006.

[46] Christel Loic, L. Torres, and M. Robert. Person identification technique using human iris recognition. In *Vision Interface*, pages 294–299, 2002.

[47] P. Gupta, A. Sana, H. Mehrotra, and C. Jinshong Hwang. An efficient indexing scheme for binary feature based biometric database. volume 6539, page 653909. SPIE, 2007.

[48] U. Jayaraman, S. Prakash, Devdatt, and P. Gupta. An indexing technique for biometric database. In *International Conference on Wavelet Analysis and Pattern Recognition*, volume 2, pages 758–763, 2008.

[49] U. Jayaraman, S. Prakash, and P. Gupta. Indexing multimodal biometric databases using kd-tree with feature level fusion. In *4th International Conference on Information Systems Security*, pages 221–234, Berlin, Heidelberg, 2008. Springer-Verlag.

[50] R. Mukherjee and A. Ross. Indexing iris images. In *19th International Conference on Pattern Recognition*, pages 1–4, 2008.

[51] N. B. Pusan and N. Sudha. A novel iris database indexing method using the iris color. In *3rd IEEE Conference on Industrial Electronics and Applications*, pages 1886–1891, 2008.

[52] S. K. Pal and P. Mitra. *Pattern Recognition Algorithms for Data Mining: Scalability, Knowledge Discovery, and Soft Granular Computing*. Chapman & Hall, Ltd., London, UK, UK, 2004.

[53] A. K. Pujari. *Data Mining Techniques*. Universities Press, India, 2001.

[54] C. Harris and M. Stephens. A combined corner and edge detection. In *Proceedings of The Fourth Alvey Vision Conference*, pages 147–151, 1988.

[55] R.C. Gonzalez and R.E. Woods. *Digital Image Processing (3rd Edition)*. Prentice Hall, 2007.

[56] B. Lipinski. Iris recognition: Detecting the pupil. Connexions website, 2004. http://cnx.org/content/m12487/1.4/.

[57] L. Masek and P. Kovesi. Matlab Source Code for a Biometric Identification System based on Iris Patterns. The School of Computer Science and Software Engineering, The University of Western Australia., 2003.

[58] L.V. Birgale and M. Kokare. Iris recognition using discrete wavelet transform. In *International Conference on Digital Image Processing*, pages 147–151, 2009.

[59] C. Schmid, R. Mohr, and C. Bauckhage. Evaluation of interest point detectors. *International Journal of Computer Vision*, 37(2):151–172, 2000.

[60] M. I. A. Lourakis, A. A. Argyros, and K. Marias. A graph-based approach to corner matching using mutual information as a local similarity measure. In *17th International Conference on Pattern Recognition*, volume 2, pages 827–830 Vol.2, 2004.

[61] SIFT for Matlab. http://www.vlfeat.org/~vedaldi/code/sift.html.

[62] M. Brown and D. Lowe. Invariant features from interest point groups. In *In British Machine Vision Conference*, pages 656–665, 2002.

[63] T. Lindeberg. Feature detection with automatic scale selection. *International Journal of Computer Vision*, 30(2):79–116, 1998.

[64] K. Mikolajczyk and C. Schmid. An affine invariant interest point detector. In *Proceedings of the 7th European Conference on Computer Vision-Part I*, pages 128–142. Springer-Verlag, 2002.

[65] C. Valgren and A. J. Lilienthal. SIFT, SURF and Seasons: Long-term outdoor localization using local features. In *Proceedings of the European Conference on Mobile Robots (ECMR)*, pages 253–258, 2007.

[66] P. Viola and M. Jones. Rapid object detection using a boosted cascade of simple features. In *Proceedings of IEEE Computer Society Conference on Computer Vision and Pattern Recognition*, volume 1, pages 511–518, 2001.

[67] P. Simard Eon, P. Y. Simard, P. Haffner, and Y. Lecun. Boxlets: a fast convolution algorithm for signal processing and neural networks. In *Advances in Neural Information Processing Systems*, pages 571–577. MIT Press, 1999.

[68] Y. Fang, J. Cheng, K. Wang, and H. Lu. Hand gesture recognition using fast multi-scale analysis. In *Fourth International Conference on Image and Graphics*, pages 694–698, 2007.

[69] H.J. Wolfson and I. Rigoutsos. Geometric Hashing: An Overview. *IEEE Computational Science & Engineering*, 4(4):10–21, 1997.

[70] S. A. Khayam. The discrete cosine transform (dct): Theory and application. Technical report, Michigan State University, 2003.

[71] E. Albuz, E. Kocalar, and A. A. Khokhar. Scalable image indexing and retrieval using wavelets, 1998.

[72] D. Wu and L. Wu. Image retrieval based on subband energy histograms of reordered dct coefficients. In *6th International Conference on Signal Processing*, volume 1, pages 596–599, 2002.

[73] Y. Lamdan, J. T. Schwartz, and H. J. Wolfson. Object recognition by affine invariant matching. In *Computer Vision and Pattern Recognition (CVPR)*, pages 335–344, 1988.

[74] W.E.L. Grimson and D.P. Huttenlocher. On the sensitivity of geometric hashing. In *Third International Conference on Computer Vision*, pages 334–338, 1990.

[75] R. Boro and S. D. Roy. Fast and Robust Projective Matching for Fingerprints using Geometric Hashing. In *Indian Conference on Computer Vision, Graphics and Image Processing*, pages 681–688, 2004.

[76] R.S. Germain, A. Califano, and S. Colville. Fingerprint matching using transformation parameter clustering. *IEEE Computational Science & Engineering*, 4(4):42–49, 1997.

[77] H. V. Dijck. *Object recognition with stereo vision and geometric hashing*. PhD thesis, Advanced School for Computing and Imaging, University of Twente, P.O. Box 217, 7500 AE Enschede, Netherlands, 1999.

[78] I. Rigoutsos and R. Hummel. Implementation of geometric hashing on the Connection Machine. In *Workshop on Directions in Automated CAD-Based Vision*, pages 76–84, 1991.

[79] A.T.S. Au and P.W.M. Tsang. Affine invariant recognition of 2D occluded objects using geometric hashing and distance transformation. In *Proceedings of IEEE TENCON. Digital Signal Processing Applications*, volume 1, pages 64–67, 1996.

Dissemination

Published

1. **Hunny Mehrotra**, Banshidhar Majhi, and Phalguni Gupta. Robust iris indexing scheme using geometric hashing of sift keypoints. *Journal of Network and Computer Applications (Elsevier)*, In press, 2010. DOI: 10.1016/j.jnca.2009.12.005.

2. **Hunny Mehrotra**, Banshidhar Majhi, and Phalguni Gupta. Annular iris recognition using surf. In *Pattern Recognition and Machine Intelligence (PReMI)*, Volume 5909 of *Lecture Notes in Computer Science, Springer*, pages 464–469, India, December 2009.

3. **Hunny Mehrotra**, Badrinath G. S., Banshidhar Majhi, and Phalguni Gupta. An efficient iris recognition using local feature descriptor. In *IEEE International Conference on Image Processing (ICIP)*, pages 1957–1960, Egypt, November 2009.

4. **Hunny Mehrotra**, Badrinath G. Srinivas, Banshidhar Majhi, and Phalguni Gupta. Indexing iris biometric database using energy histogram of dct subbands. In *International Conference on Contemporary Computing (IC3)*, CCIS 40, Springer, pages 194–204, India, August 2009.

5. **Hunny Mehrotra**, Dakshina Ranjan Kisku, V. B. Radhika, Banshidhar Majhi, and Phalguni Gupta. Feature level clustering of large biometric database. In *IAPR International Conference on Machine Vision Applications (MVA)*, pages 324–327, Japan, May 2009.

6. **Hunny Mehrotra**, Badrinath G.S., Banshidhar Majhi, and Phalguni Gupta. An efficient dual stage approach for iris feature extraction using interest point pairing. In *IEEE Workshop on Computational Intelligence in Biometrics: Theory, Algorithms, and Applications*, pages 59–62, April 2009.

7. **Hunny Mehrotra**, Banshidhar Majhi, and Phalguni Gupta. Multi-algorithmic iris authentication system. In *International Conference on Image, Signal and Vision Computing (ICISVC)*, pages 148–152, Italy, October 2008.

Communicated

1. **Hunny Mehrotra**, Badrinath G.S., Banshidhar Majhi, and Phalguni Gupta. Enhanced scale invariant feature descriptor for iris biometrics. *Journal of Network and Systems Management, Springer*, 2010.

BIO-DATA

Hunny Mehrotra

Date of Birth: 04 September 1982

Correspondence:

Department of Computer Science and Engineering,

National Institute of Technology Rourkela,

Rourkela – 769 008, Orissa, India.

Ph: +91 94384 90587

e-mail: hunny@nitrkl.ac.in, hunny04@gmail.com

Qualification

- M.Tech. (CSE)
  NIT Rourkela, [Continuing]

- B Level
  DOEACC, New Delhi, [First division]

- +2 (Commerce)
  ISC, New Delhi, [First division]

- 10th
  ICSE, New Delhi, [First division]

Professional Experience

Teaching Assistant, NIT Rourkela, Jul 2008 – Date

Project Associate, IIT Kanpur, Jan 2005 – Dec 2007

Publications

- 02 Journal Articles

- 17 Conference Articles

- 02 Book Chapters

Permanent Address

48/227, General Ganj,
Kanpur, 208 001, UP.